

S. Vernu, S. Sritharan

**Section, Member and System Level Analyses for
Precast Concrete Hybrid Frames**

**ISU-ERI-Ames Report ERI-04635
Submitted to the Precast/Prestressed Concrete Institute
Chicago, Illinois**

JUNE 2004

Final

REPORT

IOWA STATE UNIVERSITY

**Department of Civil, Construction
and Environmental Engineering**

Section, Member and System Level Analyses for Precast Concrete Hybrid Frames

by

**Sivakkolundu Vernu
Graduate Research Assistant**

**Sri Sritharan
Assistant Professor**

ISU-ERI-Ames Report ERI-04635

A Final Report to the Precast/Prestressed Concrete Institute

**Department of Civil, Construction and Environmental Engineering
Iowa State University
Ames, IA 50011**

June 2004

ABSTRACT

Experimental studies have shown that precast concrete hybrid frames with dry jointed moment connections can provide adequate lateral force resistance for buildings located in high seismic zones. This framing concept, which has been approved for use by code officials, utilizes unbonded post-tensioning and mild steel reinforcement that is debonded over a short distance to establish a moment resisting connection between a precast beam and a precast column. As a result, the hybrid frames have the ability to dissipate energy and sustain minimal residual displacements when subjected to earthquake lateral forces. Due to the use of unbonded steel reinforcement, the hybrid connection concept introduces strain incompatibility between the reinforcement and the surrounding concrete, making the analysis and design of the connection difficult. Consequently, the available analysis and design methods for hybrid frame connections are based on many simplified assumptions.

The analytical investigation presented in this report examines the monolithic beam analogy concept and establishes an improved set of expressions for estimating concrete and steel strains at the connection. The accuracy of the improved set of equations is verified using experimental data through section (or connection) and system level analyses. The improved analysis procedure is then demonstrated for a member level analysis and seismic analysis of a five-story precast hybrid building under different earthquake input motions. Using the analytical response of the five-story building, the following are examined: the benefits of using flexible floor links in hybrid frames, the ability of hybrid frames to satisfy limit states when subjected to different earthquake intensities, and suitable response modification (R-) factors for the force based design of hybrid frames.

ACKNOWLEDGEMENTS

The research presented in this report was made possible by a 2001–2002 Daniel P. Jenny Research Fellowship from the Precast/Prestressed Concrete Institute (PCI), which is gratefully acknowledged. The authors would like to express their gratitude to Dr. Stefano Pampanin of the University of Canterbury and Mr. Onur Celik of Iowa State University for providing the necessary data and guidance during the study presented in this report.

TABLE OF CONTENTS

ABSTRACT	iii
ACKNOWLEDGEMENTS.....	iv
LIST OF FIGURES	vii
LIST OF TABLES.....	xii
LIST OF SYMBOLS	xiii
CHAPTER 1 INTRODUCTION	1
1.1 Background	1
1.2 Seismic Design of Precast Prestressed Buildings	2
1.2.1 Design Philosophy	2
1.2.2 Classification of Connections	3
1.2.3 Precast Frame Systems in Seismic Regions	5
1.3 Hybrid Connection	6
1.3.1 Hybrid Connection Analysis	8
1.3.2 Design Provisions	9
1.4 Scope of Research	9
1.5 Report Layout	11
CHAPTER 2 LITERATURE REVIEW	13
2.1 Introduction.....	13
2.2 Performance of Precast Buildings in Earthquakes.....	13
2.2.1 1964 Alaska Earthquake	14
2.2.2 1977 Rumania Earthquake.....	16
2.2.3 1985 Mexico Earthquake	16
2.2.4 1988 Armenia Earthquake	17
2.2.5 1989 Loma Prieta Earthquake.....	20
2.2.6 1994 Northridge Earthquake.....	20
2.2.7 1995 Kobe Earthquake.....	24
2.2.8 1999 Kocaeli Earthquake.....	25
2.2.9 1999 Chi-Chi, Taiwan Earthquake	25
2.2.10 2001 Bhuj Earthquake.....	25
2.3 Experimental Studies	26
2.3.1 Background.....	26
2.3.2 Emulative Connections	26

2.3.2.1 Ductile-Wet Connections.....	26
2.3.2.2 Strong-Wet Connections.....	40
2.3.2.3 Ductile-Dry Connections	42
2.3.2.4 Strong-Dry Connections	43
2.3.3 Non-Emulative Connections.....	47
2.4 Analytical Studies for Hybrid Connection.....	60
2.4.1 Introduction.....	60
2.4.2 Englekirk(1989).....	61
2.4.3 Priestley and Tao (UCSD, 1993).....	63
2.4.4 Cheok, Stone and Nakaki (NIST, 1996).....	66
2.4.5 Pampanin, Priestley and Sritharan (2000)	70
2.4.5.1 Concrete Strain	71
2.4.5.2 Strain in the Mild Steel Reinforcement	73
2.4.5.3 Strain in the Post-Tensioning Tendon	75
2.4.5.4 Moment-Rotation Response.....	76
2.5 Design Provisions	76
2.5.1 Recommended Design Procedures	76
2.5.1.1 Cheok, Stone, and Nakaki (1996).....	77
2.5.1.2 ACI Innovative Task Group 1 (2001).....	79
 CHAPTER 3 CONNECTION AND MEMBER LEVEL ANALYSIS	 81
3.1 Section Analysis.....	81
3.1.1 Assumptions.....	83
3.1.2 Quantifying Strains	84
3.1.2.1 Concrete Strain.....	84
3.1.2.2 Steel Strains	86
3.1.3 Moment-Rotation Envelope.....	88
3.1.4 Experimental Validation	93
3.1.4.1 Moment Rotation Envelopes.....	94
3.1.4.2 Neutral Axis Depth	96
3.1.4.3 Elongation of Prestressing Steel	98
 3.2 Member Level Analysis.....	 100
3.2.1 Procedure	100
3.2.2 Results.....	102

CHAPTER 4 ANALYSIS OF A HYBRID FRAME BUILDING	107
4.1 Introduction.....	107
4.2 Model Formulation	108
4.2.1 Five-story Hybrid Frame Building.....	108
4.2.2 Hybrid Connection Model	111
4.2.3 Hybrid Frame Model	115
4.3 Validation of the Analytical Model	117
4.3.1 Overview.....	117
4.3.2 Pushover Analysis.....	118
4.3.3 Dynamic Analyses	119
4.4 Performance Based Seismic Analysis.....	125
4.5 Influence of Flexible Floor Link.....	127
4.6 Response Modification Factor	129
 CHAPTER 5 CONCLUSIONS AND RECOMMENDATIONS	 135
5.1 Overview.....	135
5.2 Literature Review.....	136
5.2.1 Performance of precast concrete building in past earthquakes	136
5.2.2 Experimental investigation	137
5.2.3 Analytical investigation of hybrid systems.....	137
5.2.4 Design Methods for Hybrid Frame Systems.....	138
5.3 Section Analysis of Hybrid Connections.....	138
5.4 Analysis of a Five-story Hybrid Frame Building	139
5.5 Recommendations.....	141
 REFERENCES	 143

LIST OF FIGURES

Figure 1.1 Classification of precast concrete frame connections based on different criteria.	4
Figure 1.2 Two different inelastic frame mechanisms.	5
Figure 1.3 A typical hybrid precast frame connection.	7
Figure 1.4 Relationship between steel and concrete strains.	9
Figure 2.1 Partially collapsed building with poorly connected precast floor panels.	15
Figure 2.2 Collapse of floor panels leaving walls standing in a building in Leninakan	19
Figure 2.3 Damage to a four-story building in Leninakan due to inadequate connection between precast floors and infill walls.	19
Figure 2.4 Collapse of floor planks leaving external precast frame standing in a building in Spitak.	20
Figure 2.5 Collapse of center columns, floors, and external moment frames of a parking structure at the California State University in Northridge.	23
Figure 2.6 Another view of the collapsed parking structure at the California State University in Northridge.	23
Figure 2.7 Details of Unit 1.	27
Figure 2.8 Cyclic load sequence used by Blakeley and Park.	28
Figure 2.9 Curvature distribution along precast members of Unit 1.	29
Figure 2.10 Details of a frame connection tested by Pillai and Kirk connection.	30
Figure 2.11 Loading criteria used by Pillai and Kirk.	31
Figure 2.12 Detail of the bonded post-tensioned connection tested by French et al.	32
Figure 2.13 Cyclic load history used by French et al.	33
Figure 2.14 Precast framing concept using flexural and shear plates.	34
Figure 2.15 Schematic diagrams showing test configurations used by Restrepo et al.	35
Figure 2.16 Precast frame connection details tested by Restrepo et al.	36
Figure 2.17 Cyclic load sequence used in the tests by Restrepo et al.	36
Figure 2.18 Connection details used for precast beam-column frames by Alcocer et al.	39
Figure 2.19 Displacement-controlled cyclic load sequence adopted by Alcocer et al.	39
Figure 2.20 Cross-section details of the frame system with a welded plate connection investigated by French et al.	41

Figure 2.21 Two types of precast connections investigated by Ersoy and Tankut.	44
Figure 2.22 The test setup used by Ersoy and Tankut.	45
Figure 2.23 The cyclic load sequence used by Ersoy and Tankut.	45
Figure 2.24 Typical connection details adopted by Ochs and Ehsani.	47
Figure 2.25 Ductile connector components adopted by Nakaki et al.	48
Figure 2.26 Ductile frame connection details adopted by Nakaki et al.	48
Figure 2.27 Details of test specimens used in Phase I of the NIST research program.	50
Figure 2.28 Cyclic load sequence used in Phase I of the NIST test program.	51
Figure 2.29 Lateral force-displacement hysteresis behavior of two specimens tested in Phase I of the NIST test program.	51
Figure 2.30 Lateral load-displacement behavior of precast frames with connections utilizing fully and partially bonded prestressing stands.	54
Figure 2.31 Precast frame subassembly with hybrid connection tested in Phase IV-B by Stone et al.	56
Figure 2.32 Hysteresis responses obtained for two hybrid frame subassemblages tested by Stone et al.	57
Figure 2.33 Subassembly of the interior precast frame connection tested by Priestley and MacRae.	59
Figure 2.34 The cyclic loading history used by Priestley and MacRae.	59
Figure 2.35 Lateral force-drift behavior observed for the interior precast frame connection by Priestley and MacRae.	60
Figure 2.36 Curvature and displacement distribution for a cantilever beam.	62
Figure 2.37 Displacement components for a beam-column subassembly.	63
Figure 2.38 Force-deformation response idealization suggested for a beam-column subassembly by Priestley and Tao.	64
Figure 2.39 Forces and displacements at the hybrid connection interface.	67
Figure 2.40 The equivalent monolithic beam analogy concept.	71
Figure 2.41 A hybrid connection with imposed interface rotation of θ	74
Figure 3.1 The iteration procedure adopted for the section analysis of a hybrid frame connection.	92
Figure 3.2 Connection details used in three hybrid frames.	93

Figure 3.3 Test configuration used for specimens M-P-Z4 and O-P-Z4.	95
Figure 3.4 The beam end moment vs. interface rotation obtained for M-P-Z4.	95
Figure 3.5 The beam end moment vs. interface rotation obtained for O-P-Z4.....	96
Figure 3.6 An illustration showing the displacement transducers mounted to the face of the interior column at the first floor of the hybrid frame in the PRESSSS test building.	97
Figure 3.7 A comparison between the analytical and experimental neutral axis depths obtained for the PRESSSS first floor connection.	99
Figure 3.8 Comparison of predicted stand elongations with experimental values.	99
Figure 3.9 A cantilever beam and the moment diagram.	101
Figure 3.10 Variation of curvatures along the beam length.	102
Figure 3.11 Variation of strains in the tension mild steel reinforcement along the beam. ...	103
Figure 3.12 Variation of the extreme fiber concrete compressive strains along the beam. ...	105
Figure 3.13 Variation of strains in the compression mild steel reinforcement along the beam.	106
Figure 4.1 Elevation view of the seismic frame with hybrid and pretensioned connections in the PRESSSS test building.	109
Figure 4.2 Elevation of the PRESSSS seismic frame with TCY and TCY gap connections. .	110
Figure 4.3 Typical plan of the PRESSSS test building at the first three floors.	110
Figure 4.4 Typical plan of the five-story hybrid frame building.	111
Figure 4.5 Finite element model of a hybrid frame connection.	112
Figure 4.6 Components of bending moment resistance of a hybrid frame connection.	113
Figure 4.7 The moment-rotation behavior of the mild steel reinforcement at a hybrid connection.	114
Figure 4.8 The moment-rotation behavior of the prestressing steel at a hybrid connection.	114
Figure 4.9 The total moment-rotation response envelope of a hybrid connection and its representation in a RUAUMOKO model.	115
Figure 4.10 Finite element model of the five-story hybrid frame	116
Figure 4.11 Details of an X-plate used in the PRESSSS building.	117
Figure 4.12 Comparison of experimental and calculated responses.	119
Figure 4.13 Acceleration time histories of the original input motions prepared for the PRESSSS building that represented the prototype structure at 60% scale.	120

Figure 4.14 Modified input motions for the acceleration time histories shown in Figure 4.13.....	121
Figure 4.15 Third floor lateral displacement time histories obtained for the PRESSS and hybrid frame building.	122
Figure 4.16 Base moment time histories obtained for the PRESSS and hybrid frame building.....	123
Figure 4.17 Third floor displacement time histories obtained from the PRESSS building and analytical models for the modified input motions.....	124
Figure 4.18 Linear and non-linear pushover analysis results for the hybrid frame model shown in Figure 4.10.	130

LIST OF TABLES

Table 2.1 Details of earthquakes considered in Section 2.2.	14
Table 2.2 Summary of damage of precast buildings in the 1988 Armenia Earthquake.	17
Table 2.3 Degree of damages to precast parking structures during the 1994 Northridge Earthquake.	22
Table 3.1 Material properties used in the connection analyses	94
Table 4.1 A summary of hybrid frame connection details.	109
Table 4.2 Comparison of peak lateral displacements obtained at the third floor of the PRESSS and hybrid buildings.	125
Table 4.3 Peak inter-story drifts obtained for different levels of earthquake input motions.	127
Table 4.4 Comparison of peak top floor displacements and total base moments obtained for the hybrid frame building with flexible and rigid floor links.	128

LIST OF SYMBOLS

A_{pt}	Cross-section area of the post-tensioning steel
A_s	Cross-section area of the mild steel reinforcement
b	Beam width
c	Neutral axis depth
C	Resultant compression force in concrete
d	Depth to the mild steel reinforcement from the extreme compression fiber
d_b	Bar diameter of the mild steel reinforcement
E_c	Young's modulus of concrete
E_{ps}	Young's modulus of the post-tensioning steel
E_{sec}	Secant modulus of concrete
E_{st}	Young's modulus of the mild steel reinforcement
f'_1	Maximum effective lateral confinement stress from the transverse reinforcement
f'_c	Unconfined concrete compressive strength
f'_{cc}	Confined concrete compressive strength
f_{ps}	Stress in the post-tensioning steel
f_{psy}	Yield strength of the prestressing steel
f_{sc}	Stress in the compression mild steel reinforcement
f_{st}	Stress in the tension mild steel reinforcement
f_u	Ultimate strength of the mild steel reinforcement
f_x	Intermediate stress in the hardening region corresponding to ϵ_x
f_y	Yield strength of the mild steel reinforcement
h	Height of beam
L	Length of cantilever beam
L_p	Plastic hinge length
L_{sp}	Length over which the strain penetration effects are assumed
L_u, L_{ub}	Debonded length of the mild steel reinforcement
L_{ups}	Unbonded length of the post-tensioning steel reinforcement
M	Moment resistance
M_n	Nominal moment resistance
M_p	Probable moment resistance
n	Number of stories
T_{ps}	Force in the post-tensioning steel reinforcement
T_s	Force in the mild steel reinforcement

Δ_e^*	Beam end displacement due to elastic curvature along the beam connected with a hybrid connection
Δ_E	Elastic component of the beam end displacement
Δ_e'	Member end displacement of a monolithically connected beam due to elastic curvature along the length
$\Delta_{\text{Monolithic}}$	Total beam end displacement of a monolithically connected beam
Δ_p	Plastic beam end displacement of a monolithic concrete beam
Δ_{Precast}	Total beam end displacement of a precast concrete beam with a hybrid connection
Δ_{ps}	Elongation of the post-tensioning tendon due to interface rotation θ at the hybrid connection
Δ_θ	Beam displacement component due to interface rotation θ at the hybrid connection
Δ_s, Δ_{st}	Elongation of the tension mild steel reinforcement due to interface rotation θ at the hybrid connection
Δ_{sc}	Elongation of the compression mild steel reinforcement due to interface rotation θ at hybrid connection
Δ_{sp}	Displacement component due to strain penetration effects
ε_c	Compression strain in the extreme concrete fiber
ε_{cc}	Strain corresponding to f'_{cc}
ε_{co}	Strain corresponding to f'_c
ε_e	Elastic tensile strain in the mild steel reinforcement
ε_p	Plastic tensile strain in the mild steel reinforcement
ε_{pi}	Initial prestress after losses in the post-tensioning steel reinforcement
$\varepsilon_{ps}, \varepsilon_{si}$	Strain in the post-tensioning steel reinforcement
$\varepsilon_s, \varepsilon_{st}$	Strain in the tension mild steel reinforcement
ε_{sh}	Strain in the tension mild steel reinforcement at the onset of strain hardening
$\varepsilon_{su}, \varepsilon_u$	Ultimate strain in the mild steel reinforcement at fracture
ε_x	Intermediate strain in the hardening region corresponding to f_x
ε_y	Yield strain of the mild steel reinforcement
ϕ_e	Elastic curvature
ϕ_u	Total or ultimate curvature
ϕ_y	Yield curvature
θ	Rotation at the hybrid connection interface
θ_P	Total plastic rotation at the beam-column connection

CHAPTER 1

INTRODUCTION

1.1 Background

Catastrophic structural damage observed in several recent major earthquakes, including those occurring in the United States, Japan, Turkey, and India, has once again emphasized that seismic damage is largely induced by deficiencies in design concepts, detailing, and/or construction methods [1–5]. Safety of structures in future earthquakes continues to mandate development of reliable seismic design procedures and implementation of good construction practice.

Among the various technologies available to date for construction of buildings, precast, prestressed concrete offers unique advantages:

- Slender structural members resulting from utilization of high strength materials;
- Improved building quality due to construction of structural components under controlled environment;
- Speedy construction resulting from the use of prefabricated components;
- Reduced formwork and scaffolding at the construction site;
- Incorporation of architectural features in factory settings; and
- Potential for automation in the construction industry that will result in reduced labor cost.

However, the economical and other recognized benefits of precast, prestressed concrete have not been fully exploited in seismic regions for two main reasons:

1. Poor performance of precast prestressed structures in past earthquakes [1].

2. Lack of reliable guidelines for seismic design of precast, prestressed concrete in the current building codes [6].

For these reasons, the design codes such as UBC 97 [7] have typically permitted the following alternatives for construction of precast concrete buildings in seismic regions [6, 8]:

1. Emulation design, in which the behavior of a precast building system is expected to be similar to that of an equivalent monolithic system, or
2. Non-emulative design that requires experimental confirmation showing adequacy of the precast systems through large-scale simulated seismic testing.

As discussed subsequently, the use of the emulation concept does not fully utilize the unique properties of precast, prestressed concrete in seismic design of buildings structures, and thus this alternative will not result in efficient precast systems. The second option introduces delays and additional costs, making the precast option unnecessarily expensive.

1.2 Seismic Design of Precast, Prestressed Buildings

1.2.1 Design Philosophy

Seismic design of structures is now based on the capacity design philosophy, which was suggested by Hollings and developed by discussion groups of the New Zealand Society for Earthquake Engineering in the 1970s [8]. This philosophy requires that structures be designed to exhibit appropriate inelastic deformation modes when they are subjected to moderate to large earthquakes. Suitable lateral load resisting systems are first selected, which are then designed for adequate ductility. Accordingly, in the case of precast, prestressed concrete buildings with moment frames as the lateral load resisting system, plastic hinge locations can be conveniently selected at the precast beam ends. The connections between the

columns and beams may be designed to achieve the rotational ductility demand expected under design-level earthquakes. At the same time, the remaining structural members and other possible failure mechanisms are designed with sufficient strength. This design concept prevents brittle failure of precast members and development of undesirable failure mechanism in the structure. Consequently, when subjected to design-level earthquake lateral loads, the precast structure will exhibit a desirable response by deforming through the predetermined ductile mechanism [9].

1.2.2 Classification of Connections

Several different beam-to-column connection types have been investigated for moment resisting ductile frames consisting of precast members [6]. These connections may be classified into several categories as shown in Figure 1.1. The first classification differentiates emulative connections from non-emulative type connections. If a precast beam-to-column connection is established to provide performance equivalent to that of a monolithic concrete connection in terms of strength and toughness, this connection is said to be an emulative connection. In contrast, a non-emulative connection utilizes unique properties of precast concrete technology to ensure sufficient ductile performance for the frame systems. Non-emulative connections that have been successfully introduced to precast frame systems are the “jointed” connections [10, 11].

At the next level, connections may be divided into strong or ductile connections depending on the locations where inelastic deformations are permitted to develop [12]. In frames with strong connections, precast members are designed to be weaker than the connections, forcing the inelastic actions at designated locations in the precast members. On

the other hand, ductile connections are detailed to be weaker than the precast elements, confining inelastic actions to the connection regions, while the precast elements remain elastic during seismic response of the structure.

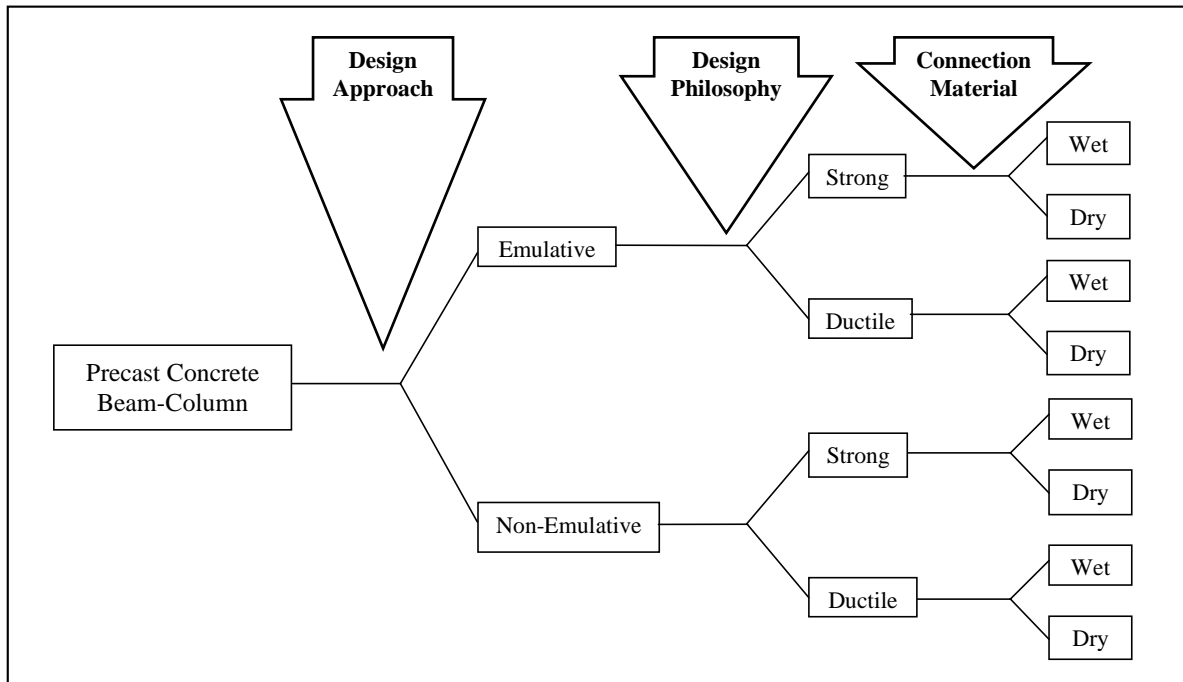


Figure 1.1 Classification of precast concrete frame connections based on different criteria.

Finally, both strong and ductile connections may be classified into wet or dry connections. Wet connections are those that utilize concrete or grout in the field to splice reinforcement of precast members. All connections other than the wet connections are classified as dry connections [11]. Although Figure 1.1 identifies eight different connection types as discussed above, researchers have not studied every connection type. A review of the connection types that have been explored by researchers is presented in Sections 2.3 and 2.4 along with their findings.

1.2.3 Precast Frame Systems in Seismic Regions

Moment frames may develop satisfactory ductile response under lateral seismic loading through several different inelastic mechanisms involving formation of plastic hinges at the beam and column ends. The two extreme mechanisms are shown in Figure 1.2. In the first mechanism as shown in Figure 1.2a, plastic hinges are formed at the beam ends and column bases and the remaining column sections are designed to be elastic, which is referred to as the strong column-weak beam mechanism. In the second mechanism, inelastic actions are concentrated in the columns of the first floor. This mode is not generally preferable since it will require significantly large rotational ductility demands in the plastic hinge locations, as illustrated in Figure 1.2b. This mode of response, which is typically referred to as the soft story mechanism, has caused buildings to collapse or reach a near collapse condition in past earthquakes [9]. Therefore, seismic design of building frames requires strong column-weak beam approach to ensure satisfactory ductile response [8].

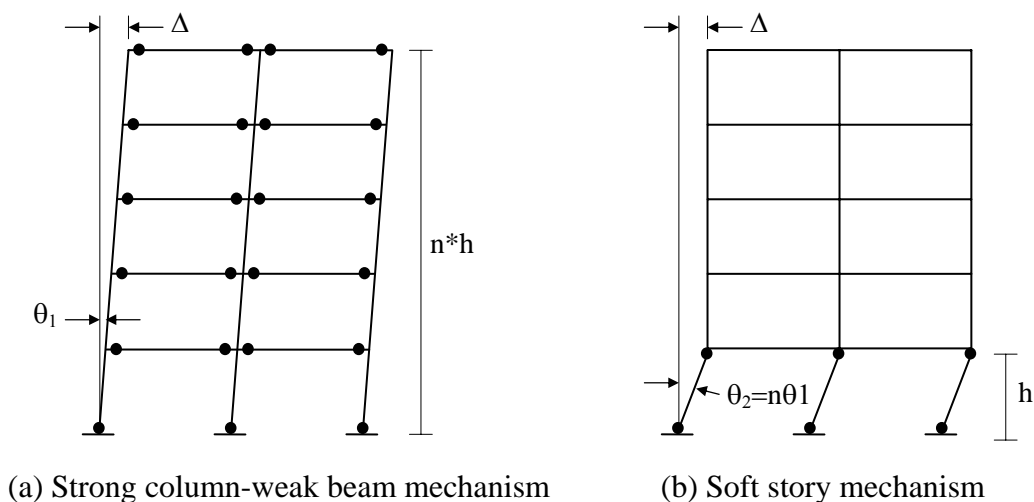


Figure 1.2 Two different inelastic frame mechanisms.

Based on the precast connection classification discussed in the previous section, either strong or ductile connections may be used to develop the strong column-weak beam mechanism. Since seismic behavior of precast frames with strong connections is expected to be similar to that of monolithic concrete frames, they can be designed with existing code provisions. Consequently, early studies on seismic design of precast beam-to-column connections subjected to earthquake loads focused on developing emulative connections [6].

However, if precast frames are provided with ductile connections, the precast members do not require ductile details, but they need to be designed with adequate margin of strength with respect to the strength of the connections. Benefits of ductile connections include cost efficiency and use of replaceable connections if they are damaged during seismic response of the frame.

1.3 Hybrid Connection

Figure 1.3 illustrates a jointed connection known as the hybrid connection that is suitable for developing the desirable ductile mechanism in moment resisting frames. In this concept, precast single-bay beams are connected to multi-story high precast columns using dry-ductile connections based on unbonded post-tensioning steel and mild steel reinforcing bars. The post-tensioning steel is located at the mid-height of the beam and is typically designed to remain elastic during seismic loading in order to minimize residual displacements and stiffness degradation of the frames. At the column-to-beam interface, shear transfer is assumed to be by a friction mechanism. Mild steel reinforcing bars are provided at the top and bottom of the beams as continuous reinforcement through the column. During seismic loading, the mild steel reinforcement is subjected to strain reversals, which provides energy

dissipation capability for the hybrid frames. The mild steel bars are debonded over a short distance on either side of the column to prevent them from premature fracture due to accumulation of large inelastic strains. Both the post-tensioning and the mild steel reinforcement contribute to the moment resistance of the precast connections.

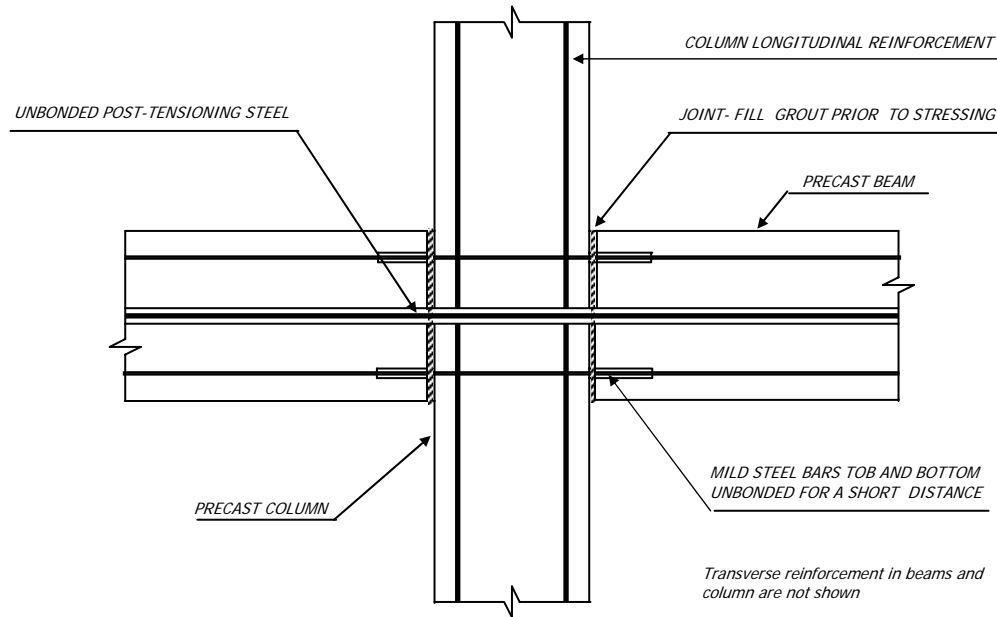


Figure 1.3 A typical hybrid precast frame connection.

The main benefit of using post-tensioning steel at the precast connections is that it gives the necessary restoring force to control the residual displacements, whereas it was previously noted that mild steel reinforcement provides energy dissipation capability for the frame. Because the restoring force and energy dissipation are achieved by two different means, this dry-ductile connection is referred to as the hybrid connection. The design of a hybrid connection relies on optimizing the following design parameters:

- The area of the post-tensioning and mild steel reinforcement

- The debonded length of the mild steel reinforcement
- Initial prestress in the post-tensioning steel

1.3.1 Hybrid Connection Analysis

In monolithic concrete section analysis, the plane sections remain plane assumption and the condition of strain compatibility establishes a relationship between the steel strain, concrete strain and neutral axis depth as illustrated in Figure 1.4a. However, the strain incompatibility that exists between concrete and unbonded steel reinforcement at a hybrid connection makes the section level analysis impossible with conventional means. Figure 1.4b shows the incompatibility between strains due to the presence of unbonded steel reinforcement in a hybrid connection. An analytical procedure is needed to develop a complete moment-rotation behavior for this connection type, which can be used in the design and performance assessment of precast hybrid frames. Limited research has been conducted on the development of a rational connection level analysis method. The studies conducted to date have used either several simplified assumptions or not provided thorough validation of the proposed methods using experimental data.

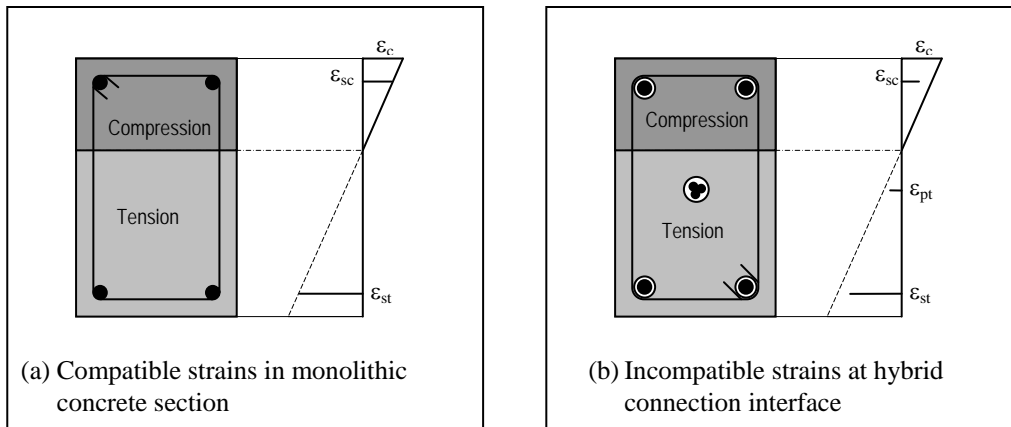


Figure 1.4 Relationship between steel and concrete strains.

1.3.2 Design Provisions

Using experimental research studies, design procedures for hybrid frame connections have been developed [13, 14]. A detailed description on the findings of these studies and a summary of design guidelines are included in Sections 2.3 and 2.5, respectively. Based on the recommendations of these studies, the American Concrete Institute (ACI) has also published a technical document that defines requirements that may be used to design special hybrid moment frames [15]. However, no provisions are available in the building codes of the United States for the design of hybrid connections. It is widely expected that provisions for hybrid connections will be incorporated into ACI 318-05 or the International Building Code to be published in 2006 [16]. As a step towards achieving this goal, validation of the different design procedures for the hybrid frame is performed in a parallel investigation [17].

1.4 Scope of Research

Considering the current state of knowledge on precast hybrid frame systems, the research presented in this report focuses on the following areas:

1. Development of an analytical model to predict the behavior of a hybrid connection as a function of rotation at the precast interface by adequately modeling:
 - a. the stress-strain behavior of concrete, mild steel reinforcement, and post-tensioning tendons
 - b. strain penetration of the mild steel reinforcement into the joint
 - c. confinement effects on the behavior of concrete
2. Development of a computer tool that will enable the connection analysis and validation of analysis results against test data.
3. Extend the connection level analysis to predict behavior at the member level.
4. Demonstrate the benefits of predicting the moment resistance of a hybrid connection as a function of the interface rotation by performing nonlinear pushover and dynamic analyses on a precast hybrid moment resisting frame building. In these analyses, the moment-rotation behavior of the hybrid connections will be characterized using the computer tool described in (2) above.

In the first phase of this research, the analytical procedure based on the monolithic beam analogy proposed by Pampanin et al. [18] to characterize the behavior of jointed connections is investigated for improvements with emphasis on application of this procedure to hybrid connections. This includes accurate modeling of the strain penetration term for the mild steel reinforcement and representing the stress-strain characteristics of the unbonded post-tensioning steel using Mattock's model [19]. Although Pampanin et al. indicated that the

moment contribution of the compression steel located at the connection was included in the analysis, no detail was provided as to how this was achieved given the section level strain incompatibility between this steel reinforcement that has a short debonded length (see Figure 1.3) and the surrounding concrete. The contribution of the compression steel in the connection analysis is addressed and an expression relating the strain in the compression steel and interface rotation is provided in this report. With improvements, the analysis results are verified against data obtained from the hybrid frame tests conducted at NIST (National Institute of Science and Technology) as well as the PRESSS (PREcast Seismic Structural System) building test. Pampanin et al. also provided validation of their analysis results against these test data. However, their validation was largely limited to overall connection and structural behavior and did not include parameters such as the change in the post-tensioning force and neutral axis depth as a function of interface rotation.

The structure chosen for the pushover and dynamic analyses is a five-story building with dimensions similar to those of the PRESSS test building. With the input ground motions from the PRESSS test, this building choice enabled its predicted behavior to be verified using the test data from the PRESSS building. Furthermore, through dynamic analyses of the hybrid building, the effects of using flexible floor links and performance-based issues are examined. Finally, an R-factor suitable for the design of the five-story hybrid building and future research directions for establishing the R-factor for the design of hybrid frame buildings are provided.

1.5 Report Layout

This report contains five chapters. Following an introduction to precast concrete design of buildings under seismic loading and hybrid frame systems in this chapter, Chapter 2 summarizes performance of precast buildings in past earthquakes, experimental and analytical studies of precast beam-column frame connections subjected to simulated seismic loads, and details of the seismic design provisions developed for precast concrete buildings.

Chapter 3 presents the theoretical background and development of an improved analytical model for the section level analysis of hybrid connections and extension of this analysis concept to predict behavior at the member level. This chapter also provides comparison between analysis results and experimental data at the connection level. Description of the building chosen for the nonlinear pushover and dynamic analyses and the analysis results are presented in Chapter 4. In addition to a summary of the research findings, conclusions and recommendations are given in Chapter 5.

CHAPTER 2

LITERATURE REVIEW

2.1 Introduction

Application of precast concrete in seismic regions varies from the use of only architectural members (e.g., claddings) to designing the building using precast structural members such as floor panels, gravity frames, and lateral load resisting systems. Precast members have been frequently used in conjunction with other structural material types such as cast-in-place concrete and steel building systems. Moment resisting frames and structural walls are two different systems that are used to resist lateral loads in building structures. Given the focus of this report on precast hybrid frames, this chapter presents a literature review on precast and/or prestressed moment resisting seismic frames in four specific areas:

1. The performance of precast concrete buildings in earthquakes
2. Experimental investigations of several types of precast, prestressed concrete beam-to-column connections that may be suitable for applications in seismic regions
3. The hybrid precast frame
4. Design methods for hybrid connections

2.2 Performance of Precast Buildings in Earthquakes

A review of reports on the performance of buildings, with precast members and/or precast structural systems, in earthquakes is presented in this section. These reports generally contained limited information on the performance of lateral load resisting precast moment frames, which may be attributed to restricted application of precast concrete in high seismic

regions. Presented in the subsequent sections are summaries of seismic performance of buildings that contained precast members in several earthquakes, whose details are given in Table 2.1.

Table 2.1 Details of earthquakes considered in Section 2.2.

Earthquake Name	Date of Event	Local Magnitude (M_L)	Maximum Horizontal Acceleration	Duration (s)
1964 Alaska Earthquake [20, 21]	March 27	8.4	0.40g	>150
1977 Rumania Earthquake [20, 22]	March 4	7.2	0.20g	25
1985 Mexico Earthquake [23]	Sept. 19 and 20	8.1, 7.5	0.17g	60
1988 Armenia Earthquake [1, 4, 20]	December 7	6.9	0.25g	90
1989 Loma Prieta Earthquake [24]	October 17	7.1	0.64g	20
1994 Northridge Earthquake [2, 20, 25]	January 17	6.8	0.94g	10
1995 Kobe, Japan Earthquake [26]	January 17	7.2	0.83g	20
1999 Kocaeli, Turkey Earthquake [3]	August 17	7.4	0.41g	15–20
1999 Chi-Chi, Taiwan Earthquake [27]	September 21	7.6	0.50g	20–30
2001 Bhuj, India Earthquake [5]	January 26	7.7	0.60g	18–21

2.2.1 1964 Alaska Earthquake

This event mainly affected Anchorage, a city about 75 miles from the epicenter of the earthquake. Precast prestressed elements were used in the construction of at least 28 buildings in Anchorage. Five of these buildings experienced partial or total collapse. All collapsed structures consisted of either reinforced concrete or masonry walls as primary lateral load resisting systems with precast floor panels, except in one structure, in which precast hammerhead frames and precast single tee beams were also used to transfer gravity

loads [21]. Figure 2.1 shows a partially collapsed building, which utilized precast floor panels as well as relatively thick precast nonstructural reinforced concrete cladding panels [20].



Figure 2.1 Partially collapsed building that contained poorly connected precast floor panels [20].

Three possible reasons were attributed to the poor performance of these structures [21]:

1. Ground accelerations were several times greater than the design value,
2. Detailing was not adequate to ensure satisfactory inelastic behavior of the structural systems responsible for resisting lateral loads, and
3. Poor connections were used between floor diaphragms and members of the lateral load resisting systems.

2.2.2 1977 Rumania Earthquake

The damage was mainly reported in the city of Bucharest, which is located 100 miles from the epicenter of this earthquake [22]. In Rumania, seismic design provisions including ductility requirements were not strictly enforced prior to this earthquake and these provisions were generally less stringent than those were in the 1977 Uniform Building Code [28]. Almost all of the residential buildings in the range of 10 stories and above constructed in the late 1950s and beyond utilized structural systems based on the precast and cast-in-place concrete technology. Precast floors with cast-in-place columns, precast floors with cast-in-place walls and precast beams and columns with cast-in-place connections were commonly used in these structural systems. All precast concrete buildings withstood the earthquake shaking satisfactorily, except for one, in which inadequate construction procedures and inferior quality of materials were reported to be the causes for the collapse of that building [22].

2.2.3 1985 Mexico Earthquake

The earthquake damage was largely in Mexico City, although the epicenter was about 250 miles away [23]. Mexican building code [29] included seismic provisions through lateral load requirements prior to this earthquake, but these requirements were less stringent than those published in UBC 1977 [28] and the ACI building standard 318-83 [30]. Precast concrete structural members in the form of slabs, beams, and columns were used only in a small percentage of buildings in Mexico City. In most structures, cast-in-place concrete was used as topping on precast slabs and for connecting precast beams and columns. Only five of the 265 collapsed or severely damaged buildings utilized precast structural members, but

none of the damage could be attributed to the use of precast concrete technology. In fact, failure modes of the buildings with precast members were found to be similar to the buildings made up of only cast-in-place concrete. Interestingly, three large precast concrete silos (224 ft wide, 918 ft long, and 92 ft high) experienced the earthquake without any damage [23].

2.2.4 1988 Armenia Earthquake

Three major cities were affected by this earthquake; the distances to these cities from the epicenter are listed in Table 2.2. Because of the closeness of the epicenter, the damage in these cities was devastating [1].

A summary of damage to precast buildings in the Armenia earthquake is given in Table 2.2. Large panel precast concrete structures performed very well in all three cities, while 95 percent of the precast concrete frame structures in Leninakan either collapsed or experienced damage beyond repair, and none of these buildings was reported to have escaped the earthquake damage. On the other hand, none of the precast frame structures in Kirovakan, a city closer to the epicenter than Leninakan, was reported to be collapsed or damaged beyond repair. Furthermore, 18 percent of the precast concrete frame structures in Kirovakan experienced the earthquake unscathed, while the rest of the precast structures suffered only repairable damage. The difference in the performance of precast concrete frame structures in these two cities was attributed to the poor soil condition in Leninakan, which was suspected to have amplified the seismic motion in the period range close to the fundamental periods of several collapsed frame buildings [1, 4].

Table 2.2 Summary of damage to precast buildings in the 1988 Armenia Earthquake [1]

City	Epicenter distance (miles)	Large panel precast Concrete structures				Precast concrete frame structures			
		A	B	C	D	A	B	C	D
Spitak	5.6	-	-	-	1	-	-	-	-
Kirovakan	15	-	-	-	4	-	-	88	20
Leninakan	20	-	-	-	16	72	55	6	-
Total	-	-	-	-	21	72	55	94	20
Total in Armenia	-	-	-	13	65	72	57	130	77

Key: Damage to precast structures in the Armenian earthquake was reported using four different damage levels, which are:

- A – Collapsed
- B – Heavily damaged-beyond repair
- C – Repairable damage
- D – No significant damage

Figure 2.2 shows the remains of a three-story building, one of the 72 buildings that collapsed in Leninakan. Failure of precast floor panel initiated the collapse of this building. Also in Leninakan, a four-story precast concrete building experienced a partial collapse, as shown in Figure 2.3, due to poorly detailed connections between precast floor panels and infill walls. The precast building shown in Figure 2.4 is another victim of not adequately tying the hollow-core floor planks together, causing middle portions of the building to collapse [20].



Figure 2.2 Collapse of precast floor panels, leaving walls standing in a building in Leninakan [20].



Figure 2.3 Damage to a four-story building in Leninakan due to inadequate connection between precast floors and infill walls [20].



Figure 2.4 Collapse of floor planks leaving external precast frames standing in a building in Spitak [20].

2.2.5 1989 Loma Prieta Earthquake

The epicenter of this earthquake was located near Santa Cruz in the southeastern part of San Francisco. Several parking structures constructed with topped double-tee diaphragms and cast-in-place concrete shear walls or frames experienced this earthquake, but no severe damage to precast structures was reported. Except for some cracking, the performance of parking structures in Oakland, Emeryville, and Berkeley were reported to be satisfactory [24].

2.2.6 1994 Northridge Earthquake

The epicenter was located in Northridge, California, where precast concrete members were commonly used in parking structures. The precast concrete was also found in residential buildings in Northridge, but it was generally limited to architectural components [25].

Seismic performance of parking structures constructed with precast components was compared with performance of other types of parking structures in this event by Iverson and Hawkins [25]. Of the 30 parking structures located within a 20-mile radius of the epicenter, 15 of them utilized precast concrete gravity columns, while 10 of them used precast double-tee slabs. Most of these structures used cast-in-place shear walls and/or moment resisting frames as the lateral load resisting systems. Precast lateral load resisting systems were found in one parking structure located at California State University, Northridge. This system included precast exterior frames with precast interior beams and precast interior columns. The exterior frames were designed as special lateral load resisting moment frames. Haunches in the exterior frames and the interior columns supported the interior beams.

The earthquake damage to precast and non-precast parking structures in Northridge is summarized in Table 2.3. Five structures incorporating precast concrete gravity columns with cast-in-place lateral load resisting systems experienced no damage, while four such structures exhibited minor cracks. However, four similar structures and the structure with precast exterior moment resisting frames experienced partial collapse due to the Northridge earthquake. In comparison, only two of the 15 structures that had no precast components partially collapsed, while damage to the rest of the structures was localized and generally confined to structural members [25].

Table 2.3 Degree of damage to precast parking structures during the 1994 Northridge Earthquake.

Parking Structures	Quantity	Collapsed		Damage to structural members	Minor damage	No damage
		Extensive	Partial			
Precast exterior frames and precast gravity columns	1	–	1	–	–	–
Precast gravity columns	14	1	4	–	4	5
No precast elements	15	–	2	13	–	–
Total	30	1	7	13	4	5

The collapsed portion of the parking structure at the California State University in Northridge is shown in Figure 2.5. Failure of the interior columns due to overloading in the vertical direction was reported to have initiated the collapse, as this failure caused the interior beams to unseat from the haunches of the failed interior columns and to rotate vertically downward [2, 25]. This in turn caused sagging of the floor slabs and pulling of the exterior frames inwards in the out-of-plane direction. Figure 2.5 shows the separated exterior frames at a corner, as the frames in the orthogonal direction were not connected to one another. Another view of this collapsed parking structure is shown in Figure 2.6.



Figure 2.5 Collapse of center columns, floors, and external moment frames of a parking structure at the California State University in Northridge [20].



Figure 2.6 Another view of the collapsed parking structure at the California State University in Northridge [20].

The following were reported to be the common shortcomings in the design of the parking structures presented in Table 2.3 [25]:

1. Inability of the gravity load frames to experience large lateral deformations in tandem with the lateral load resisting systems,
2. Presence of insufficient number of lateral-load resisting systems in the plan of the structure,
3. Improper transfer of horizontal inertia forces through the intermediate elements, referred to as the collector elements, to the lateral load resisting systems, and
4. Brittle behavior of gravity load elements when overloaded in the vertical direction.

2.2.7 1995 Kobe Earthquake

The epicenter of this event was located about 12 miles southwest from downtown Kobe, Japan. In the region where damage to structures was mainly reported, there were 11 buildings that utilized precast concrete structural members, while non-structural precast components were found in another 49 buildings. Buildings with precast structural members were relatively new and regular in shape with uniform distribution of mass and stiffness. Most of these structures with precast elements performed remarkably well except for a few buildings, in which some structural damage was evident. Typical damage included the following [26]:

1. Failure of cast-in-place concrete columns prior to yielding of the prestressed beams that were connected to the columns,
2. Unseating of roof panels from peripheral beams due to the failure of steel bolts connecting the panels to the beams, and
3. Failure of cast-in-place concrete columns causing precast roof panels to unseat.

2.2.8 1999 Kocaeli Earthquake

In Turkey, precast frame buildings have been widely used in single-story warehouses [3]. The lateral load resisting frames used in these structures were designed by modifying the connection details of gravity load resisting frames that have been typically used in Western Europe. Performance of the precast structures in the epicentral region of this earthquake was reported to be unsatisfactory due to inadequate details used at the base of the columns that inhibited the formation of dependable flexural plastic hinges. Another reason attributed to the poor performance of these structures was pounding of precast elements at the roof level [3].

2.2.9 1999 Chi-Chi, Taiwan Earthquake

Most of the mid-rise buildings were constructed with reinforced concrete while high-rise buildings were built with structural steel. Although several building failures were reported, information specific to precast buildings was not available in the literature [27].

2.2.10 2001 Bhuj Earthquake

This was an intra-plate earthquake and was compared to the 1811 and 1812 New Madrid earthquakes in the midwestern region of United States [31]. The application of precast concrete was limited to some single-story school buildings in the region where this event caused structural damage. These single-story buildings consisted of precast concrete columns and large precast concrete panels as roofs and walls. It was reported that about one-third of such buildings experienced roof collapse due to the following reasons [5]:

1. Poor connections between roof panels, and

2. Inadequate seating of roof panels that were supported on walls and beams.

2.3 Experimental Studies

2.3.1 Background

Over the past three decades, there has been a significant number of experimental studies that have investigated framing aspects of precast members for seismic resistance. These investigations were motivated by

- potential benefits of precast concrete technology,
- absence of code provisions to design reliable precast systems for seismic applications,
- hysteretic energy dissipation requirement in seismic design, and
- poor performance of precast building systems in past earthquakes.

A review of various experimental studies is presented below for both emulative and non-emulative type precast frame systems.

2.3.2 Emulative Connections

2.3.2.1 Ductile-Wet Connections

Research on ductile-wet emulative connections for precast systems suitable for seismic applications has been conducted in New Zealand, the United States, and Canada. As previously noted, this connection type emulates performance of equivalent monolithic systems in terms of strength, stiffness, ductility, story-drift and energy dissipation capacity. Inelastic actions and energy dissipation mechanisms are concentrated within the connections.

Blakeley and Park (New Zealand, 1971) [32]

Four full-scale precast frame subassemblies were tested by Blakeley and Park. The amount of transverse confining steel in the beam-to-column connection region and the location of the plastic hinge were varied between test units. Reinforcement details used in one of the test specimens are shown in Figure 2.7. The columns and beams of the specimens were pretensioned and cement mortar was used at the precast joint interface to ensure continuity between members. The beam in each specimen was post-tensioned with grouted cables through the column into an exterior block. Figure 2.8 shows the cyclic loading history used for testing the specimens.

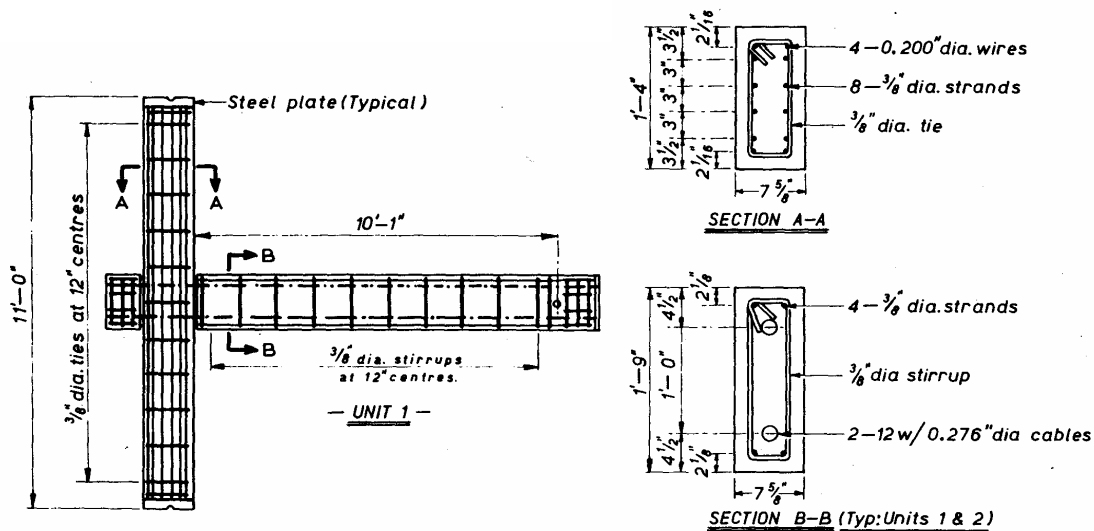


Figure 2.7 Details of Unit 1 [32].

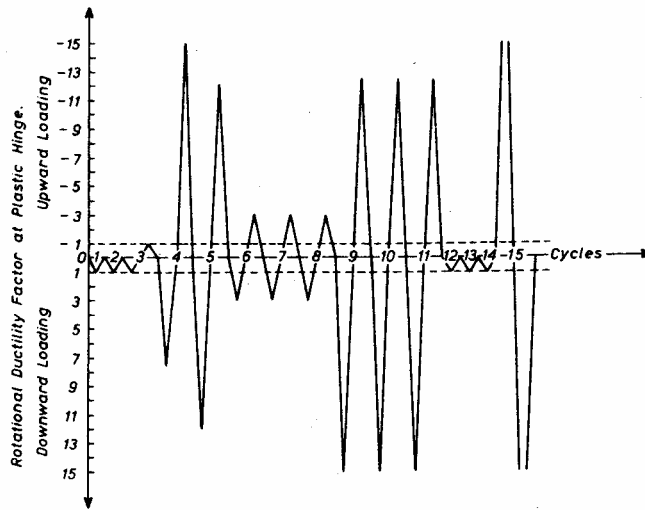


Figure 2.8 Cyclic load sequence used by Blakeley and Park [32].

Variation of curvature along the beam and column, as shown in Figure 2.9 for Unit 1, indicated that this emulative connection enabled the precast frame to experience large post-elastic deformation and to behave similarly to an equivalent monolithic frame. However, as a result of stiffness degradation and bond failure of prestressing ducts in the column at extremely large loading, the connections used between precast members were concluded to be adequate for a moderate level of earthquakes and were expected to cause structural damage in severe earthquakes. The transverse reinforcement in all specimens remained elastic and it was reported that no significant advantage would be gained by increasing this reinforcement content. Further studies were recommended for improving energy dissipating capacity of the precast frames at large displacements.

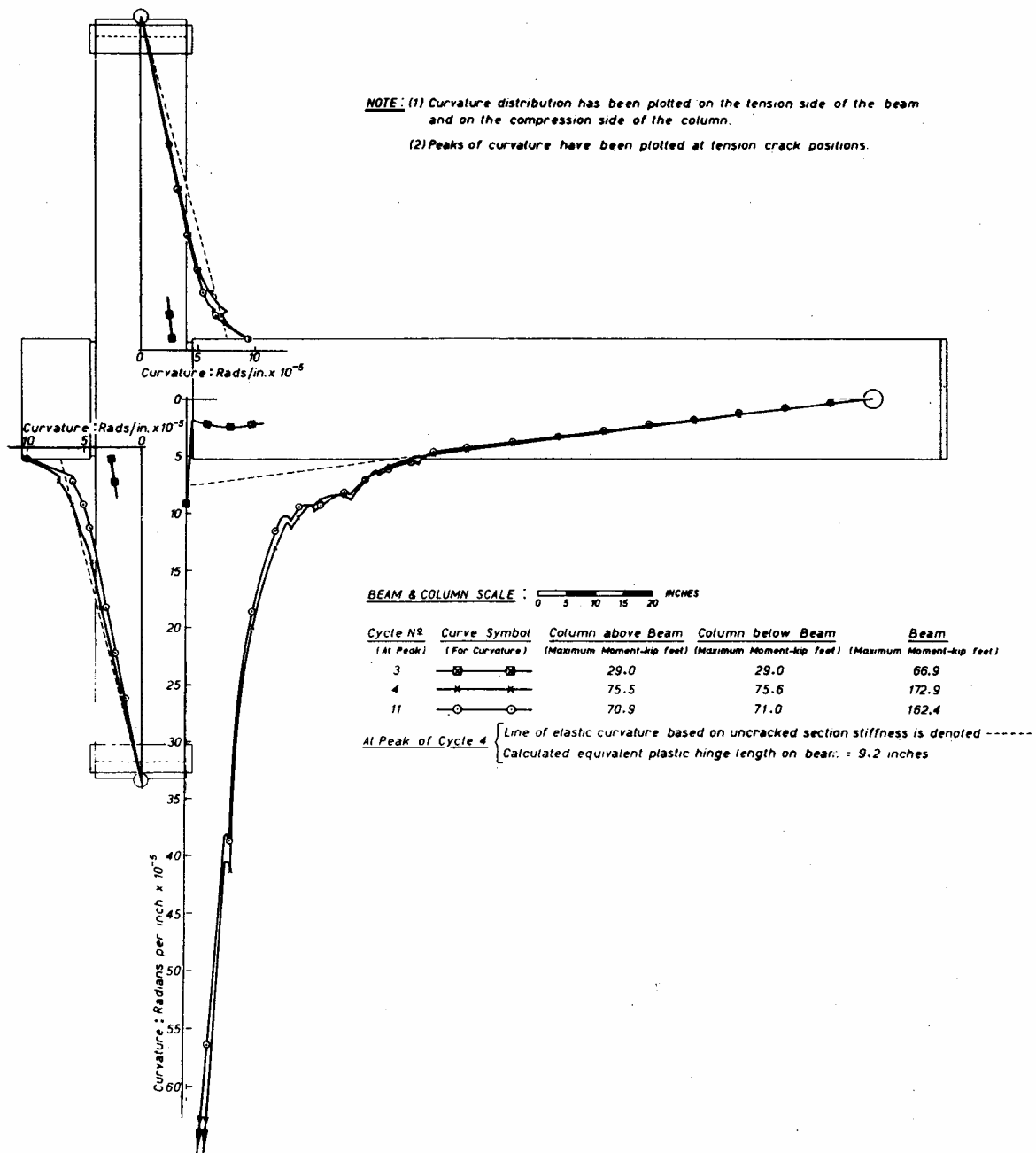


Figure 2.9 Curvature distribution along precast members of Unit 1 [32].

Pillai and Kirk (Canada, 1981) [33]

Nine precast concrete and two monolithic concrete beam-column frames were tested. Typical precast concrete beam-to-column connection details are shown in Figure 2.10. This connection was established by butt welding the top beam longitudinal reinforcement to the top portion of short U-bars anchored into the column and welding both types of bars to a plate embedded near the top of the beam. At the bottom end section of the beam, a steel angle was embedded, to which the bottom reinforcing bars were butt welded.

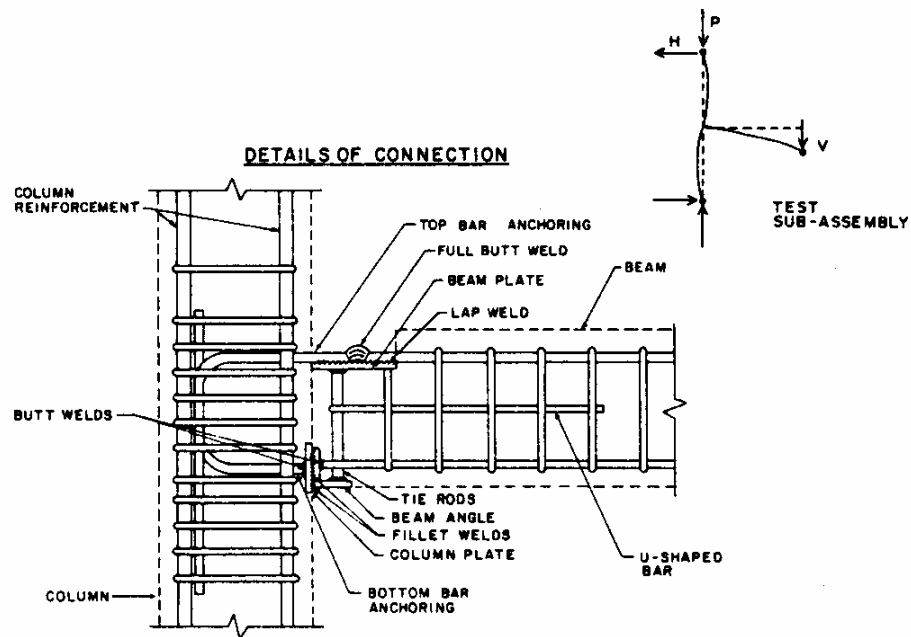


Figure 2.10 Details of a frame connection tested by Pillai and Kirk [33].

Both monolithic and precast beam-column systems were subjected to cyclic loading sequence shown in Figure 2.11a. It was observed that the number of load cycles sustained by the precast systems was equal to or greater than the number of load cycles experienced by the monolithic frame systems. Rotations at the beam ends were measured over a distance of 400

mm as shown in Figure 2.11b, which resulted in rotational ductility values in the range of 5 to 13 for the precast specimens.

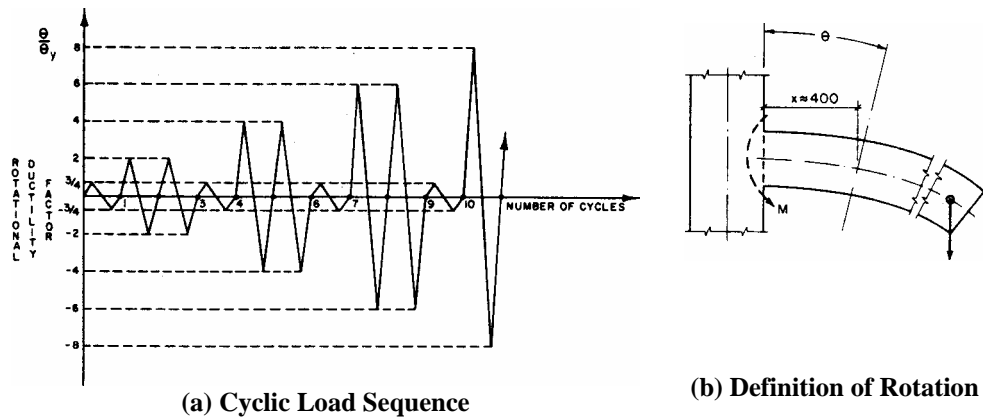


Figure 2.11 Loading Criteria used by Pillai and Kirk [33].

Even though no significant stiffness degradation was observed, the precast frames experienced residual rotations at the end of the lateral load cycles. It was reported that all precast systems had behavior comparable to the monolithic systems in terms of strength, stiffness, energy absorption capacity, and ductility.

French, Hafner, and Jayashankar (USA, 1989) [34]

Seven connection details suitable for precast beam-column frames were tested. These connections utilized

- bonded post-tensioning in one specimen;
- threaded reinforcing bars in three specimens: the first specimen with no couplers, the second specimen with ordinary couplers, and the third specimen with tapered threaded couplers;
- cast-in-place concrete topping with post-tensioning in one specimen;

- cast-in-place concrete topping with bolted details in one specimen; and
- cast-in-place concrete topping with welded details in one specimen.

The first and the last connections were detailed to be strong connections, forcing hinging to develop in precast beams away from the connection interface, while the rest of them were designed as ductile connections. Figure 2.12 shows a longitudinal cross section of the post-tensioned framing concept. All of the specimens were tested under cyclic load history shown in Figure 2.13 by controlling the beam end displacement.

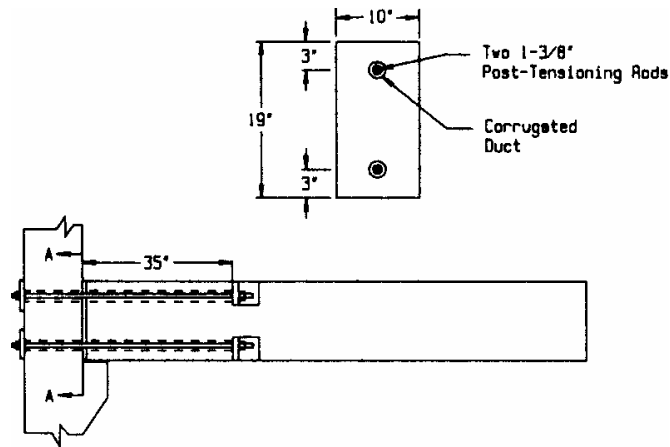


Figure 2.12 Detail of the bonded post-tensioned connection tested by French et al. [34].

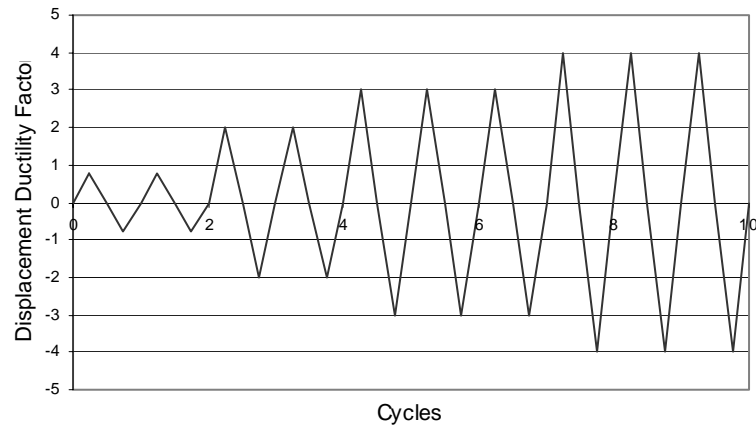


Figure 2.13 Cyclic load history used by French et al. [34]

All the connections performed well providing satisfactory strength, ductility, and energy dissipation, except for specimens with strong connections, which exhibited limited ductile behavior. Overall, the specimen that utilized threaded bars with tapered-threaded splices exhibited the most favorable performance.

Seckin and Fu (Canada, 1990) [35]

Three precast and one monolithic beam-column frames were tested by Seckin and Fu. The connections between the precast beam and column members were made by welding two sets of embedded beam plates to two sets of embedded column plates as shown in Figure 2.14. One set of horizontal plates connected the top and bottom of the beam to the column to provide moment connection, while the other set of plates was used to transfer shearing forces.

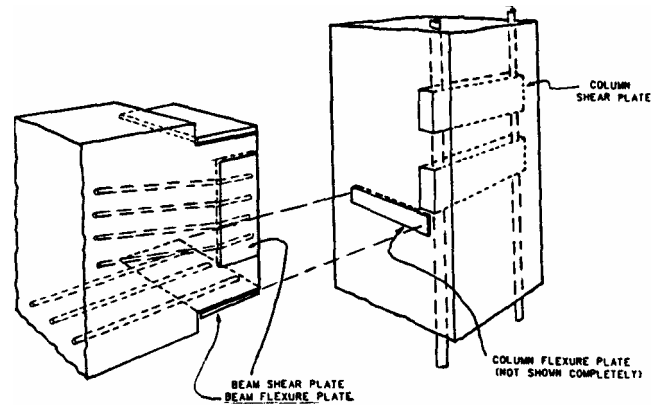


Figure 2.14 Precast framing concept using flexural and shear plates [35].

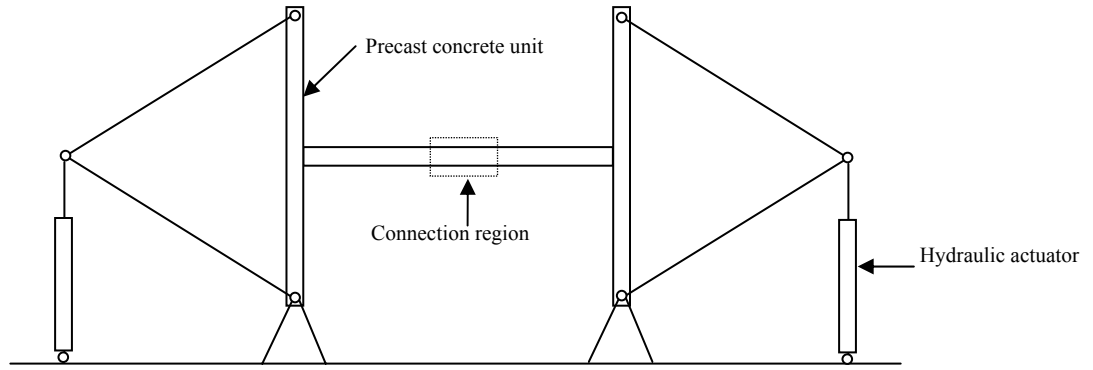
It was reported that the precast beam-column connections with the simple and economic flexural and shear plates performed in a manner comparable to the performance of their monolithic counterpart. However, authors suggested further research prior to formalizing design recommendations for this type of precast frames for seismic applications.

Restrepo, Park and Buchanan (New Zealand, 1995) [36]

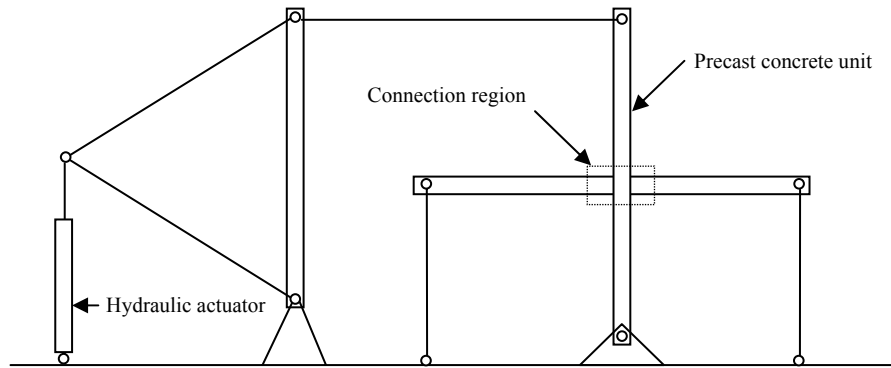
Six subassemblages with different connection details that had been used in precast concrete perimeter frames were tested. These perimeter frames were designed to resist seismic lateral forces in mid-rise buildings. Of the six specimens tested, three were designed with strong-wet connections; details and test results of those specimens are presented in Section 2.3.2.2. Details and tests results of the other three specimens designed with ductile-wet connections, referred to as Units 4, 5 and 6 are presented in this section.

The researchers used two types of configurations for testing of these specimens. Unit 4 used a midspan beam connection between precast frames as shown in Figure 2.15a while Units 5 and 6 utilized beam-to-column connections between precast beams and columns as shown in Figure 2.15b. Reinforcement details of the connection region of Units 4, 5, and 6

are shown in Figures 2.16a, 2.16b, and 2.16c, respectively. The cyclic load sequence applied to the test specimens is depicted in Figure 2.17.

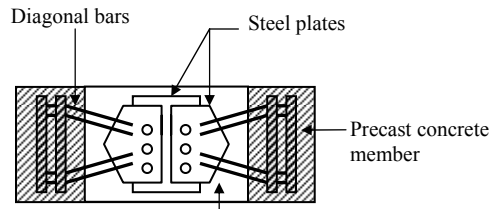


(a) Test unit arrangement for the specimen with a midspan

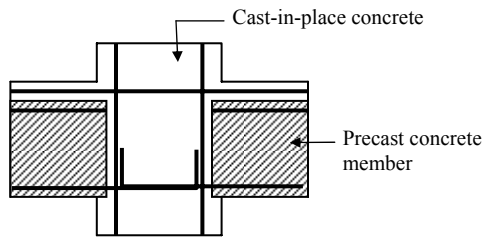


(b) Test unit arrangement for the specimens with a beam-to-column connection

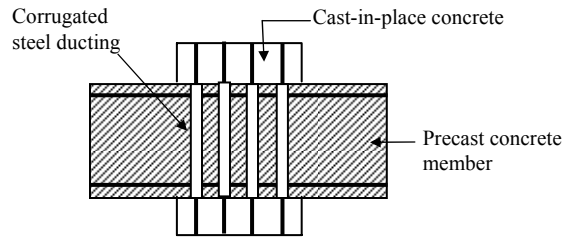
Figure 2.15 Schematic diagrams showing test configurations used by Restrepo et al. [36]



(a) Connection detail of Unit 4



(b) Connection detail of Unit 5



(c) Connection detail of Unit 6

Figure 2.16 Precast frame connection details tested by Restrepo et al. [36].

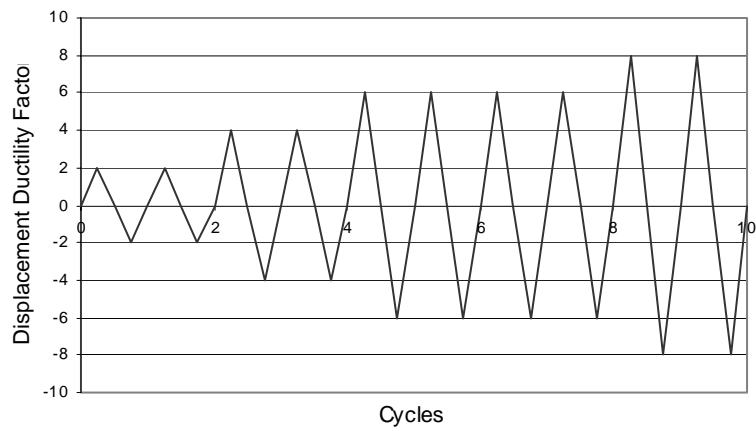


Figure 2.17 Cyclic load sequence used in the tests by Restrepo et al. [36].

The midspan connection used in Unit 4 was made up of diagonal reinforcement bars and bolted steel plates with an intention of accommodating inelastic deformations in the diagonal reinforcement. The beam-to-column connection in Unit 5 was established by anchoring the extended bottom bars from the precast beams into the beam-to-column joint using cast-in-place concrete. Additional top reinforcement bars were provided when placing the cast-in-place concrete topping over the precast beams (see Figure 2.16b). In Unit 6, a continuous precast beam was placed on top of a cast-in-place concrete column, and the column reinforcement bars were extended through the vertical corrugated steel ducts placed in the precast beam (see Figure 2.16c). These ducts were then grouted.

A summary of the test observations is as follows:

- Units 5 and 6 exhibited satisfactory responses up to a displacement ductility factor of at least 6.0 and an inter-story drift of at least 2.4 percent during the tests by resisting at least 80 percent of the measured maximum lateral load.
- In Unit 5, in-situ concrete was suspected to be of poor quality as a result of observing excessive bleeding and plastic settlement for the fresh concrete. Consequently, bond failure occurred to the top beam bars anchored into the cast-in-place beam-to-column joint. Despite the good performance of this unit in terms of displacement ductility, the bond failure of the reinforcement caused larger inter-story drifts than those observed for the other test units.
- Unit 4 exhibited only limited ductile response due to the presence of a three-dimensional stress field between the bend of the diagonal bars and the beam longitudinal reinforcement in the strong regions. Taking this stress field into account,

the unit was repaired with extra transverse ties and short transverse rods, which provided fully ductile performance for Unit 4.

- Performance of the beam-to-column joint region of Unit 6 was satisfactory.
- The New Zealand concrete code requires that the compressive strength of grout in precast connection be larger than the compressive strength of precast concrete elements. In the test units, the grout strength was at least 1.45 ksi greater than the average compressive strength of precast elements, which was found to be satisfactory.

Alcocer, Carranza, Navarrete and Martinez (Mexico, 2002) [37]

Two full-scale subassemblies consisting of precast beams and columns were tested. The framing of these subassemblies was established using a cast-in-place concrete joint core and cast-in-place concrete topping on the beams. The precast column was discontinuous through the joint and was made continuous using cast-in-place concrete in the joint and over a column region above the joint, as shown in Figure 2.18. The cyclic load sequence used for this test series is given in Figure 2.19.

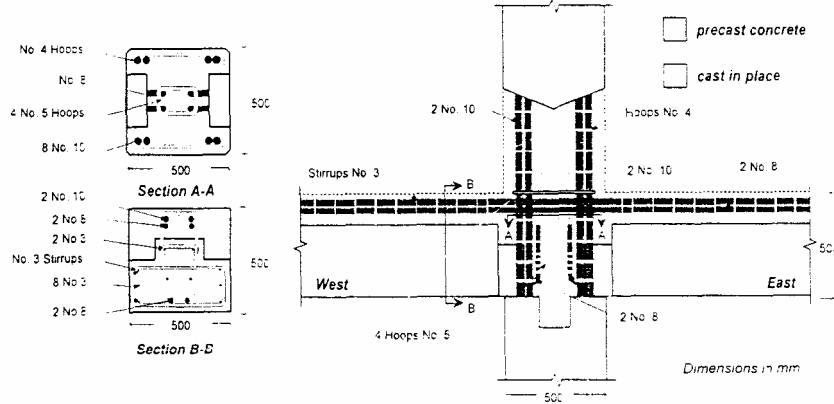


Figure 2.18 Connection details used for precast beam-column frames by Alcocer et al. [37].

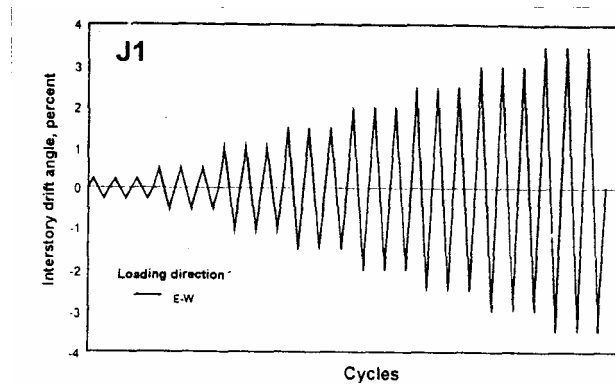


Figure 2.19 Displacement-controlled cyclic load sequence adopted by Alcocer et al. [37]

Both test specimens exhibited ductile behavior with no significant reduction in the lateral load resistance up to an inter-story drift of 3.5 percent. The test specimens also attained shear strength values of at least 80 percent of the expected values from equivalent monolithic systems. It was concluded that, even though the connections did not fully emulate monolithic systems, the tested precast concept would be appropriate for use in seismic regions.

2.3.2.2 Strong-Wet Connections

Limited studies have been conducted on emulative type strong-wet connections. This connection type requires formation of plastic hinges in the precast elements at preselected locations and designing of the connections for overstrength flexural capacities of the plastic hinges [12]. In addition to the test specimens summarized in Section 2.3.2.1, French et al. [38] and Restrepo et al. [36] conducted further experiments on strong-wet connections, which are summarized below.

French, Amu, and Tarzikhham (USA, 1989) [38]

Four different types of specimens were tested:

1. one connection with post-tensioning tendon
2. one connection with threaded bars
3. one composite connection with post-tensioning tendons in the bottom of the beam and a cast-in-place concrete top that included longitudinal mild steel reinforcement
4. one connection with welded plates

The connections and the precast elements were designed to form plastic hinges 35 inches from the beam-column connection interface. The details of the welded plate connection used in a test specimen are shown in Figure 2.20. The cyclic load history used for this series of tests was the same as that shown in Figure 2.13.

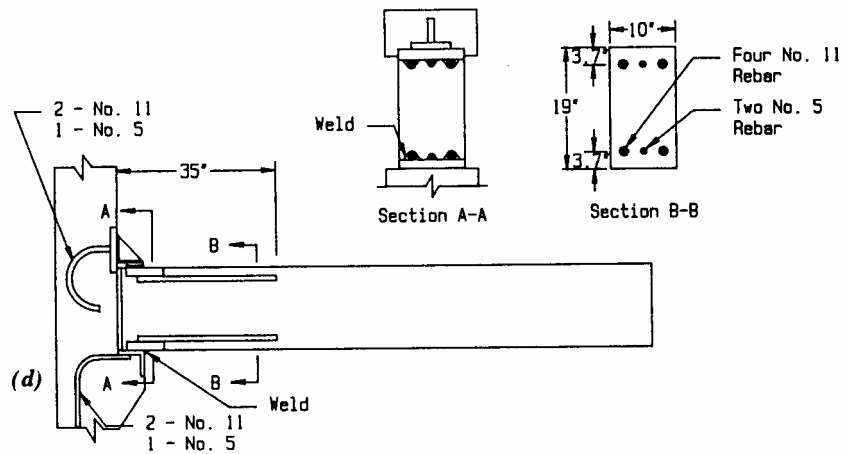


Figure 2.20 Cross-section details of the frame system with a welded plate connection investigated by French et al. [33].

The plastic hinge was concentrated at a single location in the post-tensioned connection whereas hinging was distributed along the beam in other connections. As a result of poor stirrup detail, some deterioration to the plastic hinge region was observed in all specimens except in the specimen with a welded connection. The threaded rebar and composite connections were reported to be the most promising connections, although all frames exhibited good ductility characteristics. The threaded rebar detail was the easiest of the four connections to fabricate. The study concluded that the strong-wet connections evaluated in this study could be designed effectively for adequate strength, ductility, stiffness, and energy dissipation capacity to resist earthquake loading.

Restrepo, Park, and Buchanan (New Zealand, 1995) [36]

As noted in Section 2.3.2.1, Restrepo et al. designed Units 1, 2, and 3 as H-shaped frames having short strong-wet connections at the beam midspan and tested them using the configuration and load sequence shown in Figures 2.15a and Figure 2.17, respectively.

Plastic hinges in these units were designed to develop in the beams at the column faces away from the connections. In each unit, the connection was located at a distance of two times the beam effective depth from the column faces. It was designed by splicing the beam longitudinal reinforcement and filling the connection region with cast-in-place concrete. Details with overlapping 180-degree hooks, double 90-degree hooked drop in bars, and non-contact straight lap splices were used in the connections of Units 1, 2 and 3, respectively.

The outcomes of the experimental study reported by the authors may be summarized as follows:

- The mid-span connections in all three units performed satisfactorily.
- No significant strength degradation was observed for the test units up to displacement ductility factors of at least ± 6 , which corresponded to inter-story drifts of about 2.5 percent. Some pinching in the hysteresis loops was seen at large inter-story drifts, which was attributed to shear deformations in diagonally cracked end regions of the beams as a result of smaller span-to-depth ratio of 3.
- The proximity of the connection to the critical hinge region did not affect the performance of the units.
- The beam longitudinal bars were adequately anchored in the mid-span connections.
- The longitudinal reinforcement splice can be permitted at a distance of the beam effective depth from the column faces.

2.3.2.3 Ductile-Dry Connections

The dry joint concept is intended to exploit intrinsic features of precast concrete technology and promote speedy construction of concrete structures. However, the literature

reviewed as part of the current study indicated that the ductile-dry connection concept has not been explored by researchers. The lack of research in this area may be attributed to the successful introduction of non-emulative systems with ductile-dry joints, which are discussed in Section 2.3.3.

2.3.2.4 Strong-Dry Connections

There are two logical approaches to establish a strong-dry connection based on the definition of this framing concept given in Section 1.2.2. In the first approach, precast beams are connected to brackets located away from the precast column face where plastic hinges are developed, while the interface between the beam and column is designed to be stronger than the precast beam and column members. In the second approach, the precast beams, which are designed to form plastic hinges at selected intermediate locations away from the beam ends, are connected to precast columns such that the moment resistance of the connections is greater than that of the plastic hinges [12]. A summary of experiments that investigated the two possible strong-dry precast connections is presented below.

Ersoy and Tankut (Turkey, 1993) [39]

Five precast frame units simulating two different types of precast connections and two monolithic frame units were tested to qualify the use of dry connections in four-story precast concrete buildings for the FEGA-GAMA construction company. The different types of precast connections investigated by the researchers are shown in Figure 2.21. The Type I connection was used in two specimens while the Type II connection was employed in three specimens.

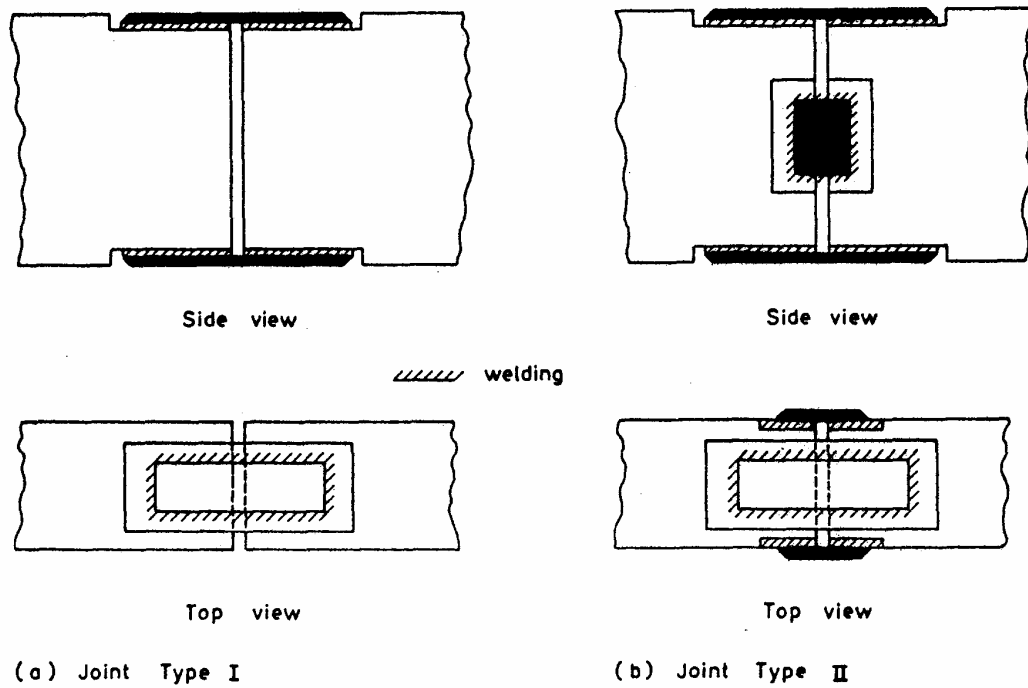


Figure 2.21 Two types of precast connections investigated by Ersoy and Tankut [39].

In both connection types, the precast members were connected at 30 inches away from the column face primarily by two steel plates, one at the top and the other at the bottom of the beam. The use of the site plates and the joint width were the main variables in the tests. Figure 2.22 shows a typical specimen along with the support and loading arrangements, in which the central block represented the column. The cyclic load sequence used in the tests is given in Figure 2.23.

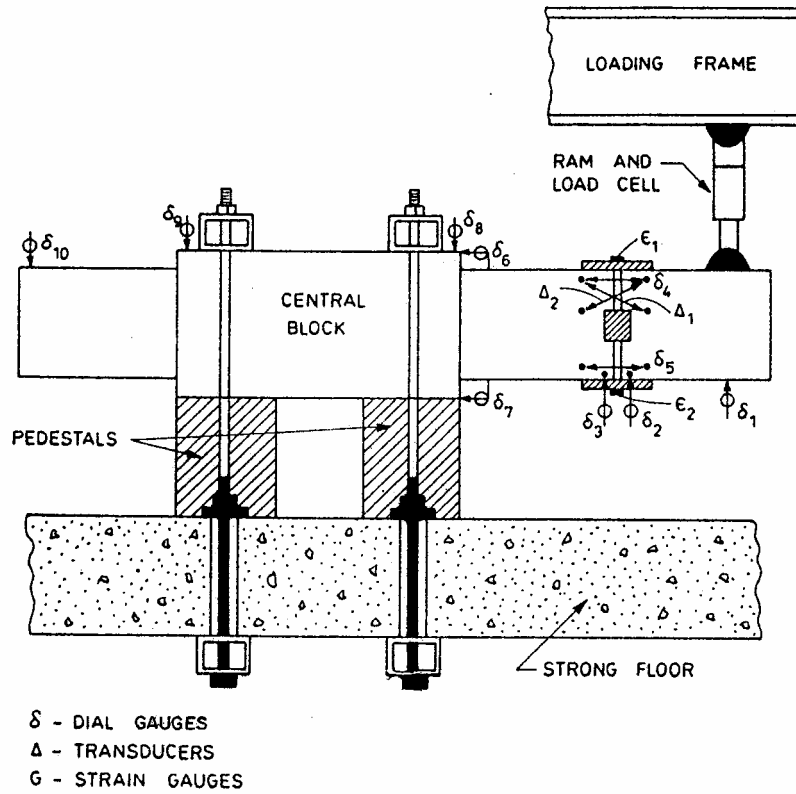


Figure 2.22 The test setup used by Ersoy and Tankut [39].

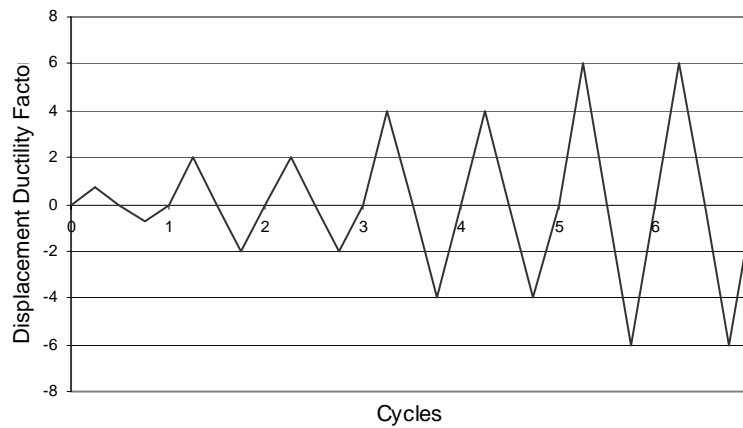


Figure 2.23 The cyclic load sequence used by Ersoy and Tankut [39].

As a result of premature failure observed in the previous tests due to the poor reinforcement detailing at the beam ends, three further specimens (one with Type I and two

with Type II connections) were designed and tested under the same load sequence. During these tests, it was found that the use of the side plates reduced the deformations and increased the load carrying capacity of the connection. The joint width was found to be an important factor when the member was subjected to cyclic loadings and needed careful attention in the design stage. The strength, stiffness and energy dissipating capacity of the dry joints were comparable to those of monolithic connections. The improved design connection details tested in the study were used in several dormitory buildings constructed by the FEGA-GAMA construction company.

Ochs and Ehsani (USA, 1993) [40]

Ochs and Ehsani tested two subassemblages of precast frames with plastic hinges located at the column face, two subassemblages of precast frames with relocated plastic hinges, and one monolithic concrete frame. The relocated plastic hinges were designed to form in the beams at a distance equal to one beam depth away from the column face. The precast connections were made by welding a fabricated steel tee-section embedded in the column to a steel angle embedded in the beam. The welded connection was applied at the top and bottom of the beam as shown in Figure 2.24.

The tests confirmed that the plastic hinges can be successfully relocated with intermediate layers of tension and compression beam longitudinal reinforcement. The connection regions in both precast and monolithic units, which had the same amount of confinement reinforcement, exhibited comparable behaviors in terms of strength and ductility. Therefore, the researchers concluded that the confinement requirement of the monolithic concrete frame is also adequate for use in precast frames.

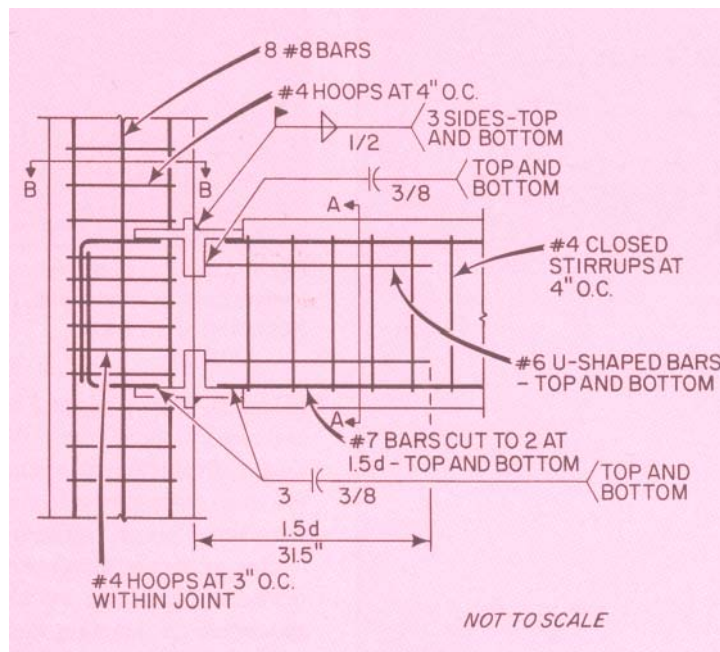


Figure 2.24 Typical connection details adopted by Ochs and Ehsani [40].

2.3.3 Non-Emulative Connections

A non-emulative design approach exploits intrinsic features of the precast, prestressed concrete technology and introduces efficient construction techniques. A ductile link connection for precast frames was investigated by Nakaki et al. [41]. A series of experiments on non-emulative type ductile-dry connections, often referred to as the jointed connections, was conducted by researchers at the National Institute for Standards and Technology (NIST). A review of published information on these investigations is presented below. Several jointed connections were also tested as part of the PREcast Seismic Structural System (PRESSSS) research program. The unbonded post-tensioning frame tests from Phase II of the PRESSSS program is summarized below while information on the connections studied under Phase III are briefly discussed in Section 4.2.1.

Nakaki, Englekirk, and Plaehn (1994) [41]

An embedded ductile link was used to connect precast beams and precast columns by bolting the beams to the column faces. The prime element in this connection is a ductile rod, which was made up of high quality steel with well-defined strength characteristics and high elongation capacity. Components used in the precast connection are shown in Figure 2.25 and a plan view of a frame connection is shown in Figure 2.26.

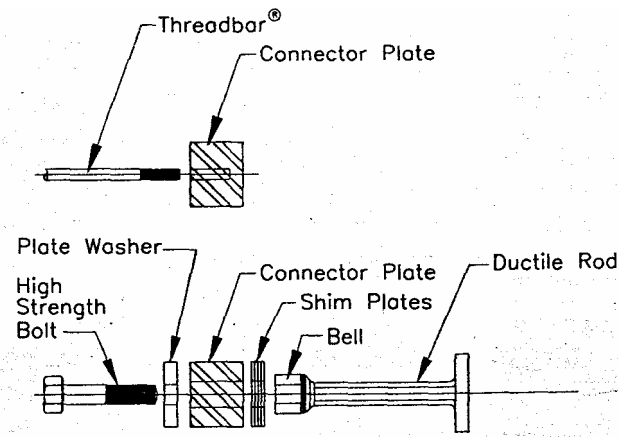


Figure 2.25 Ductile connector components adopted by Nakaki et al. [41].

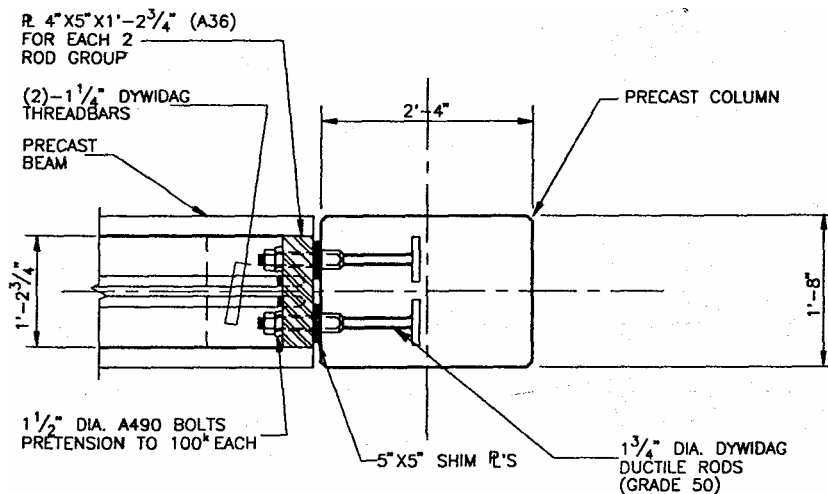


Figure 2.26 Ductile frame connection details adopted by Nakaki et al. [41].

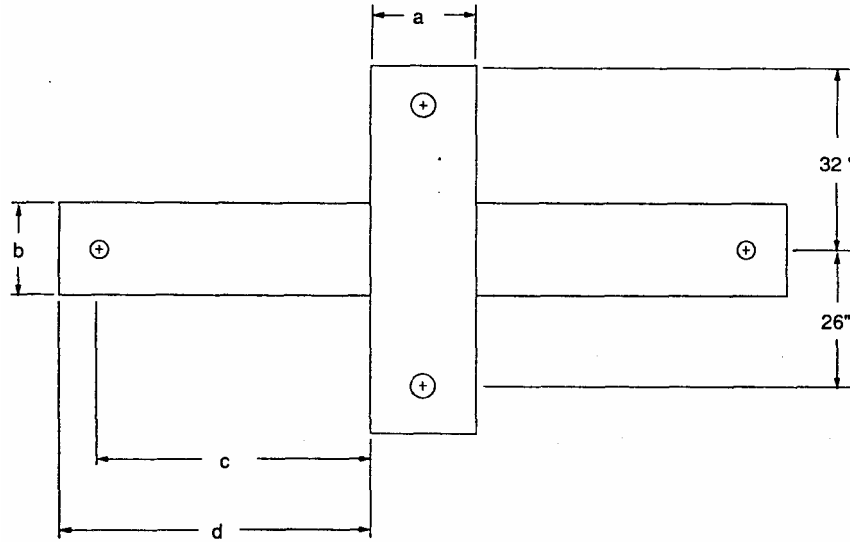
Cyclic load sequence used in the frame test subjected the connection rod to stress reversals, but no horizontal cracks developed in the beam-to-column joint region. A significant number of joint diagonal cracks were visible on the test units, which appeared to be more severe than that expected in equivalent monolithic frames. The researchers concluded that the proposed system utilized the inherent attributes of precast concrete technology to provide a satisfactory framing concept for applications in seismic regions without significantly increasing the erection costs.

Cheok and Lew (NIST, 1991) [42]

An extensive experimental investigation was conducted at NIST on concrete frame sub-assemblages with the objective of developing rational design procedures for precast frame connections for seismic regions. The tests were performed in three phases on one-third scale monolithic and precast beam-column frame connections by subjecting them to cyclic loading. Phase I testing was considered an exploratory stage in which the performance of precast frame connections was compared with that of the monolithic counterparts. Three units of precast frame connections with post-tensioned steel were planned for testing in Phase II. Factors such as hysteretic energy dissipation, strength, and ductility of the precast frame connections were investigated in Phase III, which was intended to be coordinated with the PRESSS program.

Four monolithic and two precast specimens were tested in Phase I of the NIST research program. The monolithic connections were designed in accordance with UBC 1985 [43], with two specimens suitable for Zone 4 and the remaining two specimens representing the design for Zone 2. The precast specimens, which used grouted post-tensioning, were similar

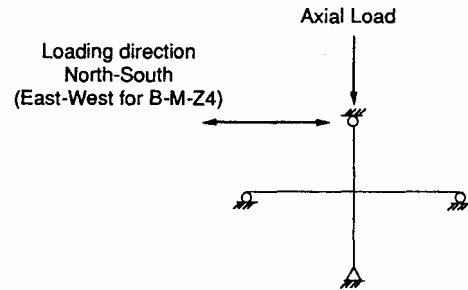
in dimensions to the monolithic specimens designed for Zone 4. The gap between the precast beams and columns were filled with fiber-reinforced grout.



(a) Schematic diagram of a typical specimen

	ZONE 2	ZONE 4	
	A-M-Z2 & B-M-Z2	A-M-Z4 & B-M-Z4	A-P-Z4 & B-P-Z4
a	10"	18"	18"
b	10	16	16
c	40	41-3/4	37
d	46	47-3/4	43

(b) Dimensions of the test Specimens



(c) Support conditions

Figure 2.27 Details of test specimens used in Phase I of the NIST research program [42].

Dimensions and support conditions used for specimens tested in Phase I are shown in Figure 2.27. Each of these specimens was identified by three letters followed by a numeral. The middle letter is either M or P corresponding to monolithic or precast, respectively, and

the last two letters are either Z2 or Z4 representing Zone 2 or Zone 4, respectively. For example, B-M-Z4 indicates a monolithic type B frame designed for Zone 4.

These specimens were subjected to the cyclic load sequence shown in Figure 2.28. The precast specimens generally exhibited behavior equivalent to that of monolithic specimens in terms of strength, ductility, and drift level. However, the energy dissipation capacity of the precast concrete specimens needed improvements. Figure 2.29 shows lateral force-displacement behavior of one set of monolithic and precast specimens designed for Zone 4.

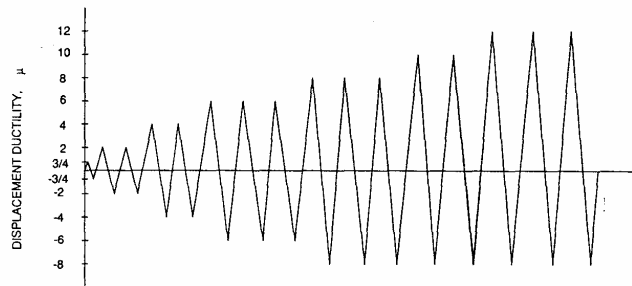


Figure 2.28 Cyclic load sequence used in Phase I of the NIST test program [42].

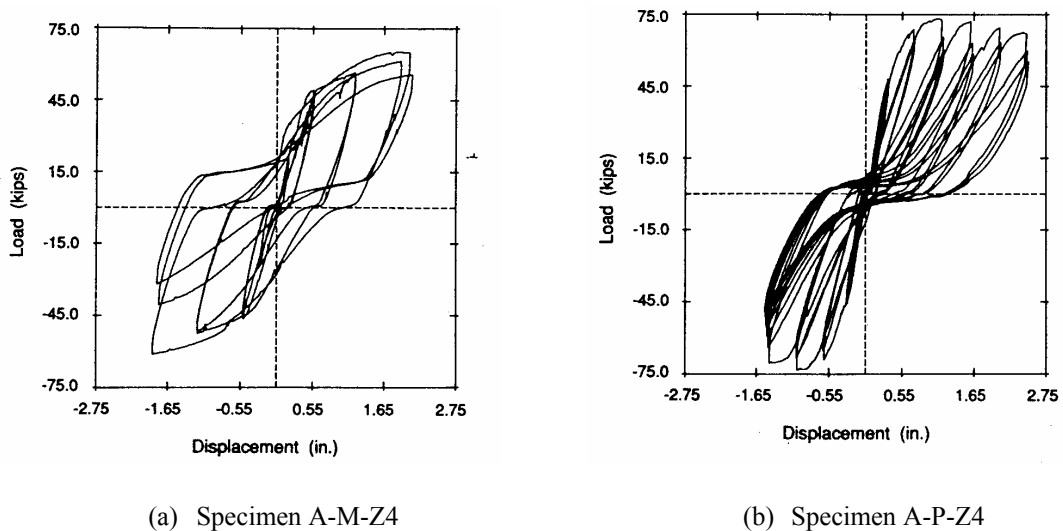


Figure 2.29 Lateral force-displacement hysteresis behavior of two specimens tested in Phase I of the NIST test program [42].

In comparison with the monolithic specimens, the energy dissipated per load cycle by the precast concrete frames designed for Zone 4 was only 30 percent. In order to enhance the energy dissipation capability of the precast frames, positioning the prestress bars closer to the mid-height of the beam and debonding the prestressing strands were suggested for consideration in Phase II and Phase III testing, respectively.

Cheok and Lew (NIST, 1993) [44]

In Phase II of the NIST test program, six precast specimens, two for Zone 2 and four for Zone 4, were designed and tested. In addition to changing the location of the prestressing steel, the effect of using the prestressing strands instead of high strength prestressing bars was investigated in Phase II.

Two specimens with partially debonded prestressing strands were tested in Phase III. The strands were left unbonded in the beam-to-column connection region to avoid zero slopes introduced to the hysteresis loops during load reversals. Precast frame specimens tested in Phases I and II exhibited hysteresis loops with zero slopes (see example in Figure 2.29b). This observation was believed to be mainly due to the development of inelastic strains in the prestressing strands and associated prestress loss. The concept of using partially unbonded post-tensioning steel to improve the behavior of prestressed frames was suggested by Priestley and Tao [45].

The connection strength, and ductility and drift capacities of the precast frame connections tested in Phase III were superior to those tested in Phase II as well as their monolithic counterparts tested in Phase I. Even though the Phase III precast specimens designed for Zone 4 provided accumulated energy dissipation more than that obtained for the

monolithic specimens, the energy dissipated by the precast frames was about 60 percent of the equivalent monolithic frames when energy dissipated within a particular load cycle was examined. It was also reported that the use of the unbonded post-tensioning strands increased the crack opening at the beam-column interface. However, the increased crack opening at the precast interface did not significantly affect the strength of the frame connection.

With respect to a precast frame response with fully bonded strands, the specimens tested in Phase III with partially bonded post-tensioning strands did not result in zero stiffness for the frames during unloading of the lateral load (see an example in Figure 2.30). However, the hysteresis loops obtained for the frames with partially bonded strands were narrower than those produced by specimens having fully bonded prestressing strands. The elastic behavior of the post-tensioning steel limits the energy dissipation of prestressed frames with partially bonded strands. By extending the NIST test program to Phase IV, the researchers examined the possibility of adding mild steel reinforcement as a means of energy dissipating elements in this phase.

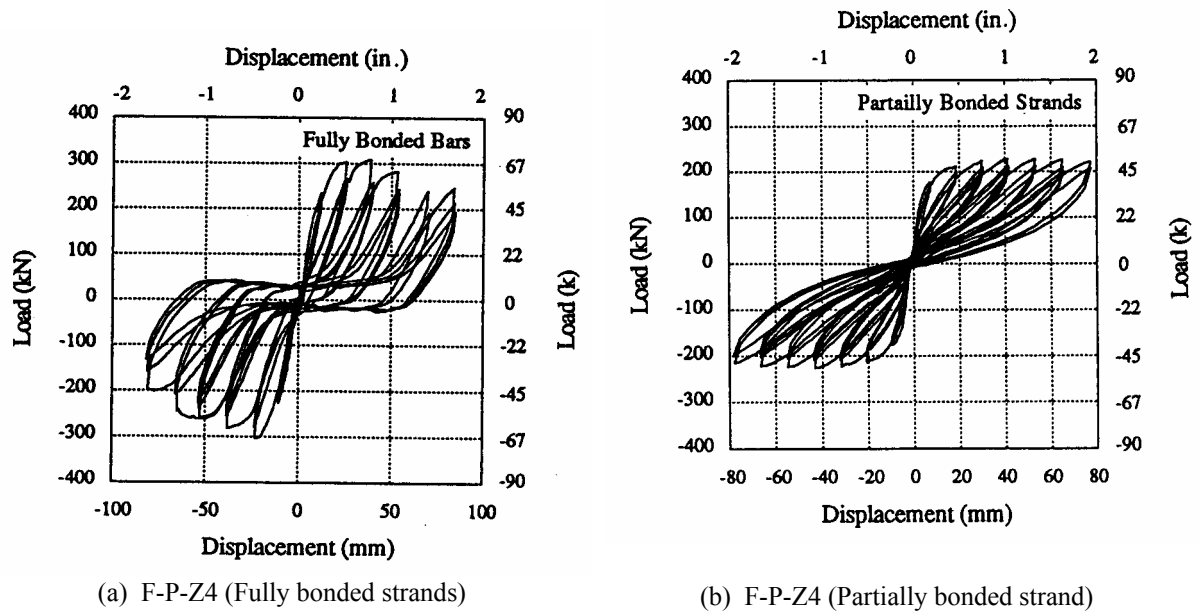


Figure 2.30 Lateral load-displacement behavior of precast frames with connections utilizing fully and partially bonded prestressing strands [44].

Stone, Cheok and Stanton (NIST, 1995) [46, 47]

In Phase IV of the NIST test program, 10 hybrid frame connections consisting of unbonded post-tensioning and mild steel reinforcement were tested in two sub-phases, Phase IV-A and Phase IV-B. Phase IV-A involved cyclic load testing of six specimens with three different connection details. Two frame connections were designed with fully bonded mild steel reinforcement at the top and bottom of the beam and the post-tensioning steel located at the mid-height of the beam. The next frame connection was designed with fully bonded mild steel reinforcement and unbonded post-tensioning steel, both of which were located at the top and bottom of the beam. The remaining three frame connections were designed with unbonded mild steel reinforcement and post-tensioning strands. The variables investigated in

the Phase IV-A tests were the location of the post-tensioning steel, and the amount and type of the energy dissipation steel.

Phase IV-A test results were used as guidance to detail the precast frame connections in Phase IV-B. It was found in Phase IV-A that placing the post-tensioning steel at the mid-height of the beam was appropriate to provide adequate shear resistance at the precast connection interface. It was also found to be appropriate to debond the mild steel reinforcement in the beam over a short distance on either side of the precast column to prevent accumulation of inelastic strains and premature fracture of this reinforcement, which was observed in the Phase IV-A tests.

Four hybrid connections, M-P-Z4 through P-P-Z4, were designed and tested in Phase IV-B. The dimensions and test configuration used for these specimens are shown in Figure 2.31. The specimens were provided with three 0.5-in. diameter Grade 270 prestressing strands at the mid-height of the beams. The strands were stressed to an initial prestress of 118.8 ksi. The main test variables in Phase IV-B were the amount and type of the passive steel reinforcement at the precast frame connection. Two No. 3 and three No. 3 mild steel reinforcing bars at the top and bottom of the beam were used in Specimens M-P-Z4 and O-P-Z4, respectively. Two 0.31-inch and three 0.31-inch diameter stainless steel bars at the top and bottom of the beam were used in Specimens N-P-Z4 and P-P-Z4, respectively. All reinforcing bars placed at the top and bottom of the beam were debonded over an inch length on either side of the column, except in P-P-Z4. Fully bonded reinforcement was provided in P-P-Z4 to avoid the bond failure of the stainless steel bars observed during the test of Specimen N-P-Z4.

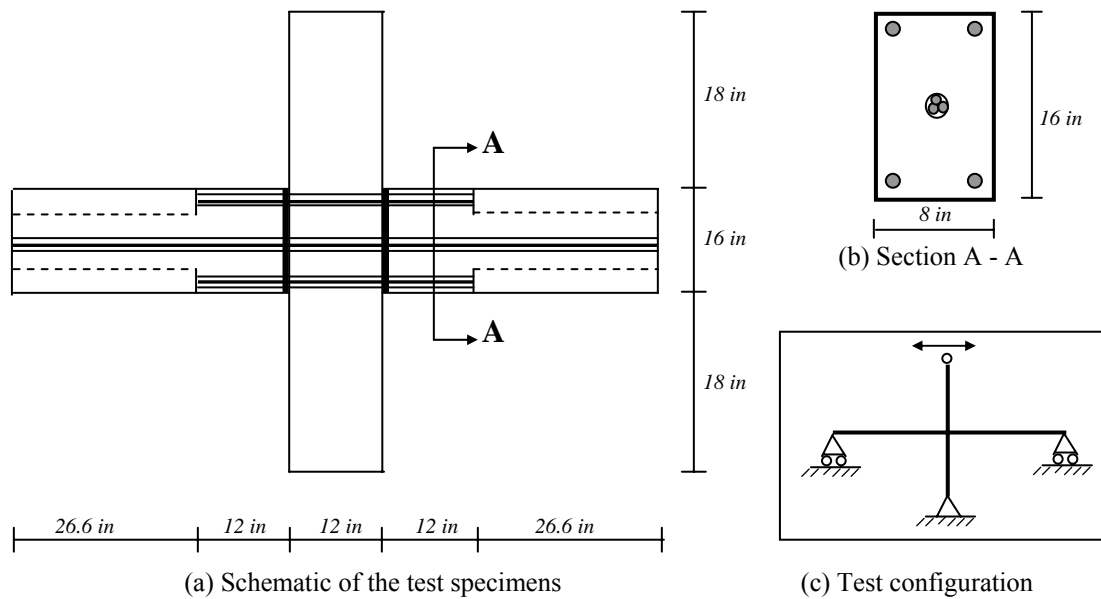


Figure 2.31 Precast frame subassembly with the hybrid connection tested in Phase IV-B by Stone et al. [46].

The lateral load vs. story drift hysteresis responses obtained for two hybrid precast frames (M-P-Z4 and O-P-Z4) are shown in Figure 2.32. Fracture of the mild steel bars at a column drift greater than 3.5 percent initiated the failure of both of these specimens. As noted above, bond failure of the stainless bars resulted in premature failure of N-P-Z4. For PPZ4, bond failure of stainless steel bars was avoided and satisfactory response was obtained up to 3 percent lateral drift. When PPZ4 was retested simulating load due to an after-shock stainless steel bars fractured at 2.9 percent drift.

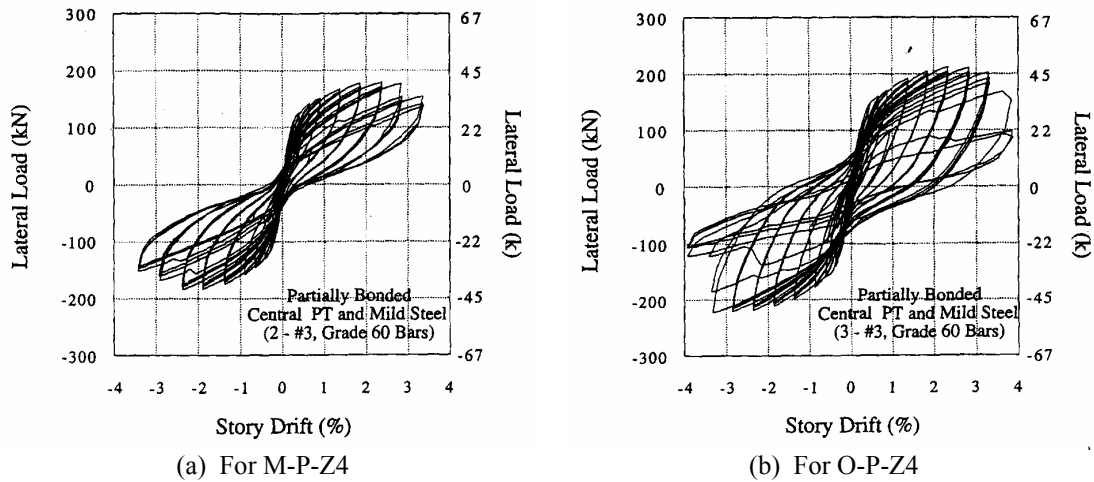


Figure 2.32 Hysteresis responses obtained for two hybrid frame subassemblages tested by Stone et al. [46].

The post-tensioning steel remained elastic throughout the test in all specimens with the average peak stress recorded in the post-tensioning steel during testing being less than 90 percent of the ultimate strength. The loss in the initial prestressing force that was encountered during testing was reported to be negligible.

The followings conclusions were drawn from the test observations:

- No significant strength degradation was observed for the test specimens prior to fracturing of the passive steel reinforcing bars.
- The hybrid frame has a very large drift capacity. At drift levels of ± 6 percent, it was found that the precast frames provided 55 percent of the maximum lateral resistance.
- Up to 1.5 percent story drifts, hybrid frames dissipated more energy per load cycle than the equivalent monolithic systems. At larger drifts, the energy dissipated by the hybrid frames was 75 percent of the energy dissipated by the equivalent monolithic frames.

- The level of damage in hybrid frames was negligible when compared to that observed for the equivalent monolithic frames. Furthermore, the hybrid frame exhibited re-centering capability when the lateral load was removed.
- The transverse reinforcement in the beams and columns remained elastic. No shear cracks were visible on the precast beams after removal of the lateral load. In contrast, shear cracks were observed in the beams of the equivalent monolithic frames at the end of the test.

Priestley and MacRae (UCSD, 1996) [48]

Modeling an exterior and an interior building frame, two precast beam-column connection subassemblages with partially bonded prestressing tendons were tested. The subassemblages were designed based on the results obtained from theoretical analysis of this framing concept by Priestley and Tao [45].

Details of the specimen modeling the interior frame connection are shown in Figure 2.33. Prestressing tendons, which were placed at $0.25h_b$ and $0.75h_b$ distance from the beam top surface, where h_b is the beam depth, were unbonded in the beam-to-column connection region to prevent development of inelastic strains in the tendon and the corresponding loss of prestress when the frame was subjected to lateral loads. The precast frame specimens were tested under cyclic loading using the load history shown in Figure 2.34.

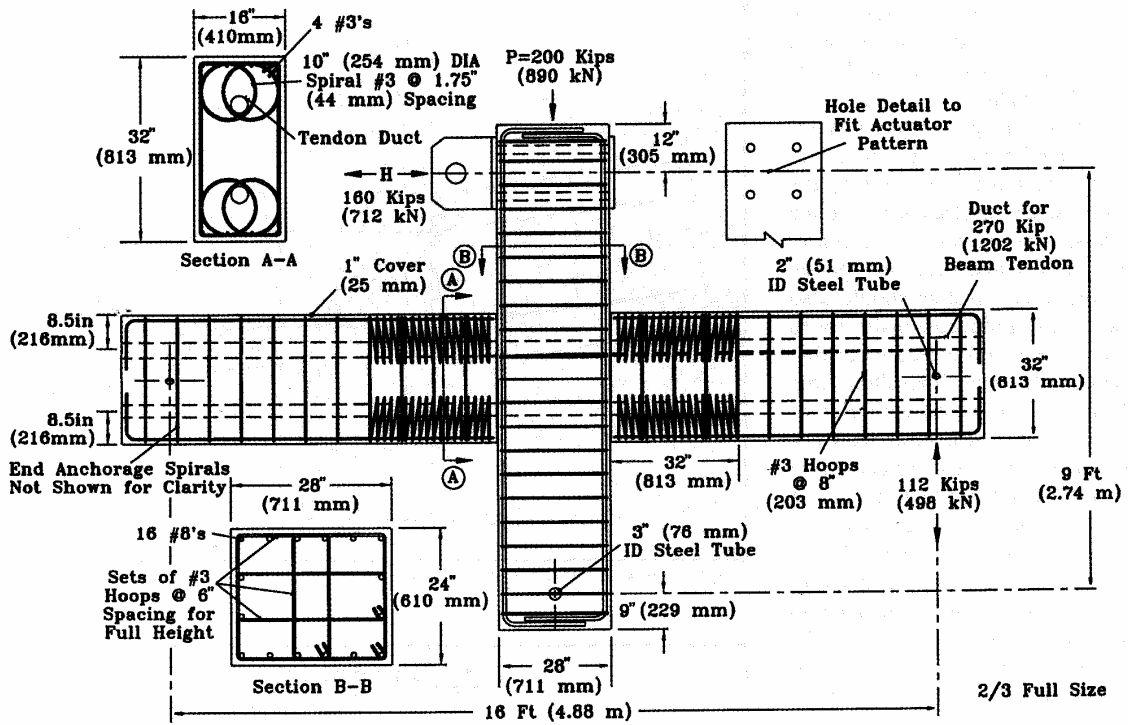


Figure 2.33 Subassembly of the interior precast frame connection tested by Priestley and MacRae [48].

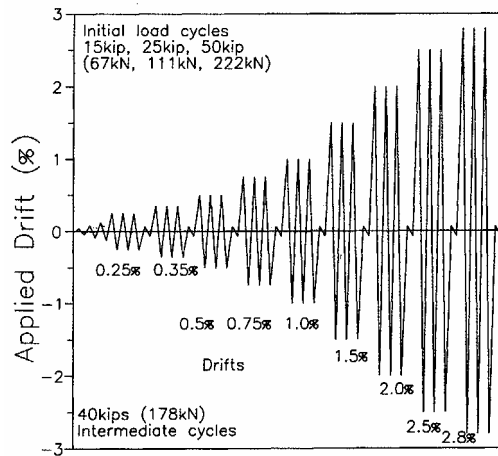


Figure 2.34 The cyclic loading history used by Priestley and MacRae [48].

The precast frame system with partially bonded prestressing exhibited inter-story drifts of 2.8 percent and 4.0 percent for the interior and exterior connections, respectively, without significant strength degradation. Compared to the equivalent monolithic frame systems, neither significant damage to the beam ends nor residual drifts were observed for the precast frames. Due to the elastic behavior of the tendons, the precast frames exhibited very low hysteretic energy dissipation, which can be seen in Figure 2.35. Additional research was recommended for the optimum design of the precast frame connections with partially bonded tendons.

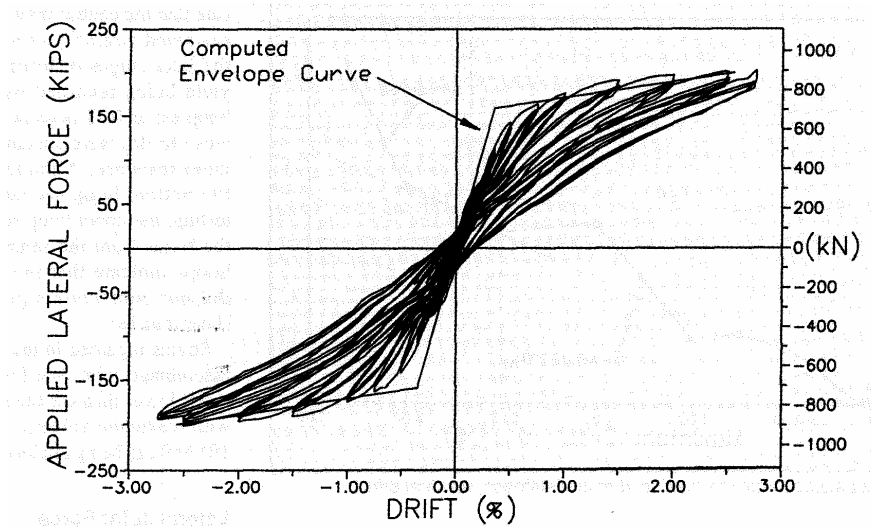


Figure 2.35 Lateral force-drift behavior observed for the interior precast frame connection by Priestley and MacRae [48].

2.4 Analytical Studies of Hybrid Frame Connections

2.4.1 Introduction

As indicated in Section 1.3.1, examining seismic behavior of hybrid frame buildings using conventional frame analysis methods requires development of a relationship between

moment resistance and rotation at the connection interface. Although such a relationship can be readily established for monolithic frame systems, strain incompatibility that exists between the concrete and unbonded mild steel and prestressing reinforcement makes the connection level analysis complicated for precast hybrid frames. Analytical investigations, which have attempted to characterize the behavior of non-emulative precast frame systems, have been limited and a summary of available literature is provided in the following sections.

2.4.2 Englekirk (1989) [49]

In order to assess performance of precast concrete ductile earthquake resistant frames, the concept of ductility was used by Englekirk. The component ductility and system ductility concepts were introduced to evaluate displacements associated with the ultimate load or the ultimate strain for individual members and beam-column subassemblages, respectively. For the cantilever beam shown in Figure 2.36, the ultimate displacement was given by:

$$\Delta_u = [1 - l_p / 2] l_p \Phi_u + \Delta_y \quad (2.1)$$

where, l is the length of the beam, l_p is the plastic hinge length, Φ_u is the plastic curvature, and Δ_y is the beam end displacement at yielding.

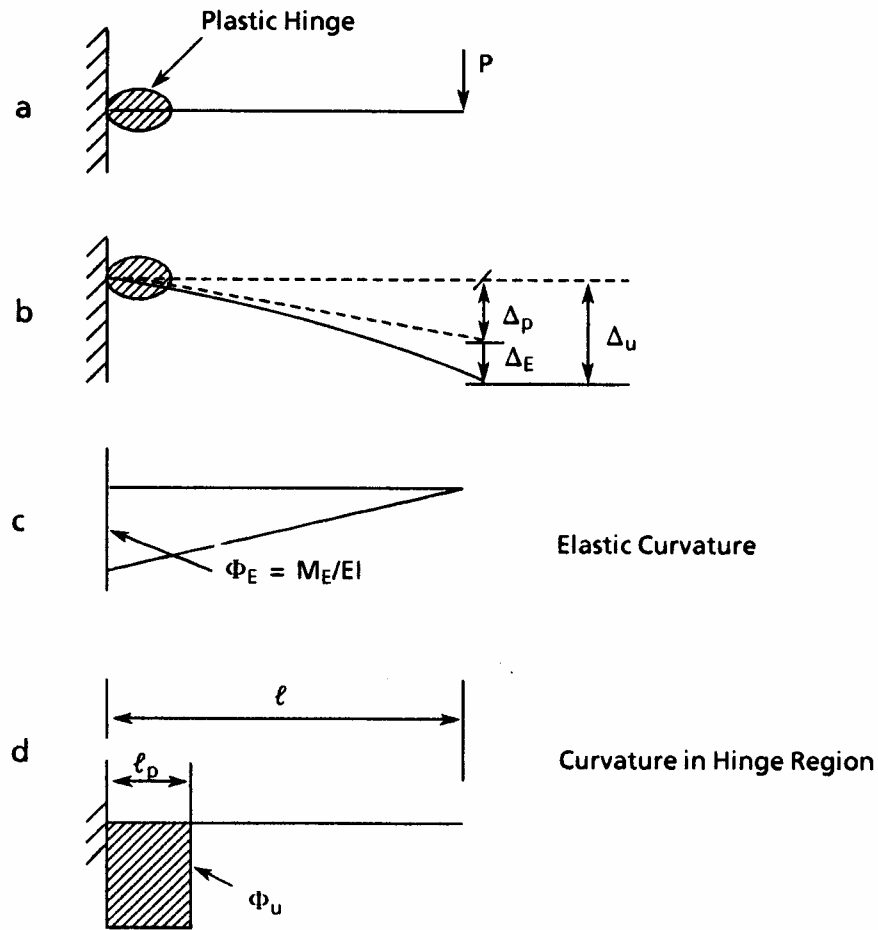


Figure 2.36 Curvature and displacement distribution for a cantilever beam [49].

The system ductility concept determines the ultimate displacement of a subassembly from three components, two of which are shown in Figure 2.37. These components include the column flexure, beam flexure, and plastic rotation of the beam at the precast connection. Using the parameters shown in Figure 2.36, the displacement components corresponding to the ultimate displacement can be expressed as follows:

Due to column flexure,
$$\delta_c = \frac{2}{3} \frac{M_p}{h} \left(\frac{1}{l_b} \right) \frac{l_c^3}{EI} \quad (2.2)$$

$$\text{Due to beam flexure, } \delta_c = \frac{2 M_p l_b^2 h}{3 EI} \quad (2.3)$$

Due to plastic rotation at the beam-to-column connection,

$$\delta_p = l_p \Phi_u \left(l_b - \frac{l_p}{2} \right) \frac{2h}{l} \quad (2.4)$$

$$\text{Therefore, the total column end ultimate displacement, } \Delta_u = \delta_c + \delta_b + \delta_p \quad (2.5)$$

Where M_p is the plastic moment, I is the moment of inertia of the beam and E is the elastic modulus of concrete (see Figure 2.37 for definition of other variables.)

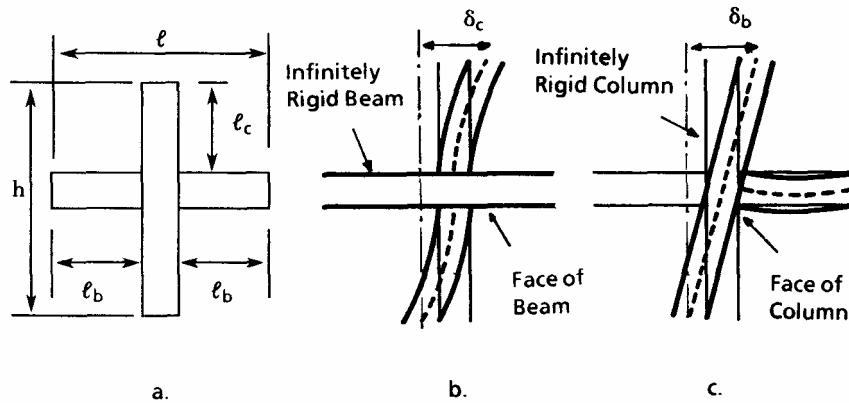


Figure 2.37 Displacement components for a beam-column subassembly [49].

The proposed analysis method is applicable to precast systems at the member and structure levels for approximate analyses. However, this analysis method was not meant for section level analysis to quantify strains at the beam-to-column precast connection interface.

2.4.3 Priestley and Tao (1993) [45]

An analysis technique was investigated for precast beam-column subassemblages with connections using partially debonded prestressing tendons and no mild steel reinforcement.

The tendons in the frames were assumed to remain elastic to avoid the loss of prestressing during seismic response as discussed in Section 2.3.3.

The authors proposed a tri-linear force-displacement idealization for precast frame subassemblages using three control points, as shown in Figure 2.38. Point 1 is called the decompression point. It corresponds to the condition at which the precompression stress in the extreme tension fiber in the beam reaches zero and a flexural crack is assumed to develop at the precast connection interface.

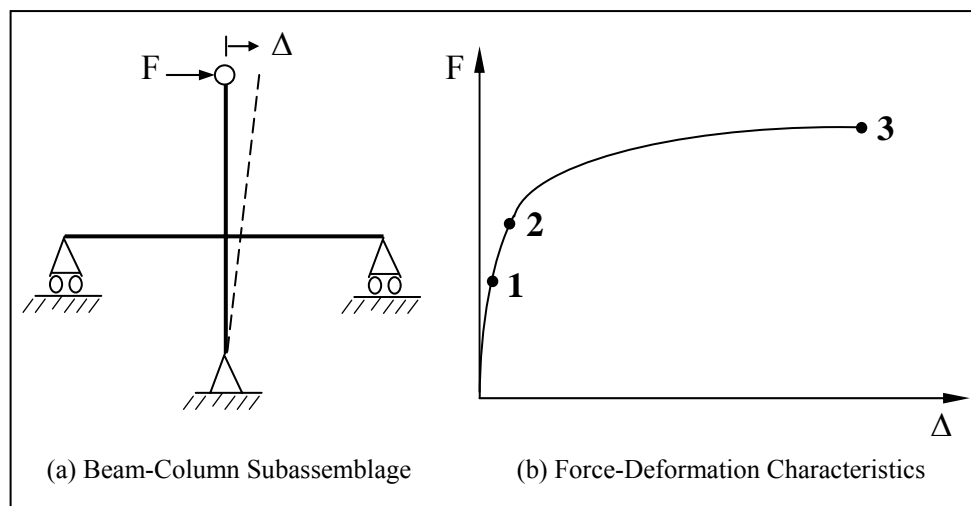


Figure 2.38 Force-deformation response idealization suggested for a beam-column frame subassembly by Priestley and Tao [45].

At Point 2, it is assumed that the interface crack has propagated from the extreme tension fiber to the centroidal axis of the beam section. Point 3 corresponds to the limit of proportionality on the stress-strain curve of the prestressing steel. At this stage, it is assumed that the concrete strain reaches the ultimate value. Furthermore, the authors suggested that the response of the precast frame in Figure 2.38b may be conservatively approximated by

linear curves between Points 1 and 2 and between Points 2 and 3, with Point 2 representing the equivalent yield condition. Note that the linear behavior assumption is also valid up to Point 1.

The moment resistance corresponding to Point 1 and Point 2 are evaluated using linear compressive stress distributions and predetermined neutral axis depths at the connection interface. The moment resistance corresponding to Point 3 is determined using the concept of equivalent rectangular compression stress block without considering the confinement effects. As a result, the section level analysis at Point 3 is not sensitive to the strains at the critical section.

The authors performed a series of dynamic inelastic analyses on single-degree-of-freedom-systems, which represented precast frame and other systems. Linear elastic, bi-linear elastic, bi-linear elasto-plastic and bi-linear degrading force-deformation characteristics were used to describe the behavior of the different frame systems. Several earthquake accelerograms were used in this analytical study, which showed that partially debonded tendons in precast frames can maintain prestressing even after subjected to large lateral displacements and provide improved shear performance and reduced residual displacements for the frames. The dynamic analyses also indicated that the precast frame systems with partially debonded tendons would experience lower ductility demand than comparable frames with fully bonded prestressing tendons. However, the need for an experimental study to confirm the observed analytical behavior was emphasized.

2.4.4 Cheok, Stone and Nakaki (NIST, 1996) [13]

The guidelines given by the authors for designing hybrid frame connections may be used for analyzing the connection behavior at two different states. The first state, which defines the nominal moment capacity, assumes that the strain in the mild steel tension reinforcement is equal to the strain at the onset of hardening. The second state determines the probable moment capacity assuming that the tensile steel has reached its ultimate strength.

To determine both moment capacities, an iterative procedure is used, in which the neutral axis depth is determined using the force equilibrium condition at the connection interface. In this procedure, the following assumptions are made:

- The Whitney equivalent rectangular compression stress block may be used to satisfactorily represent the concrete compression stress distribution.
- The contribution of the compression steel reinforcement may be neglected.
- For the state defining the probable moment capacity, the growth in the unbonded length of the mild steel reinforcing bar due to experiencing cyclic strains is taken as $5.5 d_b$, where d_b is the diameter of the mild steel reinforcing bar.

The different steps involved in the calculation of the two moment capacities are described below:

(a) Nominal Moment Capacity (M_n)

Assume, $\epsilon_s = \epsilon_{sh}$ (2.6)

where ϵ_{sh} is the strain at the onset of hardening.

Therefore, the stress in the tension reinforcing bars is

$$f_s = f_y \quad (2.7)$$

where f_y is the yield strength of the tension reinforcement.

As shown in Figure 2.39, the elongation in the tension reinforcement is given by:

$$\Delta_s = \epsilon_s L_u \quad (2.8)$$

where L_u is the unbonded length of the mild steel reinforcement. The growth in the unbonded length of the mild steel reinforcement is assumed to be zero because the reinforcement has not experienced significant inelastic strains at this state.

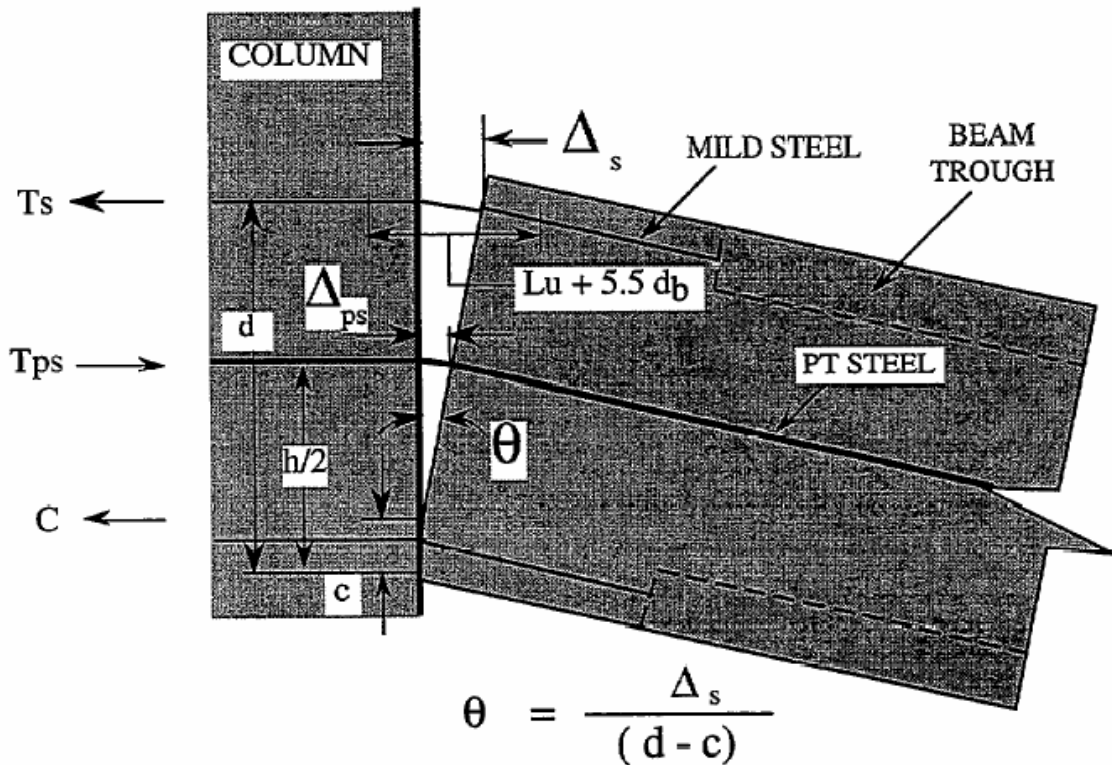


Figure 2.39 Forces and displacements at the hybrid connection interface [13].

Assuming a neutral axis depth, c , the elongation of the tendon, as shown in Figure 2.39, can be expressed as:

$$\Delta_{ps} = \left[\frac{h/2 - c}{d - c} \right] \Delta_s \quad (2.9)$$

where h is the beam height and d is the distance from the extreme compression fiber to the mild steel tension reinforcing bar. For an unbonded length of L_{ups} and an initial prestressing of ϵ_{si} , the strain in the prestressing tendon corresponding to the nominal moment capacity is given by:

$$\epsilon_{ps} = \left[\frac{\Delta_{ps}}{L_{ups}} \right] + \epsilon_{si} \quad (2.10)$$

Using Mattock's stress-strain model suggested for Grade 270 strands [19], the corresponding stress in the tendon can be determined from Equation 2.11:

$$f_{ps} = \epsilon_{ps} E_{ps} \left[0.02 + \frac{0.98}{\left[1 + \left[\epsilon_{ps} E_{ps} / 1.04 f_{psy} \right]^{3.36} \right]^{0.1196}} \right] \quad (2.11)$$

where E_{ps} and f_{psy} are, respectively, Young's modulus and yield strength of the prestressing strands.

With an area of A_{ps} for the prestressing steel, the force in the prestressing tendon is

$$T_{ps} = A_{ps} f_{ps} \quad (2.12)$$

The tension force in the mild steel reinforcement is given by

$$T_s = A_s f_s \quad (2.13)$$

where A_s is the area of the mild steel reinforcement. Using the equilibrium condition, the concrete compression force, C , at the connection interface is the summation of the two tensile forces. Hence,

$$C = T_s + T_{ps} \quad (2.14)$$

Using the equivalent rectangular compression stress block concept, the neutral axis depth required to satisfy the equilibrium condition of Eq. 2.14 is determined from Equation 2.15.

$$c = \frac{C}{0.85f'_c b \beta_1} \quad (2.15)$$

where f'_c is the unconfined concrete compressive strength, b is the beam width and β_1 is the ratio of the equivalent stress block depth to the neutral axis depth.

The procedure described above is repeated until the assumed neutral axis depth, c , converges to the calculated value in Equation 2.15. Once the neutral axis depth is determined, forces in the mild steel reinforcement and post-tensioning tendons are known, and thus the nominal moment is obtained from the following expression:

$$M = T_{ps} \left[\frac{h}{2} - \frac{\beta_1 c}{2} \right] + T_s \left[d - \frac{\beta_1 c}{2} \right] \quad (2.16)$$

The connection interface rotation corresponding to the nominal moment capacity is given by

$$\theta = \frac{\Delta_s}{d - c} \quad (2.17)$$

(b) Probable Moment Capacity (M_p)

Assume $\varepsilon_s = \varepsilon_u$ (2.18)

where ε_u is the strain corresponding to the ultimate strength, f_u , of the mild steel reinforcement. Therefore,

$$f_s = f_u \quad (2.19)$$

Using the assumed growth of $5.5 d_b$ in the debonded length, the elongation of the mild steel tension reinforcement at the connection interface is found from

$$\Delta_s = \epsilon_s [L_u + 5.5d_b] \quad (2.20)$$

Assuming a neutral axis depth, c , Equations 2.9–2.17 are used to determine the probable moment capacity and the corresponding interface rotation of the hybrid frame connection.

2.4.5 Pampanin, Priestley and Sritharan (2001) [18]

The authors proposed an analysis method to predict continuous moment-rotation envelopes for jointed precast frame systems under monotonic loading. This method, which uses an analogy between a jointed connection and an equivalent monolithic concrete connection, makes the section level analysis possible for jointed systems by assuming identical global displacements for members that are connected with both the jointed and monolithic connections, as illustrated in Figure 2.40. This concept, referred to it by the authors as the monolithic beam analogy, enables relationships between neutral axis depth, concrete strain, and steel strains to be established at the jointed connection interface. Establishing these relationships is not possible through conventional means due to the strain compatibility that exists due to the use of debonded reinforcing bars and/or unbonded prestressing tendons to establish jointed connections.

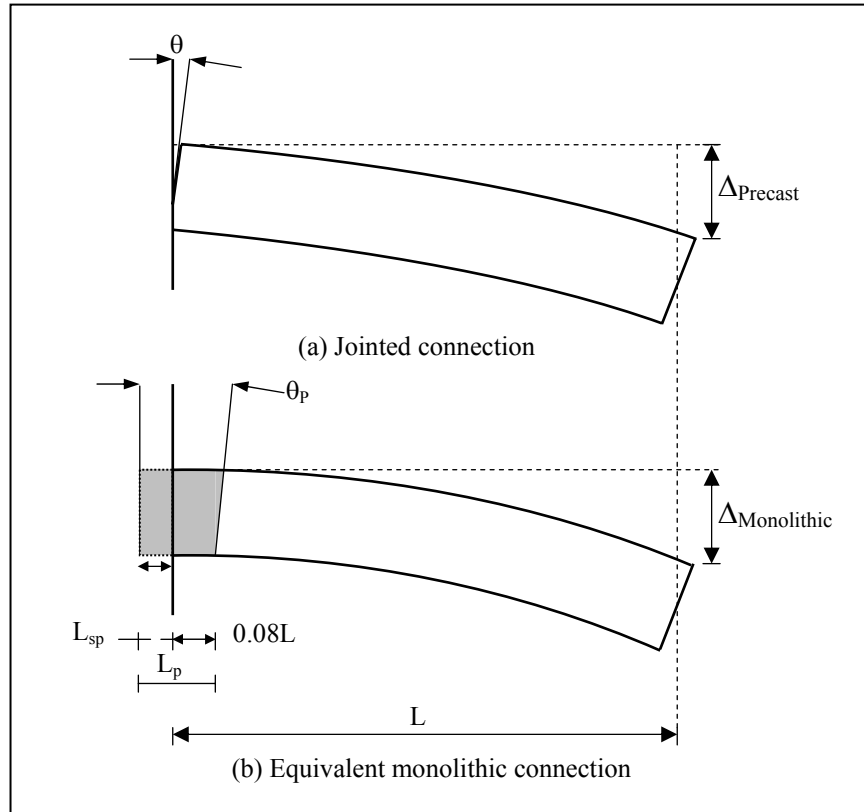


Figure 2.40 The equivalent monolithic beam analogy concept [18].

2.4.5.1 Concrete Strain

As shown in Figure 2.40, the monolithic beam analogy assumes equal displacements at the member ends. Hence,

$$\Delta_{\text{Precast}} = \Delta_{\text{Monolithic}} \quad (2.21)$$

In jointed frame systems, the precast beams are designed to behave elastically, while the beam rotations are concentrated at the connection interfaces, which result in gaps opening at the interfaces rather than distributed cracks along the beams. The displacement due to elastic curvature along the precast beam, Δ_e , and the displacement due to the concentrated rotation at

the connection interface, Δ_θ , in Figure 2.40a are the components of the total displacement at the precast beam end. Therefore,

$$\Delta_{\text{Precast}} = \Delta_e + \Delta_\theta, \text{ and} \quad (2.22)$$

$$\Delta_\theta = L\theta \quad (2.23)$$

where L is the length of the beam or the distance between the connection interface and the contra-flexure point in a beam that is part of a frame, and θ represents the elastic and inelastic components of the concentrated rotation that occurs at the connection interface.

The equivalent monolithic beam exhibits plastic behavior in the critical moment region adjacent to the beam-column interface as well as due to strain penetration in the reinforcing bars anchored into the beam-to-column joint. The shaded area in Figure 2.40b represents the idealized region over which the plastic behavior is assumed to take place. In addition, the elastic behavior along the beam and the corresponding strain penetration term should be included in the calculation of the beam end displacement. These elastic and plastic components that constitute the total member end displacement in the equivalent monolithic beam are discussed in detail by Paulay and Priestley [9].

Accordingly, the member end displacement for the monolithic beam in Figure 2.40b is

$$\Delta_{\text{Monolithic}} = \Delta_e + \Delta_p \quad (2.24)$$

$$\Delta_p = \left[L - \frac{L_p}{2} \right] \theta_p \quad (2.25)$$

$$\theta_p = L_p (\phi_u - \phi_y) \quad (2.26)$$

where L_p is the plastic hinge length, θ_p is the plastic rotation, ϕ_u is the ultimate curvature, and ϕ_y is the yield curvature. Substituting Equations 2.22–2.26 in Equation 2.21,

$$\Delta_e + L\theta = \Delta_e + L_p \left[L - \frac{L_p}{2} \right] [\phi_u - \phi_y] \quad (2.27)$$

$$[\phi_u - \phi_y] = \frac{L\theta}{L_p(L - L_p/2)} \quad (2.28)$$

$$\text{But,} \quad \phi_u = \frac{\varepsilon_c}{c} \quad (2.29)$$

where ε_c is the extreme fiber compressive strain and c is the neutral axis depth. Hence,

$$\varepsilon_c = \left[\frac{L\theta}{L_p(L - L_p/2)} + \phi_y \right] c \quad (2.30)$$

Equation 2.30 is suggested for estimating the extreme fiber concrete compression strain for a given neutral axis depth at an interface rotation θ imposed at the connection interface.

However, it was reported that ε_c in Equation 2.30 can be further approximated as follows:

$$L \approx (L - L_p/2) \quad (2.31)$$

$$\text{Hence,} \quad \varepsilon_c = \left[\frac{\theta}{L_p} + \phi_y \right] c \quad (2.32)$$

2.4.5.2 Strain in the Mild Steel Reinforcement

Based on the gap opening mechanism as shown in Figure 2.41 for a hybrid connection, an expression for the strain in the mild steel tension reinforcement at the connection, ε_{st} , was established as a function of θ in Equation 2.33, in which L_{ub} is the debonded length of the mild steel reinforcement:

$$\epsilon_{st} = \frac{\Delta_{st} - 2\Delta_{sp}}{L_{ub}} \quad (2.33)$$

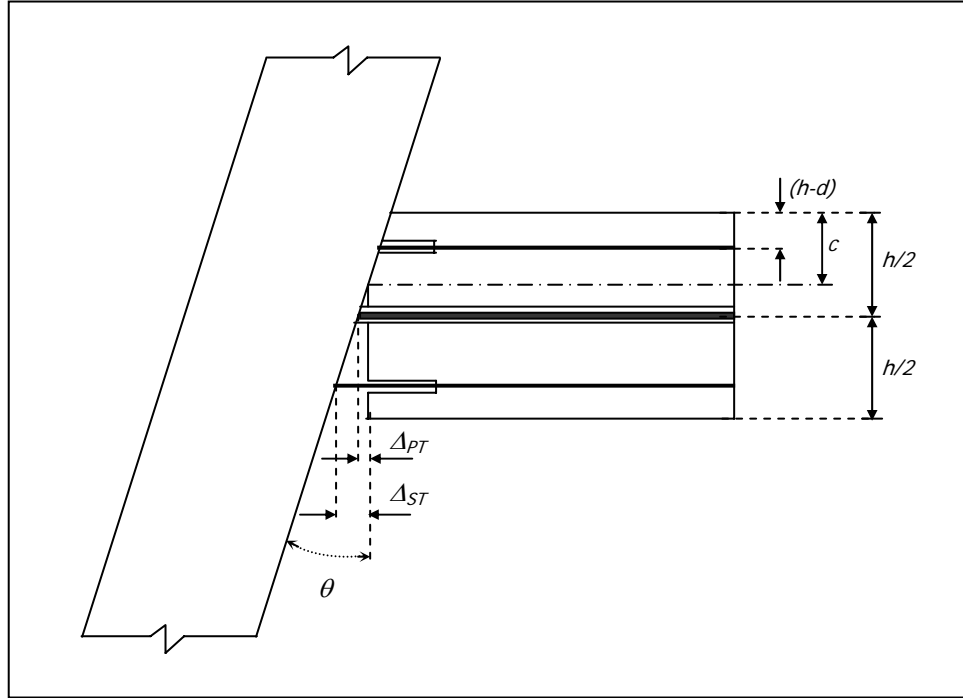


Figure 2.41 A hybrid connection with imposed interface rotation of θ .

$$\text{From geometry, } \Delta_{st} = [d - c]\theta \quad (2.34)$$

$$\text{But, } \epsilon_{st} = \epsilon_e + \epsilon_p \quad (2.35)$$

Expressing the displacement component due to the strain penetration into the joint, Δ_{sp} , as suggested by Sritharan [50],

$$\Delta_{sp} = L_{sp} \epsilon_p + \frac{2}{3} L_{sp} \epsilon_e \quad (2.36)$$

where L_{sp} is the portion of the plastic hinge length representing the strain penetration effect.

Substituting Equation 2.35 in Equation 2.36,

$$\Delta_{sp} = L_{sp}[\epsilon_{st} - \epsilon_e] + \frac{2}{3}L_{sp}\epsilon_e \quad (2.37a)$$

$$\Delta_{sp} = L_{sp}\epsilon_{st} - \frac{1}{3}L_{sp}\epsilon_e \quad (2.37b)$$

However, ϵ_e may be represented as $\epsilon_e = \frac{f_{st}}{E_{st}}$ (2.38)

where f_{st} is the elastic stress corresponding to ϵ_{st} and E_{st} is the elastic modulus of the reinforcing steel.

Substituting Equations 2.34, 2.37b and 2.38 in Equation 2.33,

$$\epsilon_{st} = \frac{(d-c)\theta + \frac{2}{3}L_{sp}\frac{f_{st}}{E_{st}}}{L_{ub} + 2L_{sp}} \quad (2.39)$$

2.4.5.3 Strain in the Post-Tensioning Tendon

Using the frame geometry shown in Figure 2.41 at the connection interface rotation of θ , the strain in the post-tensioning steel, ϵ_{pt} , may be obtained from

$$\epsilon_{ps} = \frac{\Delta_{pt}}{L_{ups}} + \epsilon_{pi} \quad (2.40)$$

where Δ_{pt} , L_{ups} and ϵ_{pi} are, respectively, the elongation, unbonded length and initial stress of the post-tensioning steel.

But
$$\Delta_{pt} = [h/2 - c]\theta \quad (2.41)$$

Hence,
$$\epsilon_{ps} = \frac{[h/2 - c]\theta}{L_{ups}} + \epsilon_{pi} \quad (2.42)$$

2.4.5.4 Moment-Rotation Response

At a given rotation θ at the connection interface and an assumed value for the neutral axis depth, Equation 2.30 or Equation 2.32, Equation 2.39 and Equation 2.42 are used to evaluate strains in the extreme concrete compression fiber, tension mild steel reinforcement and post-tensioning steel, respectively. As noted previously, the authors indicated that the contribution of the compression steel was also accounted for in the analysis, but no details were given as to how this was achieved. From the estimated strain values, stresses in concrete, mild steel reinforcement and prestressing tendons and the corresponding forces can be determined using appropriate stress-strain behavior for the materials. At a given θ , the neutral axis depth is refined iteratively using the force equilibrium condition. Once the neutral axis depth for the selected θ is finalized, the corresponding moment resistance can be readily established since the resultant forces and their location are known at the connection interface. By repeating the procedure for different interface rotations, a continuous moment-rotation envelope is established that can describe the monotonic response of a hybrid connection.

2.5 Design Provisions

2.5.1 Recommended Design Procedures

There have been only limited studies that have proposed design procedures for precast hybrid frame connections. A summary of design procedures recommended by Cheok et al. [13] and ACI Innovative Task Group [15] is presented in this section. Although the design guidelines proposed for precast seismic structural systems by Stanton and Nakaki [14] included hybrid frame connection, they are not documented as part of the current study. Similar to References [13, 15], their design method is also based on assumed stresses in the

steel reinforcement and representing the concrete stress distribution at the connection using an equivalent rectangular stress block. In addition to summarizing the design method of Stanton and Nakaki for the hybrid frame connection, Celik and Sritharan [17] have provided validation and recommendations for improving the proposed design method.

2.5.1.1 Cheok, Stone, and Nakaki (1996) [13]

The authors recommended a design procedure for hybrid frame connection based on many simplified assumptions, which are listed in Section 2.4.4. The recommended design steps are summarized below.

Design Parameters

The following design parameters are assumed at the beginning of design:

- a) Steel areas: A_{ps} , A_s
- b) Beam section details: h , b , d (see Figure 2.39)
- c) Unbonded lengths: L_{ups} , L_{ub}

Minimum Area of Mild Steel Reinforcement

If shear demands at the connection interface due to dead and live loads are V_D and V_L , respectively, and M_{p1} and M_{p2} represent the probable moment capacities of the hybrid connections at the ends of a single-bay beam, then the total shear demand at the connection interface, V_u , is:

$$V_u \leq 1.4V_D + 1.7V_L + (M_{p1} + M_{p2})/L \quad (2.43)$$

where L is the beam length.

The shear resistance in the vertical direction at the connection interface is provided by friction created by the concrete compression force. This compression force has two

components: a portion due to the force in the prestressing steel, F_p , and the other portion, C , due to gravity, live and seismic moment couple. Therefore, the shear resistance of the connection, V_n , can be expressed as:

$$V_n = \mu(F_p + C) \quad (2.44)$$

where μ is the friction coefficient and a value of 1.0 was recommended for use in accordance with UBC 94 [51], Section 1911.7.4.3.

For satisfactory transfer of shear at the connection, it should be ensured that

$$\Phi V_n \geq V_u \quad (2.45)$$

where Φ is the shear strength reduction factor.

To resist the gravity load in case of the prestressing tendon failure, a minimum area for the mild steel reinforcement is suggested using Equation 2.46, in which f_y is the yield strength of the steel reinforcement:

$$A_s \geq (V_D + V_L) / f_y \quad (2.46)$$

Minimum Force in Tendon

From Equation 2.43 – 2.46, the minimum required clamping force could be deduced to:

$$F_p \geq (1.4V_D + 1.7V_L) / \Phi\mu \quad (2.47)$$

Moment Design

If moments due to dead load, live load and earthquake load are M_D , M_L , M_E , respectively, the nominal moment, M_n , should satisfy the following conditions:

$$\phi_f M_n \geq 1.4M_D + 1.7M_L \quad (2.48)$$

$$\phi_f M_n \geq 1.4(M_D + M_L + M_E) \quad (2.49)$$

$$\phi_f M_n \geq 0.9M_D + 1.4M_L \quad (2.50)$$

where ϕ_f is the strength reduction factor for flexure. The nominal moment capacity is calculated using the procedure described in Section 2.4.4.

Flexural Strength Ratio

The moment contribution of the mild steel reinforcement should be checked to ensure that this contribution does not exceed 50 percent of the total moment capacity of the connection.

Vertical Shear Design

By using the probable moment capacities defined in Equation 2.43 and the components of the compression force at the connection, which are included in Equation 2.44 and can be obtained from the procedure described in Section 2.4.4, Equation 2.45 should be satisfied to ensure sufficient vertical shear resistance at a hybrid connection interface.

Maximum Drift

The requirements in UBC 1994 [51] were recommended for defining the maximum drift demand for the hybrid frame. The drift capacity at the probable moment of the connection can be determined using the procedure described in Section 2.4.4, which should be shown to be greater than the demand obtained from the building code.

2.5.1.2 ACI Innovative Task Group 1 [15]

The American Society of Concrete (ACI) appointed a group of experts, the ACI Innovative Task Group 1, to investigate and document a design procedure for the precast hybrid frame connection. The procedure that was recommended by the group was similar to that of Cheok et al. [13] (see Section 2.5.1.1) except for the following changes:

Shear Demand

When calculating the shear demand as per Equation 2.43, a factor of 0.75 for the shear components due to gravity loads was introduced. Accordingly, Equation 2.43 is replaced with Equation 2.51:

$$V_u \leq 0.75(1.4V_D + 1.7V_L) + (M_{p1} + M_{p2})/L \quad (2.51)$$

Moment Contribution of Compression Steel

In the probable moment capacity calculation, the contribution of the compression mild steel reinforcement was ignored by Cheok et al. [13]. The ACI Task Group 1 recommended that the steel stress in the compression steel be taken as $1.25f_y$ when determining the probable moment capacity of a hybrid connection.

CHAPTER 3

SECTION AND MEMBER LEVEL ANALYSES

3.1 Section Analysis

Two conditions that are typically used in a section analysis of reinforced concrete members are the equilibrium of forces and compatibility of strains between concrete and steel reinforcement. The latter condition is only possible because of the assumption that there exists a perfect bond between the steel reinforcement and surrounding concrete. The presence of unbonded prestressing bars and mild steel reinforcement at the hybrid connection creates strain incompatibility between the concrete and steel reinforcement at the critical section, making the section analysis difficult at the beam-column connection interface as well as along the beam.

The concept of monolithic beam analogy, which was introduced by Pampanin et al. [18] and summarized in Section 2.4.5, may be used to overcome the strain incompatibility issue and to estimate concrete and steel strains at a hybrid frame connection. In this concept, the use of a global displacement condition makes the section level analysis possible. Using the stresses obtained for the estimated strains from material constitutive relations and enforcing the equilibrium condition, the section level analysis may be performed for the hybrid connections. Pampanin et al. examined the accuracy of this methodology by comparing the analytical moment-rotation response envelopes with the experimental results obtained for specimens M-P-Z4 and O-P-Z4 tested by Stone et al. [46]. For both specimens, good agreement between the experimental and analytical moment-rotation envelopes was reported. Furthermore, application of this concept was used to quantify the response of the PRESSS

test building subjected to different segments of earthquake motions. The PRESSS building consisted of four different types of jointed frames, including a three-story hybrid frame. Satisfactory comparison between the measured and analytical responses was generally reported, but some of the response peaks were found to be underestimated by the analytical model.

Although the monolithic beam analogy was reported to be satisfactory for predicting the moment-rotation envelopes and the response of the PRESSS test building, it was not clear if the predicted stresses at the connection level are appropriate for use in the design. This is because the monolithic beam analogy concept essentially assumes that the theoretical plastic hinge length for the beams in jointed frame systems is the same as that empirically derived for the beams in monolithic frame systems. Furthermore, Pampanin et al. found that the moment-rotation analysis of the jointed frame system is not very sensitive to the concrete strain that was estimated using the monolithic beam analogy concept.

Motivated by the fact that estimation of accurate strains at the critical section is vital for introducing the monolithic beam analogy in the design of the hybrid frame connection, the current study investigates the ability of the monolithic beam analogy to predict the critical strains at the connection (section) level. Such an investigation was not included in the previous study [18]. With an intention to improve the estimates of strains, the following modifications are introduced in the analysis procedure based on the monolithic beam analogy concept:

- 1) Establish an expression to quantify the strain in the compression steel, and account for its contribution in the equilibrium equation and in the calculation of moment resistance at the hybrid connection interface.

- 2) Improve representation of the strain penetration term and elastic component of the strain in the mild steel tension reinforcement in the equation for estimating the concrete compressive strain.
- 3) Use Mattock's model [19] to represent the stress-strain behavior of the prestressing tendons.

3.1.1 Assumptions

The following assumptions are made in the development of a modified set of expressions for computing strains at a hybrid frame connection using the monolithic beam analogy:

- The plane section at the beam-column connection remains plane for all interface rotations. The compressive strain in concrete at the connection is zero at the center of rotation and varies linearly within the contact region between the beam and column.
- The steel in the unbonded region is assumed to be perfectly unbonded.
- The beam segment outside the effective unbonded length of the mild steel reinforcement is assumed to remain elastic for all rotations at the beam-column connection interface. The effective unbonded length includes the intentionally left debonded length and the growth of the debonded length due to strain penetration.
- The prestressing force used in the analysis accounts for losses due to time dependent effects such as creep and shrinkage.
- Stress-strain relations for concrete, mild steel, and prestressing steel are accurately represented by the constitutive relations presented in Section 3.3.

3.1.2 Quantifying Strains

3.1.2.1 Concrete Strain

For establishing a relation between the concrete strain in the extreme compressive fiber and neutral axis depth using the monolithic beam analogy, the global displacements obtained at the ends of cantilever beams with a hybrid and a monolithic connection were equated as shown in Figure 2.40. By re-examining this concept, some modifications to the strain equations are introduced over that proposed by Pampanin et al. [18]

Considering the strain penetration term in the monolithic connection and using the geometry and variables shown in Figure 2.40, the total member end displacement for the monolithically connected beam end can be expressed as

$$\Delta_{\text{Monolithic}} = \Delta_e + \Delta_p \quad (3.1)$$

Plastic component of the displacement,

$$\Delta_p = L\theta_p \quad (3.2)$$

Plastic rotation,

$$\theta_p = L_p[\phi_u - \phi_e] \quad (3.3)$$

where ϕ_u is the ultimate curvature and ϕ_e is the elastic curvature at the critical section.

It is noted that Pampanin et al. used ϕ_y instead of ϕ_e due to the difficulty in estimating the latter (see Equation 2.26), where ϕ_y is the first yield curvature. When using the revised approach, ϕ_e will be estimated using the value obtained for the previous θ and then iterated to find ϕ_e for the current θ , where θ is the interface rotation.

Accounting for the strain penetration contribution to Δ_e as suggested by Sritharan [50], Δ_e may be expressed as

$$\Delta_e = \frac{1}{3}\phi_e L^2 + \left[\frac{2}{3}\phi_e L_{sp} \right] L \quad (3.4)$$

where L_{sp} is the strain penetration length.

Substituting Equations 3.2–3.4 in Equation 3.1,

$$\Delta_{\text{Monolithic}} = \Delta'_e + L_p[\phi_u - \phi_e]L + \left[\frac{2}{3}\phi_e L_{sp} \right] L \quad (3.5)$$

where the beam elastic deformation

$$\Delta'_e = \frac{1}{3}\phi_e L^2 \quad (3.6)$$

The total member end displacement of the beam with a precast hybrid connection

$$\Delta_{\text{Precast}} = \Delta_e^* + \Delta_\theta \quad (3.7)$$

where Δ_e^* is the beam end displacement due to the elastic curvature along the precast beam.

The displacement due to the concentrated rotation θ at the hybrid connection can be expressed as

$$\Delta_\theta = L\theta \quad (3.8)$$

Based on the monolithic beam analogy (see Equation 2.21),

$$\Delta_{\text{Precast}} = \Delta_{\text{Monolithic}} \quad (3.9)$$

Therefore,

$$\Delta'_e + L_p[\phi_u - \phi_e]L + \left[\frac{2}{3}\phi_e L_{sp} \right] L = \Delta_e^* + L\theta \quad (3.10)$$

The strain in the tension reinforcement at the critical section may be similar in both the monolithic and hybrid beam, but not the curvature. This is because the reinforcement in the

hybrid beam is debonded over a short distance and thus a portion of the member elastic deformation is included in the displacement obtained from the interface rotation θ . Approximating the elastic displacement component included in θL to that estimated for the strain penetration effect into the column, the following assumption is made:

$$\Delta'_e \approx \Delta_e^* + \frac{2}{3} L_{sp} \phi_e \quad (3.11)$$

Hence,

$$L_p[\phi_u] = \theta + \left[L_p - \frac{4}{3} L_{sp} \right] \phi_e \quad (3.12)$$

But,

$$\phi_u = \frac{\varepsilon_c}{c} \quad (3.13)$$

where ε_c is the strain in extreme concrete compression fiber and c is the neutral axis depth.

Combining Equations 3.12 and 3.13, the compressive strain in the extreme concrete fiber may be obtained from Equation 3.14:

$$\varepsilon_c = \left[\theta + \phi_e \left[L_p - \frac{4}{3} L_{sp} \right] \right] \frac{c}{L_p} \quad (3.14)$$

For a given rotation at the beam-column interface and an assumed neutral axis depth, Equation 3.14 provides an estimate for the concrete strain.

3.1.2.2 Steel Strains

Compression Mild Steel Reinforcement

As shown in Figure 1.3, the compression reinforcing bar is also debonded over a distance of L_{ub} . Using the variables identified in Figure 2.41, Equation 3.15 is suggested for estimating the strain in the compression steel reinforcement. This expression averages estimates of strains obtained at the critical section and at a distance of L_{ub} from the critical

section. At the critical section, the steel strain is determined from the concrete compressive strain found from Equation 3.14. At the section at a distance of L_{ub} from the critical section, it is assumed that the compressive steel strain cannot exceed the steel yield strain, ε_y :

$$\varepsilon_{sc} = \frac{1}{2} \left[\frac{(c-d')}{c} \varepsilon_c + \varepsilon_y \frac{M}{M_y} \right] \quad (3.15)$$

where M is the moment resistance calculated for the connection in the previous step and M_y is yield moment at the section located at a distance L_{ub} from the critical section. The reason for using M that is calculated at the connection interface in Equation 3.15 is to keep this equation independent of member length L . If necessary, M may be more accurately represented with $M(1 - L_{ub}/L)$ in Equation 3.15.

Tension Mild Steel Reinforcement

For a given interface rotation θ at the hybrid connection, the tensile strain in the mild steel reinforcement can be obtained from Equation 3.16 which is identical to that adopted by Pampanin et al. (see Equation 2.39):

$$\varepsilon_{st} = \frac{\left[[d-c]\theta + \frac{2}{3} L_{sp} \frac{f_{st}}{E_{st}} \right]}{[L_{ub} + 2L_{sp}]} \quad (3.16)$$

where E_{sp} is the elastic modulus of the mild steel reinforcement.

Prestressing Steel

The recommendation by Pampanin et al. is used to estimate the strain in prestressing steel (see Equation 2.42). Accordingly, the strain in the prestressing steel corresponding to an interface rotation of θ is

$$\varepsilon_{ps} = \frac{[h/2 - c]\theta}{L_{ups}} + \varepsilon_{pi} \quad (3.17)$$

where L_{ups} is the unbonded length of the prestressing steel and ε_{pi} is initial strain in the prestressing steel after losses.

3.1.3 Moment-Rotation Envelope

The strain values in concrete and steel reinforcement are functions of the interface rotation and neutral axis depth as expressed in Equations 3.14–3.17. Hence, for a given rotation at the hybrid connection interface, an iterative procedure is used to find the corresponding neutral axis depth such that the equilibrium condition is satisfied at the critical section. By repeating this procedure for a range of values for θ , a continuous moment-rotation curve describing the behavior of a hybrid connection can be produced. The steps involved in the iteration procedure are described below and a summary of the procedure is presented in a flowchart in Figure 3.1.

Step 1: Quantifying Strains

For a given rotation at the connection interface and an assumed neutral axis depth, concrete and steel strains are estimated using Equations 3.14–3.17.

Step 2: Quantifying Stresses

Using the estimated strains at the critical section, stresses in the concrete, mild steel reinforcement, and prestressing tendons are determined using the stress-strain models described below:

- **Concrete**

The concrete model proposed by Mander et al. [52] is used for estimating the concrete stresses. This model describes the stress-strain behavior of confined and unconfined concrete using the following equations:

$$f_c = \frac{f'_{cc} x r}{r - 1 + x^r} \quad (3.18)$$

$$f'_{cc} = f'_c \left[2.254 \sqrt{1 + \frac{7.94 f'_l}{f'_c}} - \frac{2 f'_l}{f'_c} - 1.254 \right] \quad (3.19)$$

$$x = \frac{\epsilon_c}{\epsilon_{cc}} \quad (3.20)$$

$$r = \frac{E_c}{E_c - E_{sec}} \quad (3.21)$$

$$E_{sec} = \frac{f'_{cc}}{\epsilon_{cc}} \quad (3.22)$$

$$\epsilon_{cc} = \epsilon_{co} \left[1 + 5 \left[\frac{f'_{cc}}{f'_c} - 1 \right] \right] \quad (3.23)$$

where f_c is the stress corresponding to strain ϵ_c , f'_c is the unconfined concrete strength and the corresponding strain is ϵ_{co} , E_c is Young's modulus of concrete, and f'_l is the effective lateral confining stress, f'_{cc} is the confined concrete strength, E_{sec} is the secant modulus

of concrete at f'_{cc} , and ϵ_{cc} is the strain corresponding to f'_{cc} . When computing the stress-strain behavior of unconfined concrete, f'_c is taken as zero.

- **Mild Steel**

The stress-strain model suggested by Dodd and Restrepo [53] is used to estimate the stresses in the mild steel reinforcement. This model is represented by the following equations:

$$f_s = E_s \epsilon_s \quad \text{for} \quad \epsilon_s \leq \epsilon_y \quad (3.24)$$

$$f_s = f_y \quad \text{for} \quad \epsilon_y \leq \epsilon_s \leq \epsilon_{sh} \quad (3.25)$$

$$f_s = f_{su} + (f_y - f_u) \left(\frac{\epsilon_{su} - \epsilon_s}{\epsilon_{su} - \epsilon_{sh}} \right)^p \quad \text{for} \quad \epsilon_{sh} \leq \epsilon_s \leq \epsilon_u \quad (3.26)$$

$$p = \log \left[\frac{f_{su} - f_x}{f_{su} - f_y} \right] / \log \left[\frac{\epsilon_{su} - \epsilon_x}{\epsilon_{su} - \epsilon_{sh}} \right] \quad (3.27)$$

where (f_s, ϵ_s) is an arbitrary point on the monotonic stress-strain curve, (f_y, ϵ_y) defines the yield point, (f_y, ϵ_{sh}) is the point at the onset of strain of hardening, (f_x, ϵ_x) is a generic data point on the hardening portion of the stress-strain curve, (f_{su}, ϵ_{su}) defines the ultimate strength, and E_s is the elastic modulus of the steel reinforcement.

- **Prestressing Steel**

The stress-strain model recommended by Mattock [19] is used for determining the stress in the Grade 270 prestressing strands. Accordingly, for a given level of strain, the stress is found from Equation 3.28:

$$f_{ps} = \epsilon_{ps} E_{ps} \left[0.02 + \frac{0.98}{\left[1 + \left[\epsilon_{ps} E_{ps} / 1.04 f_{psy} \right]^{8.36} \right]^{0.1196}} \right] \quad (3.28)$$

where f_{ps} is stress corresponding to strain ϵ_{ps} , f_{psy} is the yield strength, and, E_{ps} is the elastic modulus of the prestressing steel.

Step 3: Find Forces

By multiplying the stresses with the respective cross-sectional steel areas, the forces in the mild steel reinforcement and post-tensioning steel can be readily calculated. For computing the force contribution by concrete, the compressive region is divided into a finite number of strips and the forces contributed by each strip is calculated using the concrete model described in Step 2 and assuming a linear distribution of strain within the compression region. From the forces established for the strips, the location and magnitude of the resultant concrete compression force is found.

Step 4: Check Equilibrium

In this step, the equilibrium condition is checked using the forces computed in Step 3. If the condition is not satisfied, the neutral axis depth is improved and Steps 1, 2, and 3 are repeated until the equilibrium condition is satisfied. Using the final values for the forces in the steel reinforcement and concrete, the moment resistance at the hybrid connection at interface rotation of θ can be determined.

The procedure described above is repeated for a range of values for θ to obtain a continuous moment-rotation envelope. Incorporating these steps of the analytical procedure, a computer program, hereafter referred to as HYBRID, was developed in Visual C++ to perform various analyses reported in the remainder of this report.

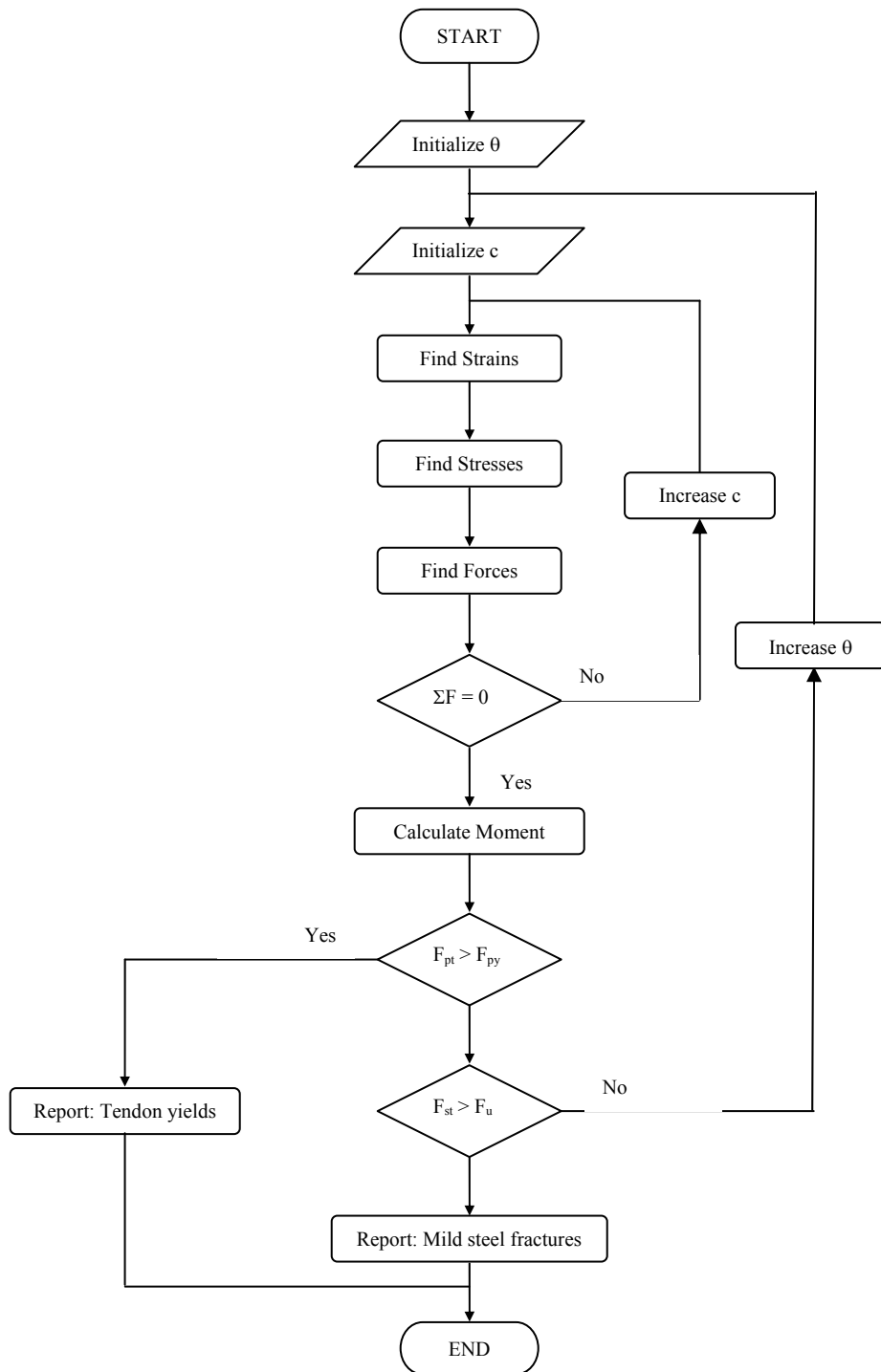


Figure 3.1 The iteration procedure adopted for the section analysis of a hybrid frame connection.

3.1.4 Experimental Validation

In order to assess the accuracy of the analysis procedure based on the monolithic beam analogy concept that was presented in Sections 3.1.2 and 3.1.3, experimental data obtained from two NIST tests and the PRESSSS test building are compared with the analysis results obtained using the computer program HYBRID. Section details of the three hybrid frame connections are included in Figure 3.2. Specimens M-P-Z4 and O-P-Z4 were interior frame tests conducted at NIST in Phase IV-B as described in Section 2.3.3. The PRESSSS section details given in Figure 3.2 are those used in the first floor of the hybrid frame in the PRESSSS test building [54–56].

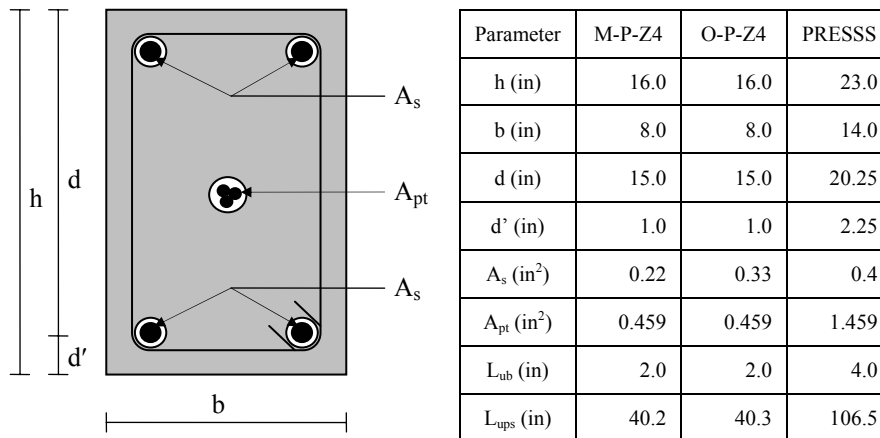


Figure 3.2 Connection details used in three hybrid frames.

The summary of details provided in Figure 3.2 are those reported in Reference [17], which also provides justification for the use of the reported unbonded lengths for the section analysis of the hybrid connections. As per this reference, the material properties summarized in Table 3.1 are also assumed for the analysis. In the PRESSSS building, the section of the

grout pad at the connection interface had dimensions of 22 in. x 13 in., which were used in the analysis as the effective beam dimensions.

Table 3.1 Material properties used in the connection analyses [17].

Parameter	MPZ4	OPZ4	PRESSS
f'_c (ksi)	6.8	6.8	8.8
f_y (ksi)	61.2	75.9	68.0
E_s, E_{ps} (ksi)	29,000	29,000	29,000
ϵ_{sh}	0.006	0.006	0.014
f_{su} (ksi)	97.6	113.1	97.9
ϵ_{su}	0.088	0.078	0.099
f_{psy} (ksi)	248.0	248.0	255.0
f_{pi} (ksi)	120.6	117.7	119.0

3.1.4.1 Moment Rotation Envelopes

Using the HYBRID program, the moment-interface rotation envelopes were established for the two NIST specimens and compared with experimental results. The typical configuration and support conditions used for these specimens are shown in Figure 3.3, whereas the dimensions of the test subassembly may be found in Figures 2.31 and 3.2. The analytical beam moment vs. interface rotation envelope is compared with the experimental results for the specimens M-P-Z4 and O-P-Z4 in Figure 3.4 and Figure 3.5, respectively. The analytical predictions are satisfactory for both cases. When presenting the original set of strain equations (see Section 2.4.5), Pampanin et al. [18] included moment-rotation envelope predictions for MPZ4 and OPZ4. In comparison to their predictions, the strain equations

presented in Section 3.1.2 appear to have led to better estimates of the elastic stiffness and the yield strength of the hybrid connections. Furthermore, the differences in the two sets of equations lead to different estimates of strains at the connection for a given interface rotation [57].

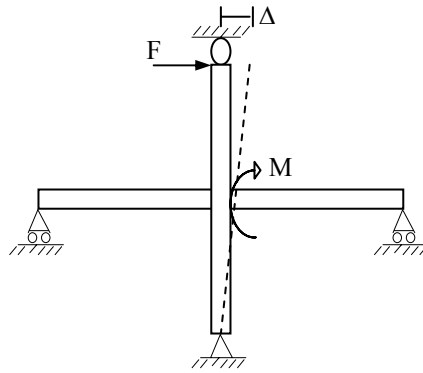


Figure 3.3 Test configuration used for specimens M-P-Z4 and O-P-Z4 [46, 47].

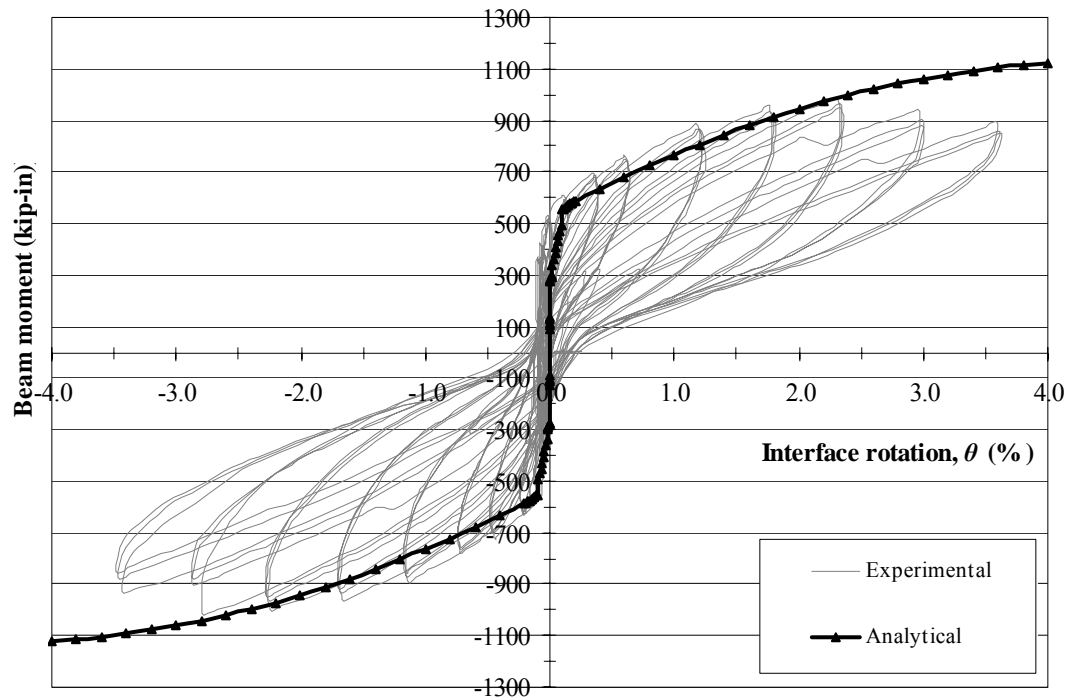


Figure 3.4 The beam end moment vs. interface rotation obtained for M-P-Z4.

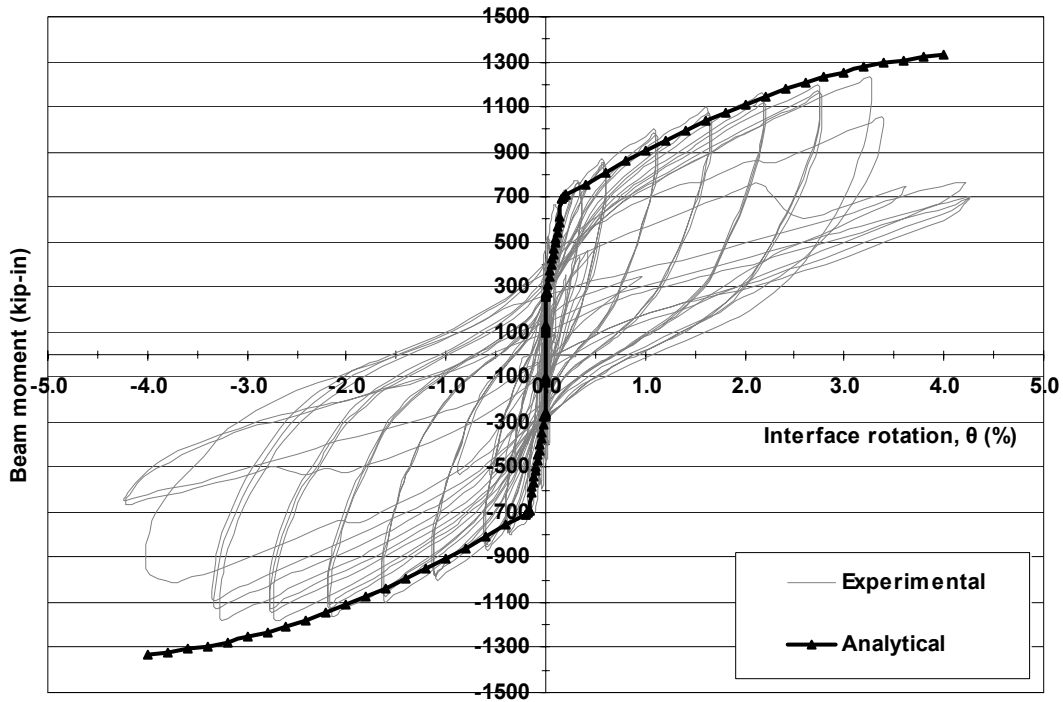


Figure 3.5 The beam end moment vs. interface rotation obtained for O-P-Z4.

3.1.4.2 Neutral Axis Depth

The PRESSS test building was instrumented with displacement transducers at the interior column-beam interface of the hybrid frame at the first floor level. Figure 3.6 shows the locations of the displacement transducers, which are identified with labels A, B, and C. As shown in this figure, let ℓ_1 , ℓ_2 , and ℓ_3 be the changes in the readings of displacement transducers A, B, and C, respectively, at an interface rotation θ and h_1 , h_2 , and h_3 define the relative locations of A, B, and C. Using the features of triangles shown in Figure 3.6 and assuming that the positive change in transducer displacement is almost equal to the gap opening at the connection interface, the neutral axis depth, c , and corresponding interface

rotation, θ , may be determined in terms of ℓ_1 , ℓ_2 , ℓ_3 , h_1 , h_2 , h_3 , and h , where h is the height of the beam.

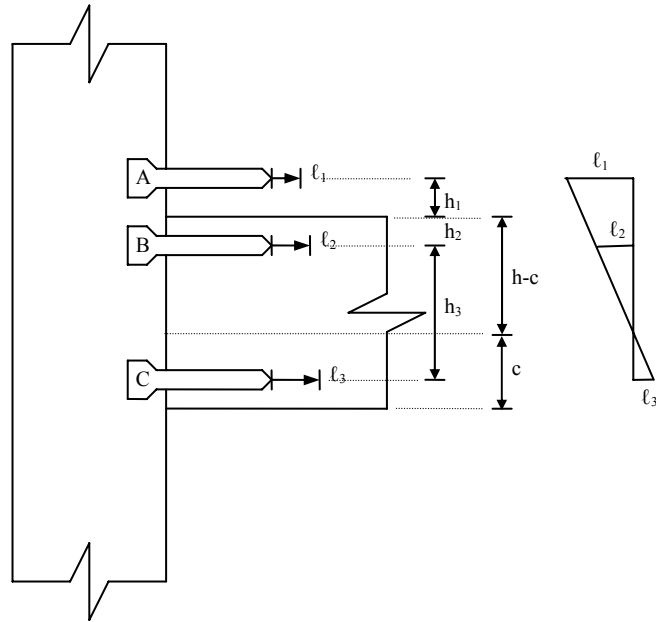


Figure 3.6 An illustration showing the displacement transducers mounted to the face of the interior column at the first floor of the hybrid frame in the PRESSS test building.

The hybrid connection at the first floor of the PRESSS test building was analyzed using HYBRID. The analytical neutral axis depth is plotted as a function of the interface rotation at the connection in Figure 3.7 along with the experimental data. The neutral axis depths were also computed at the nominal and probable moments, using the analytical procedure established from the design method proposed by Cheok et al. [13] (see Section 2.4.4), which are also included in Figure 3.7. The analytical prediction obtained from HYBRID satisfactorily captures the envelope of the experimental values. However, the neutral axis depth calculated from the analysis of Cheok et al. is unsatisfactory and, in particular, it shows an increase in neutral axis depth as the interface rotation increases. This trend, which should

be expected due to the use of the equivalent rectangular stress block to quantify forces at the connection, is contradictory to the actual behavior of the connection.

3.1.4.3 Elongation of Prestressing Steel

The measured elongations of the prestressing steel at the first floor of the hybrid frame in the PRESSSS test building are compared with the analytical prediction from HYBRID in Figure 3.8. The predicted values for the tendon elongations at the nominal and probable moments using the analytical procedure of Cheok et al. [13] (see Section 2.4.4) are also included in Figure 3.8. A good correlation found between the analytical prediction by HYBRID and the experimental elongation vs. interface rotation behavior confirms that the equations suggested for strain estimates using the monolithic beam analogy concept are satisfactory for the section level analysis. The HYBRID program appears to overestimate the elongations at large interface rotations at the connection. The cause for this discrepancy is believed to be not modeling the damage to the beam ends and grout pads that occurred to the hybrid frame of the PRESSSS building at large drifts. The analysis procedure of Cheok et al. satisfactorily predicted the elongation at the nominal moment, but not at the probable moment. The underestimation of elongation at the probable moment is due to overestimating the neutral axis depth as shown in Figure 3.7.

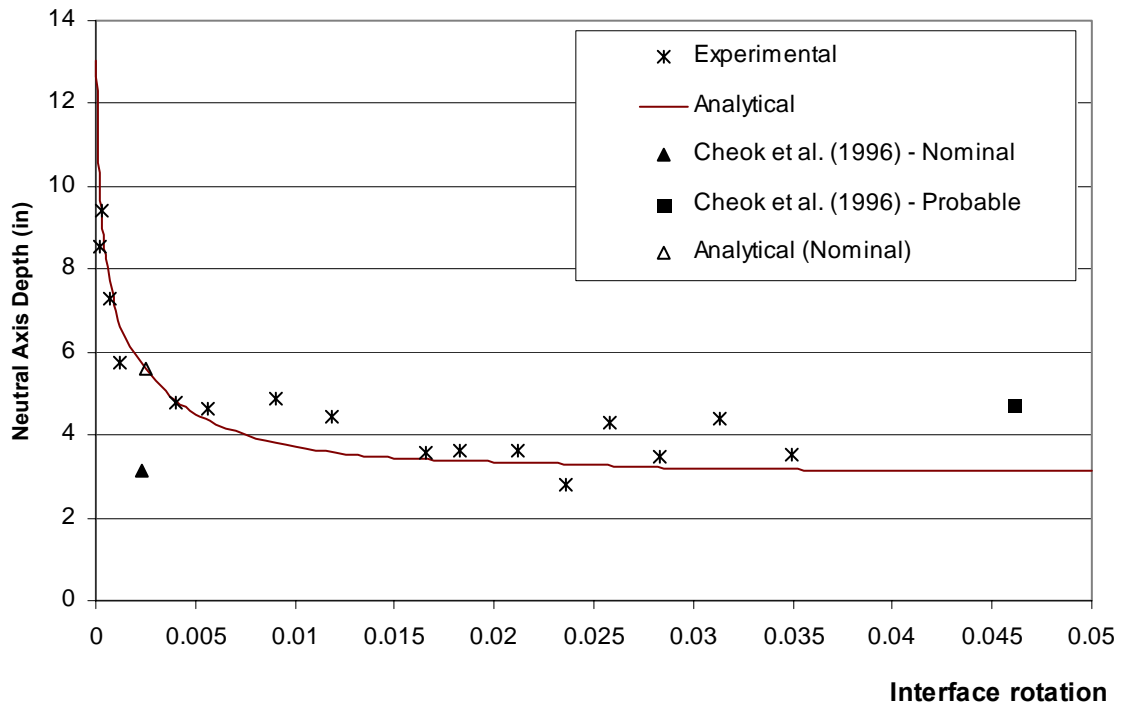


Figure 3.7 A comparison between the analytical and experimental neutral axis depths obtained for the PRESSS first floor connection.

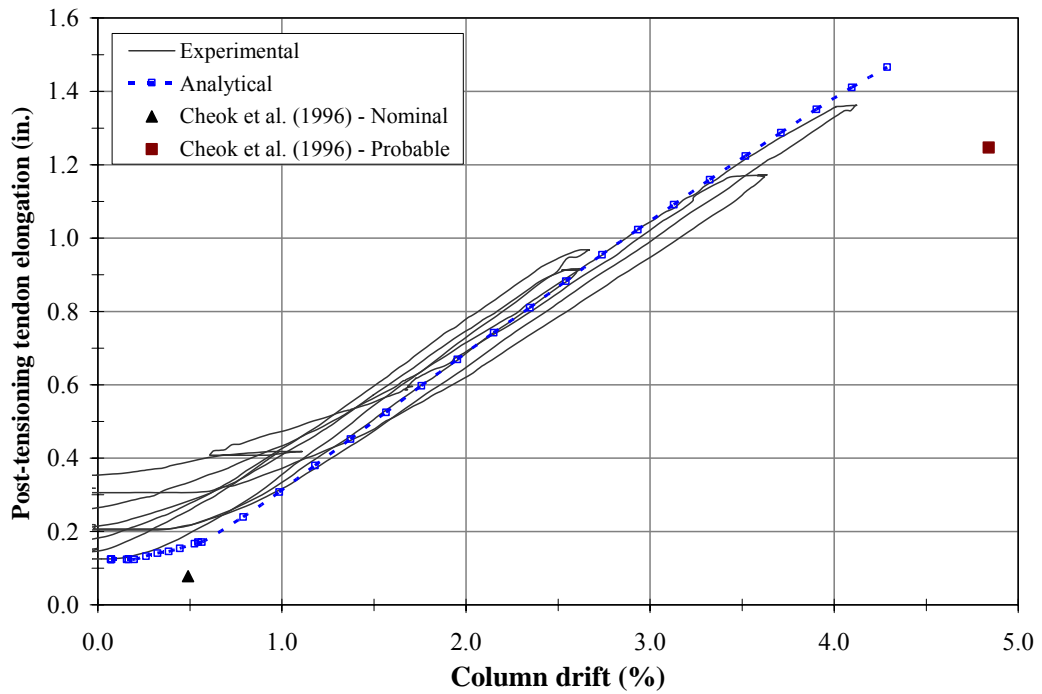


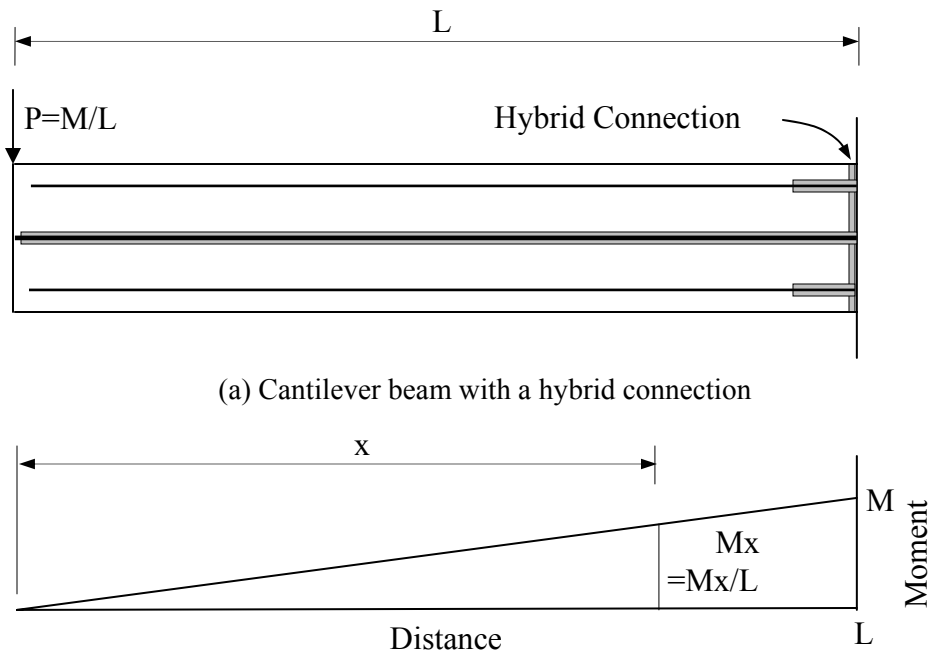
Figure 3.8 A comparison of predicted strand elongations with experimental values.

3.2 Member Level Analysis

Motivated by the fact that estimating the variation of curvature along the beam in a hybrid frame will give better understanding of the hybrid framing concept, this section presents a procedure suitable for a member level analysis and results obtained from this procedure for a beam connected with a hybrid connection. It is also demonstrated that the member level analysis will facilitate predictions of strains in concrete and steel at any beam section, including those which contain debonded steel reinforcement.

3.2.1 Procedure

The member level analysis procedure was investigated for a cantilever beam with a hybrid connection at the fixed end and a concentrated vertical force at the free end, as shown in Figure 3.9. The computer program HYBRID was used to determine the moment resistance at the critical section and the corresponding forces in the debonded mild steel reinforcement and unbonded prestressing steel for various interface rotations. These estimated forces in the steel reinforcement at the critical section are applicable at any section within the debonded length of the mild steel reinforcement. Consequently, the analysis of these sections can be performed at a given interface rotation, with the only unknowns being the neutral axis depth and compressive strain at the extreme concrete fiber. Since the moment resistance at the critical section is known for a given value of θ , the corresponding moments along the beam length can be easily found (see Figure 3.9b). Using this information and forces in the steel reinforcement, the neutral axis depth and the concrete strain can be found at any section along the debonded length of the mild steel reinforcement using an iteration procedure by enforcing the equilibrium conditions.



(a) Cantilever beam with a hybrid connection

(b) Linear variation of moment along the beam length

Figure 3.9 A cantilever beam and the moment diagram.

In the beam region where the mild steel reinforcement is bonded, the forces in the top and bottom mild steel reinforcing bars are unknown, but the prestressing tendon force is known from the analysis at the critical section. In addition to satisfying the equilibrium conditions, the compatibility between concrete compressive strains and strains in the mild steel reinforcement is enforced to determine the strains in the top and bottom mild steel reinforcing bars, the neutral axis depth, and compressive strain at the extreme concrete fiber. An iterative procedure requiring an estimate for the neutral axis depth is suggested for performing the section analysis along the beam where the mild steel reinforcement is bonded. Once the section analysis has been completed, the corresponding curvature can be found by dividing the compressive strain at the extreme concrete fiber by the neutral axis depth.

3.2.2 Results

A cantilever beam with dimensions and connection details identical to that used in test specimen M-P-Z4 was studied using the member level analysis procedure described above. Accordingly, the length of the beam was taken as 33.75 inches, which matched the beam length from the column face to the pin support in M-P-Z4. The results obtained from the member level analysis conducted at interface rotations of 0.5%, 1.0% and 2.0% are reported below.

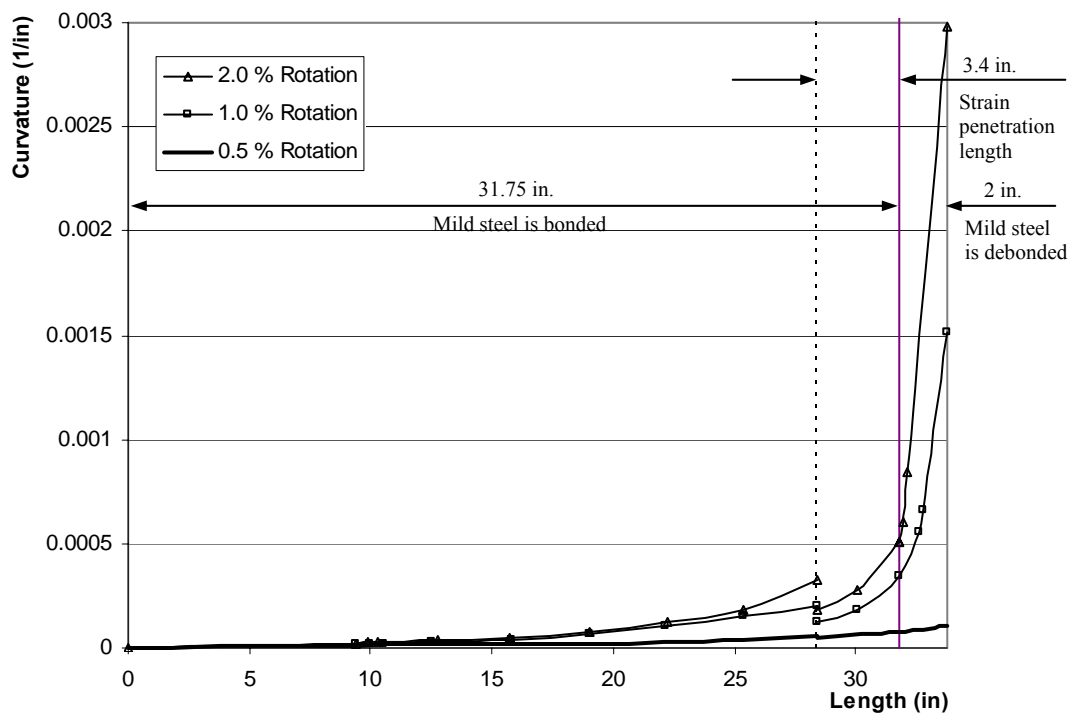


Figure 3.10 Variation of curvatures along the beam length.

The change in curvature along the beam length corresponding to the three interface rotations is presented in Figure 3.10. Similar plots showing the variation of strains in the

tension mild steel reinforcement, extreme concrete compression fiber, and compression mild steel reinforcement along the beam length are shown in Figures 3.11–3.13. In all figures, the region where the mild steel reinforcement is debonded and the theoretical strain penetration length are identified. In accordance with Equations 3.15 and 3.16, constant steel strains should be expected in these regions, which are seen in Figures 3.11 and 3.13. Furthermore, Figures 3.10–3.13 show discontinuity in curvature values or strains at the beam section defining the strain penetration length, which is located at 28.35 in. from the free end. In reality, gradual transitions of curvatures and strains should be expected at this section, but the theoretical approach that replaces gradual change of strains in the mild steel reinforcing bars with constant strains within the equivalent penetration length was expected to introduce these discontinuities.

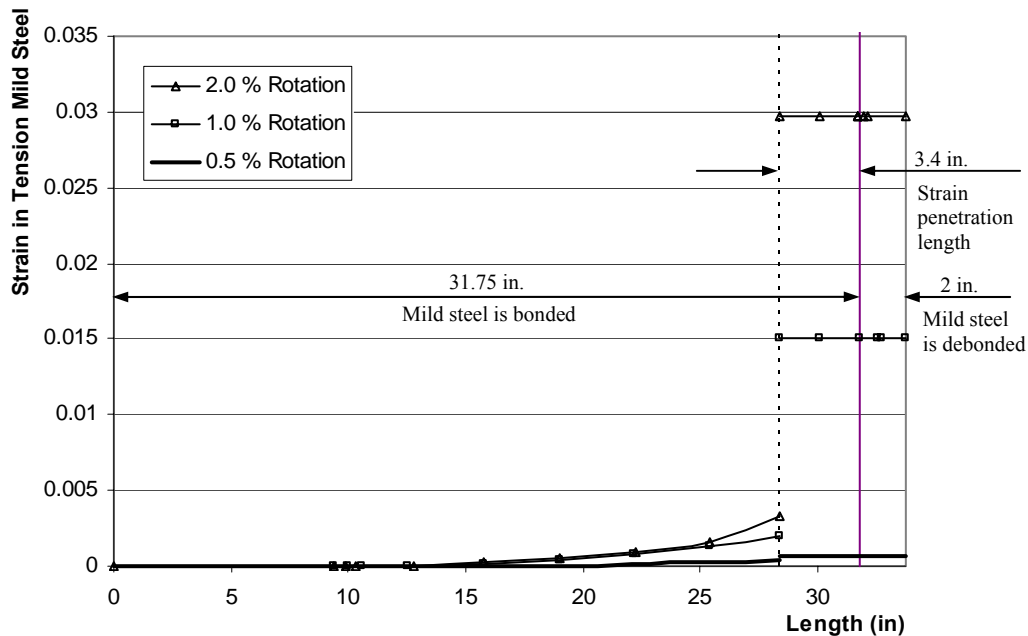


Figure 3.11 Variation of strains in the tension mild steel reinforcement along the beam.

In Figure 3.10, curvatures at sections adjacent to that at 28.35 in., where discontinuities in the curvature values are seen, show larger values on the left side than those on the right side. This may also be very unlikely to occur and is caused by the assumed strain penetration length. As discussed by Thomas and Sritharan [58], the plastic hinge length for jointed systems may be less than that assumed based on the response of monolithic connections. With a reduced plastic hinge length, higher curvatures on the right side and lower curvatures on the left side of the section at 28.35 in. and gradual change in curvatures along the beam are expected. The corresponding effect would be higher tensile strains in the mild steel reinforcement than shown in Figure 3.11. Unfortunately, the hybrid connection tests performed to date do not yield the necessary data to establish a more realistic plastic hinge length. With adequate instrumentation, this information may be obtained from future experiments.

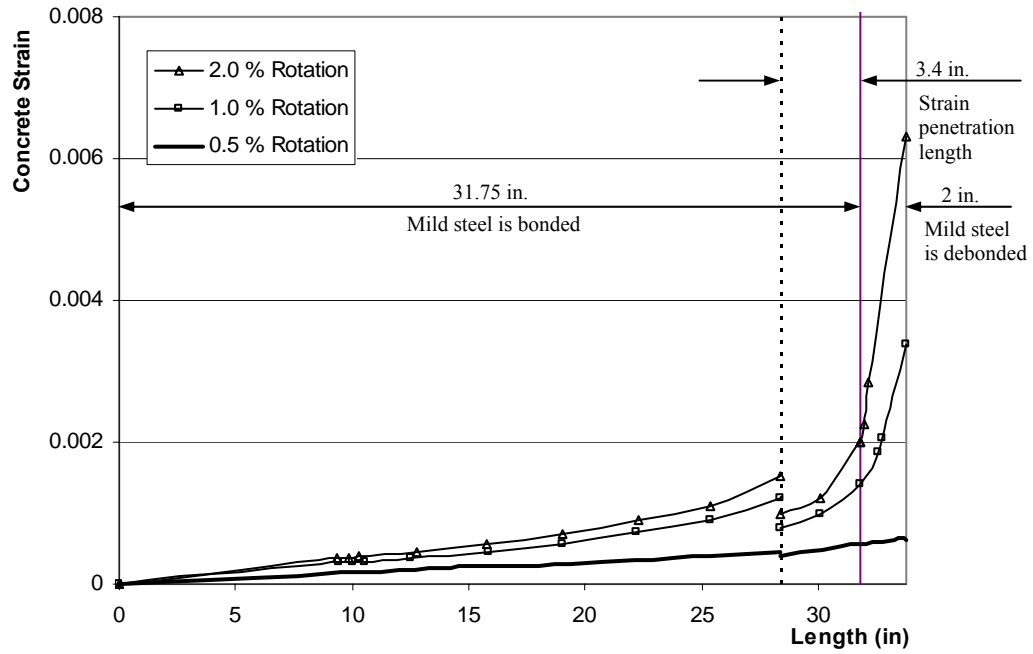


Figure 3.12 Variation of the extreme fiber concrete compressive strains along the beam.

In general, Figures 3.10–3.13 highlight the jointed hybrid frame concept with inelastic actions concentrated in the connection region and the significant portion of the beam exposed elastic behavior. In contrast, an equivalent monolithic beam will experience inelastic actions over a significant length of the beam.

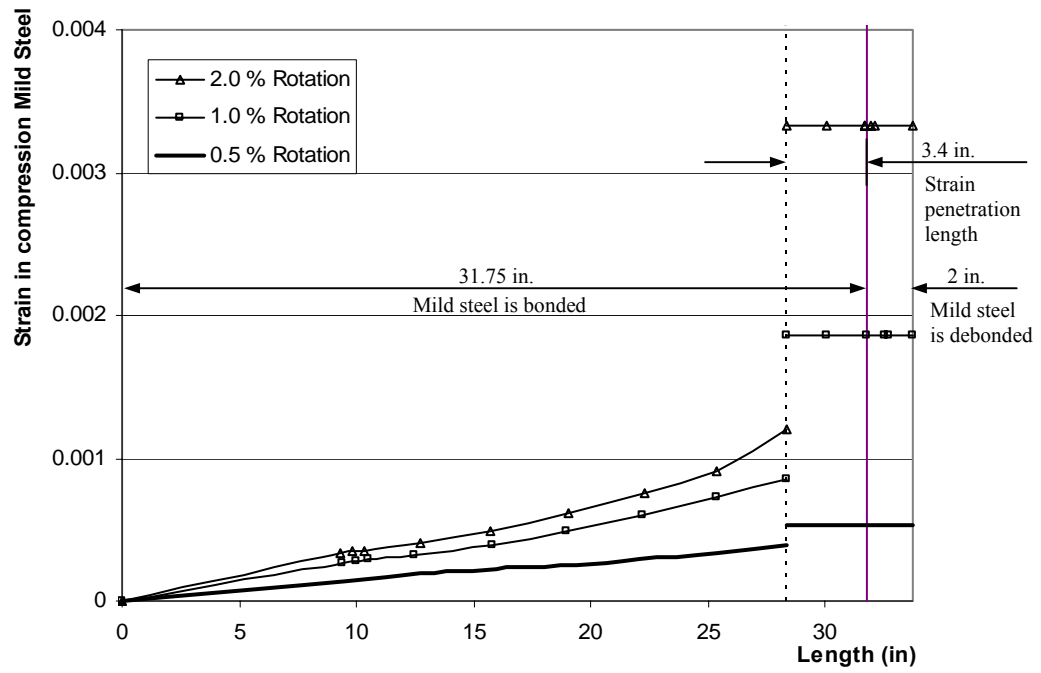


Figure 3.13 Variation of strains in the compression mild steel reinforcement along the beam.

CHAPTER 4

ANALYSIS OF A HYBRID FRAME BUILDING

4.1 Introduction

Seismic behavior of a building may be evaluated by performing static and/or dynamic analysis on a suitable model representing the lateral load resisting systems in that building. This chapter describes the model formulation of a precast hybrid frame building and presents results obtained from pushover and dynamic nonlinear analyses of the building model. The analyses of the hybrid building were performed using the finite element computer program RUAUMOKO [59], which incorporates many element types and hysteresis rules to adequately capture the inelastic behavior of structures.

The main objective of performing the pushover and dynamic analyses was to demonstrate the application of section level analysis presented in Section 3.1 to study the structure level response using a 2D frame model. For this purpose, a five-story building with dimensions similar to that of the PRESSSS test building was chosen so that the analytical results could be verified using the test data from the PRESSSS building (see more details of the building selected for the analysis in Section 4.2.1). As part of the analysis of the five-story hybrid frame building, the following issues were investigated:

- the influence of flexible floor links
- a performance-based assessment
- suitable force reduction (R-) factors that may be used in the force-based design of precast hybrid frame buildings

4.2 Model Formulation

Rapid development of the finite element technique and increasing availability of powerful micro-computers have made analysis of structures with a desired level of refinement possible. However, a reliable assessment of nonlinear dynamic behavior of structures depends on the accuracy of the mathematical models that represent the actual behavior of structural members and critical connections. This section presents the details of the five-story hybrid frame building and formulation of the analytical model.

4.2.1 Five-story Hybrid Frame Building

As previously noted, the selected five-story hybrid frame building had dimensions similar to the PRESSSS building. As used in the frame direction response of the test building, the five-story hybrid frame building consisted of two, two-bay seismic frames and represented the prototype building at 60 percent scale. Figures 4.1 and 4.2 show the elevation views of the PRESSSS test building in which four different types of jointed frame connections were investigated [54-56]. The hybrid frame connection was used in the lower three floors of one of the seismic frames (see Figures 4.1 and 4.3).

For the five-story building selected for the analysis in this report, two identical two-bay hybrid frames were used with the pretopped double-tee floors at all five levels. In the lower three floors of these hybrid frames, the connection details were assumed to be the same as those used in the PRESSSS building. In the upper two floors, new hybrid connections were designed to replace the pretensioned connections used in the PRESSSS building. Figure 4.4 shows a typical plan view of the five-story hybrid building. Hybrid details of the column-to-beam connections are summarized in Table 4.1 (see Table 3.1 for relevant material

properties). Similar to the PRESSS building, it was assumed that the column-to-footing connection consisted of 4 #6 bars and unbonded post-tensioning.

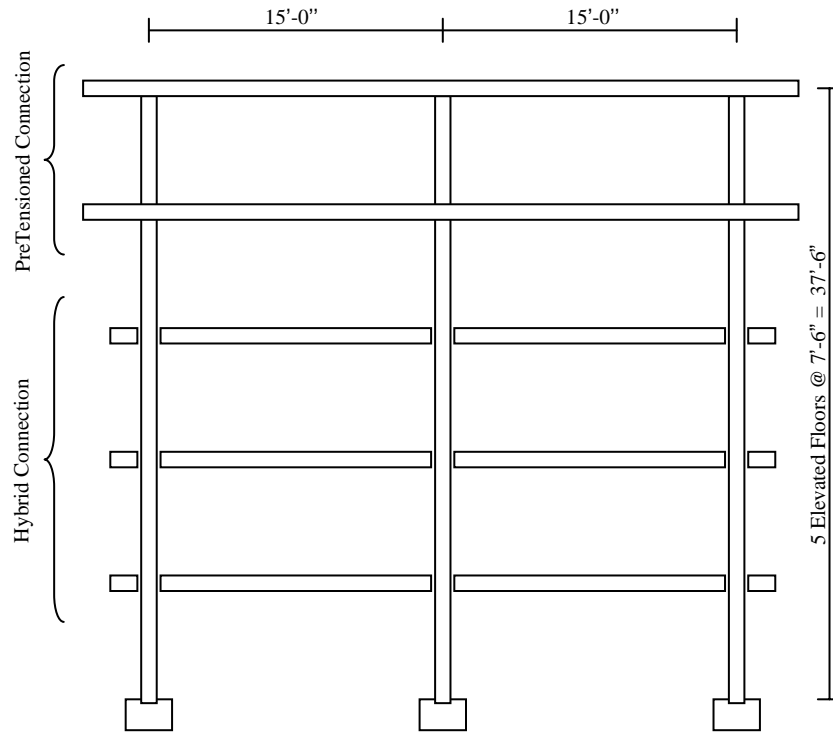


Figure 4.1 Elevation view of the seismic frame with hybrid and pretensioned connections in the PRESSS test building.

Table 4.1 A summary of hybrid frame connection details.

Location	A_s (in ²)	A_{pt} (in ²)
Floor 1	0.88	0.918
Floor 2	0.62	0.765
Floor 3	0.62	0.765
Floor 4	0.40	0.696
Floor 5	0.40	0.696
Column base	Exterior: 0.88 Interior: 0.88	Exterior: 2.50 Interior: 2.50

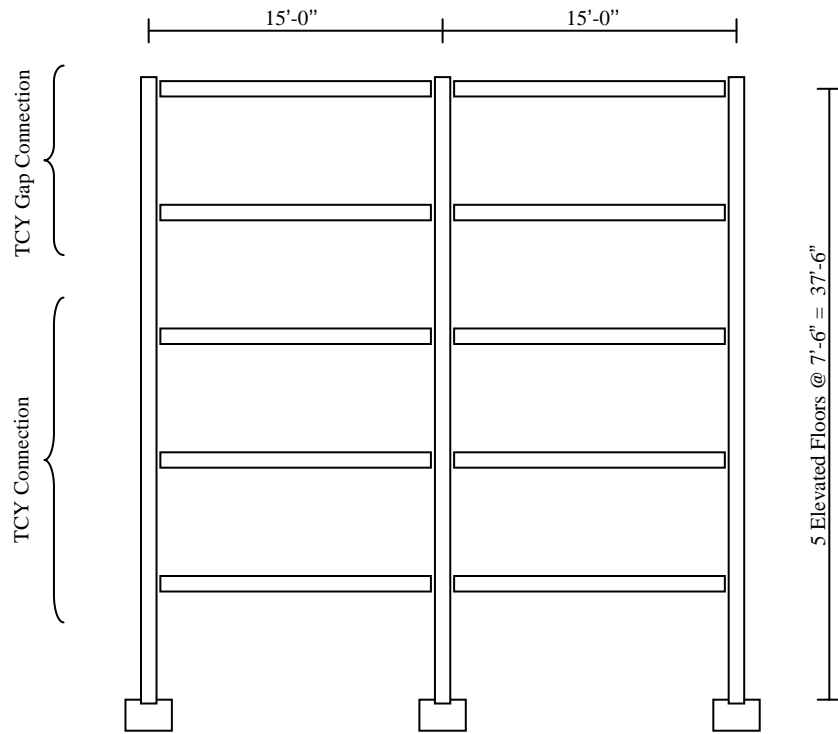


Figure 4.2 Elevation of the PRESSS seismic frame with TCY and TCY gap connections.

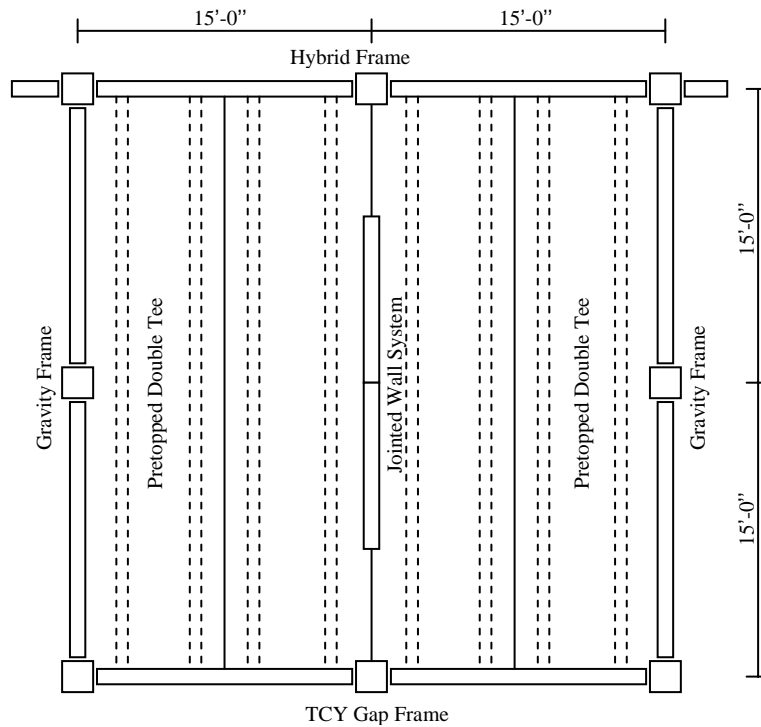


Figure 4.3 Typical plan of the PRESSS test building at the first three floors.

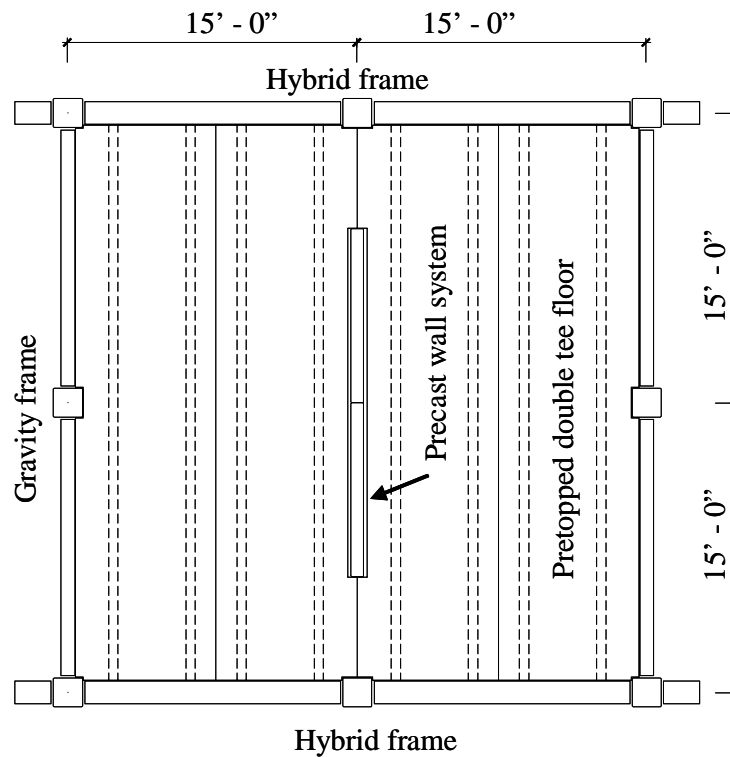


Figure 4.4 Typical plan of the five-story hybrid frame building.

By retaining the overall dimensions and hybrid connection details from the PRESSS building, it provided an opportunity to validate the analysis model of the hybrid frame building using selected data from the PRESSS test building. The measured moment resistance at the base of the seismic frame containing the hybrid connections and lateral floor displacements from the PRESSS building were used for this purpose.

4.2.2 Hybrid Connection Model

As described in Section 1.3, the hybrid connection is a ductile connection, which is designed to experience a concentrated crack and inelastic actions at the precast connection

interface. Therefore, as shown in Figure 4.5, elastic and post-elastic behavior of hybrid connections can be adequately modeled using zero-length rotational spring elements.

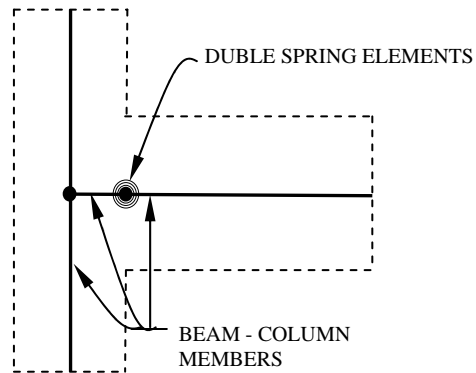


Figure 4.5 Finite element model of a hybrid frame connection.

Using the approach suggested by Pampanin et al. [18], moment resistance and hysteresis behavior of a hybrid connection could be modeled with two rotational springs and hysteresis rules available in RUAUMOKO. As illustrated in Figure 4.6, for the first floor connections used in the hybrid frame building, the two springs will represent the moment contributions from the mild steel reinforcement and prestressing tendons. The total connection resistance and moment contributions from the mild steel reinforcement and prestressing steel shown in Figure 4.6 were obtained using the program HYBRID.

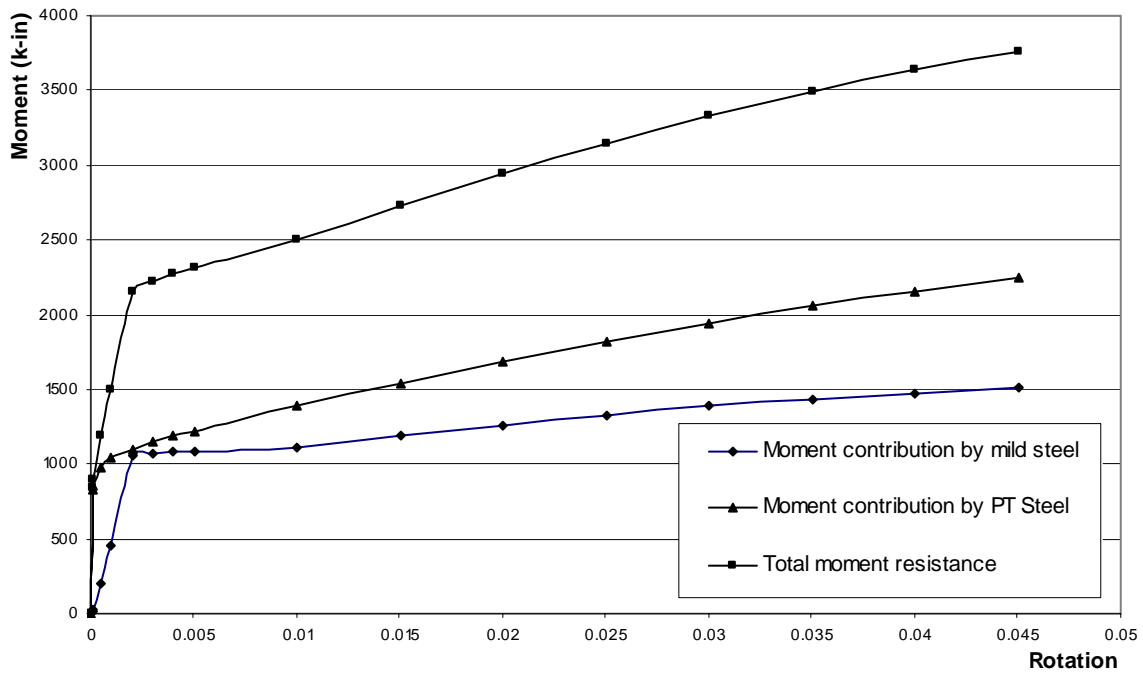


Figure 4.6 Components of bending moment resistance of a hybrid frame connection.

The use of two springs to model the hybrid connection was to adequately capture the hysteresis actions resulting from the mild steel reinforcement and elastic behavior of the prestressing steel. Having defined the moment-rotation envelopes for the springs as shown in Figure 4.6, their cyclic behavior was characterized using the modified Takeda and elastic bi-linear models for the contributions of the mild steel reinforcement and prestressing steel, respectively. Figures 4.7–4.9 show the comparison between the moment-rotation envelopes obtained for the springs and for the total resistance of the hybrid connection from HYBRID and their representations using cyclic models available in RUAUMOKO [59]. As can be seen in these figures, the results from HYBRID of a hybrid connection can be adequately represented in a RUAUMOKO model using two rotational springs.

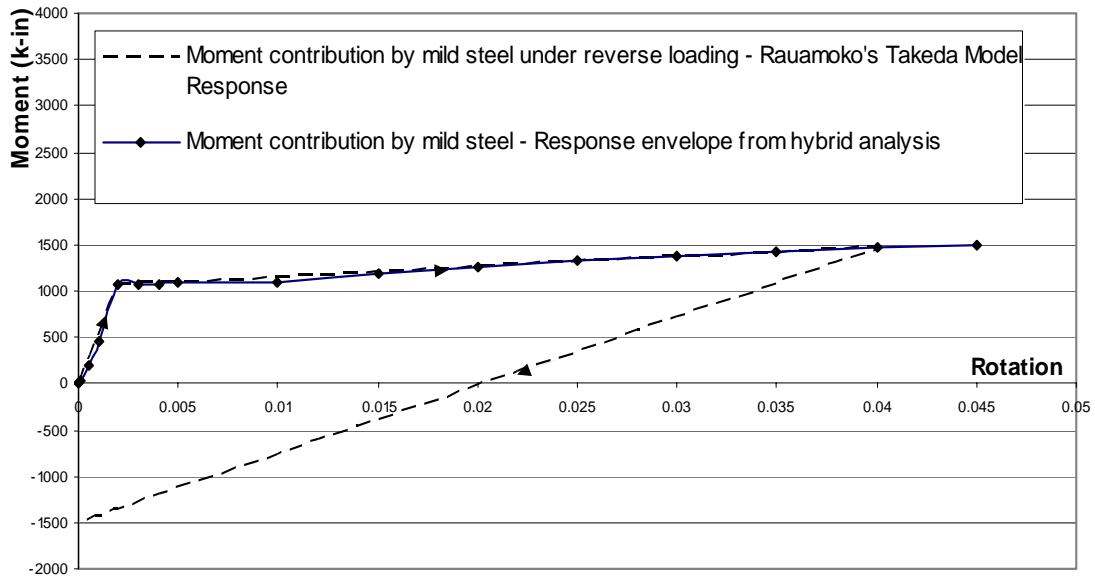


Figure 4.7 The moment-rotation behavior of the mild steel reinforcement at a hybrid connection.

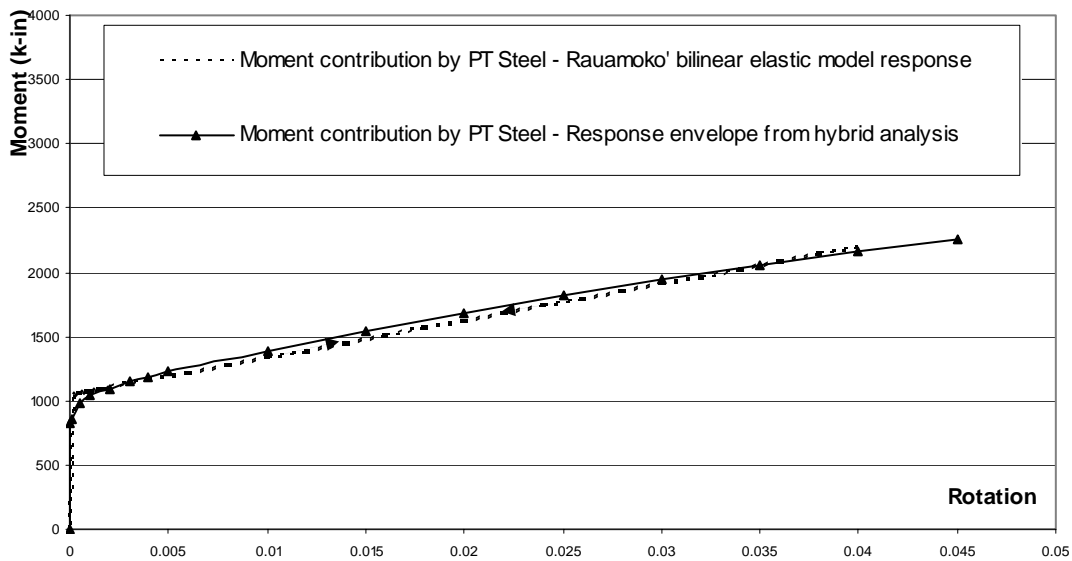


Figure 4.8 The moment-rotation behavior of the prestressing steel at a hybrid connection.

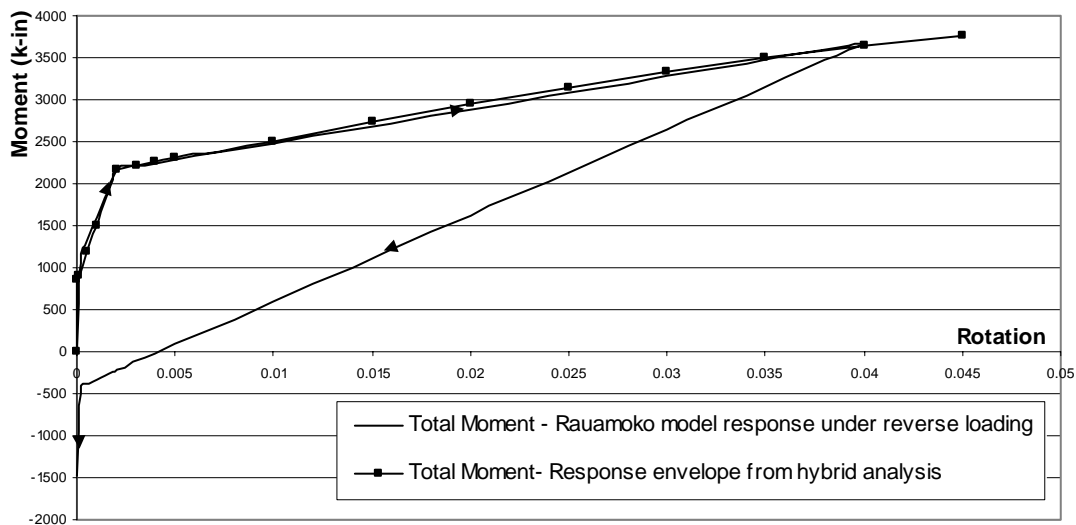


Figure 4.9 The total moment-rotation response envelope of a hybrid connection and its representation in a RUAUMOKO model.

4.2.3 Hybrid Frame Model

This subsection presents a 2-D finite element model for the hybrid frame building described in Section 4.2.1. As shown in Figure 4.10, the 2-D model consisted of only one seismic frame and a fictitious column that enabled the influence of the flexural floor links to be examined. The base resistance of the gravity columns and the out-of-plane bending of the precast wall system were small and were neglected in the analyses. As previously detailed (Section 1.3), the beams and columns jointed by hybrid connection concept were expected to remain elastic and thus, these members were represented as elastic beam-column elements in the RUAMUOKO model. To account for the influence of flexural cracking, the moment of inertia for the beam-column elements was taken as a fraction of that corresponded to the uncracked concrete gross section (I_g). Based on the test observations reported for the PRESS building [55], $0.6I_g$, I_g , and $0.51I_g$ were used for the columns in the first story, all

other columns, and beams, respectively. The reason for using larger I_g values for the columns was that they were subjected to axial compression due to prestressing and gravity loads, whereas the beams were subjected to the prestressing force required as part of the design of hybrid connections.

It was noted that the hybrid connection concept was used to connect the seismic column in the building to the footings. As detailed in the PRESSSS building, unbonded post-tensioning bars were used along the five-story height of the columns. All hybrid connections in the building model were represented with double springs as detailed in the previous section.

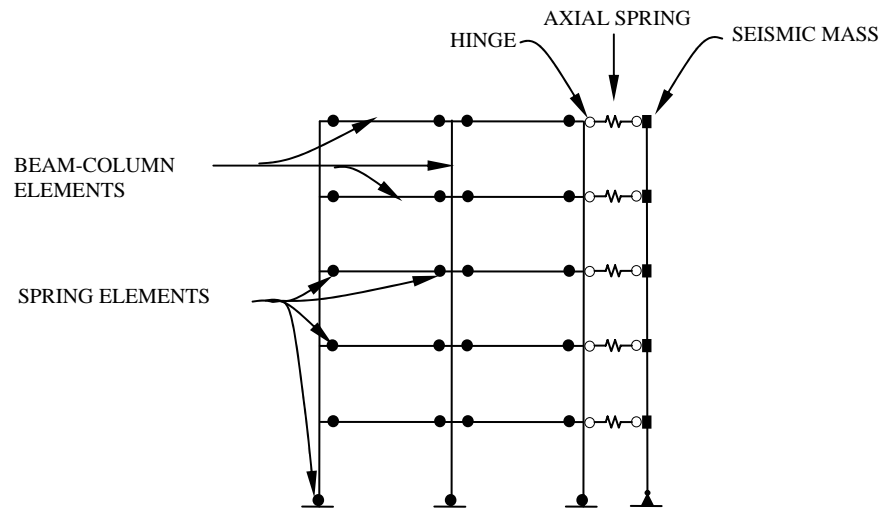


Figure 4.10 Finite element model of the five-story hybrid frame.

The 2-D model representing the hybrid frame was connected to the fictitious column using axial springs at the floor level. In the PRESSSS building, the precast double-tee floors were used in the lower three floors and were connected to the hybrid frame using flexible x-shaped steel plates (see Figure 4.11). It was envisioned that a similar floor-to-frame

connection detail could be adopted for the five-story hybrid frame building chosen for the analytical investigation in this report. The flexible floor connections were represented with equivalent axial springs in the model as shown in Figure 4.10 to simplify the investigation on the influence of flexible floor links on the response of the hybrid frame building. As with the PRESS building, each end of the double-tee floor panel was connected to the hybrid frame using two x-plates (see Figure 4.11).

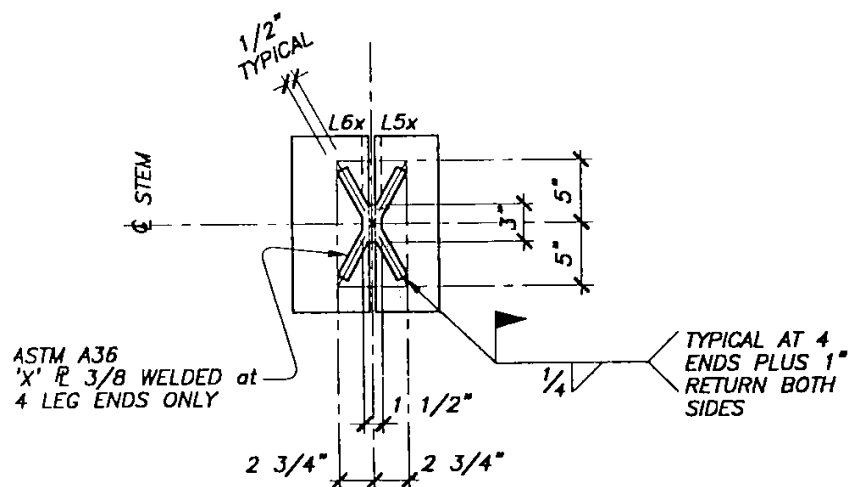


Figure 4.11 Details of an X-plate used in the PRESS building.

4.3 Validation of the Analytical Model

4.3.1 Overview

Pushover and dynamic analyses were conducted on the finite element model of the five-story hybrid frame building to examine the following issues:

- Adequacy of representing the moment-rotation behavior of hybrid connections using the model presented in Section 3.1, and
- The concept adopted for modeling hybrid frame buildings as detailed in Section 4.2.

As previously noted, the PRESSSS test building consisted of a three-story hybrid frame whose dimensions and connection details were identical to those assumed for the lower three stories of the hybrid frame building. Hence, the analysis results were compared to the test data where appropriate.

4.3.2 Pushover Analysis

The pushover analysis of the 2-D building model was performed using a monotonically increasing inverse triangular load. Because of the similarity between the hybrid building and the PRESSSS building, the lateral displacement at the third floor of the hybrid building was examined as a function of the base moment. Figure 4.12 compares the base moment-third floor lateral displacement response obtained for the PRESSSS test building with the pushover analysis results obtained for the hybrid building.

The predicted response, which satisfactorily captures the experimental response envelope of the PRESSSS test building, confirms that the 2-D analytical model accurately represents the strength and stiffness of the hybrid frame building. Furthermore, such close prediction of the strength and stiffness of the building indicates that the moment-rotation behavior of the hybrid connections was also adequately represented in the model. The failure of the analytical model to capture the experimental behavior at large displacements was expected, as some damage occurred to the beam ends and the grout pads at the interface during testing of the PRESSSS building [55]. Due to lack of information available, issues related to localized damage was not included in the analytical model.

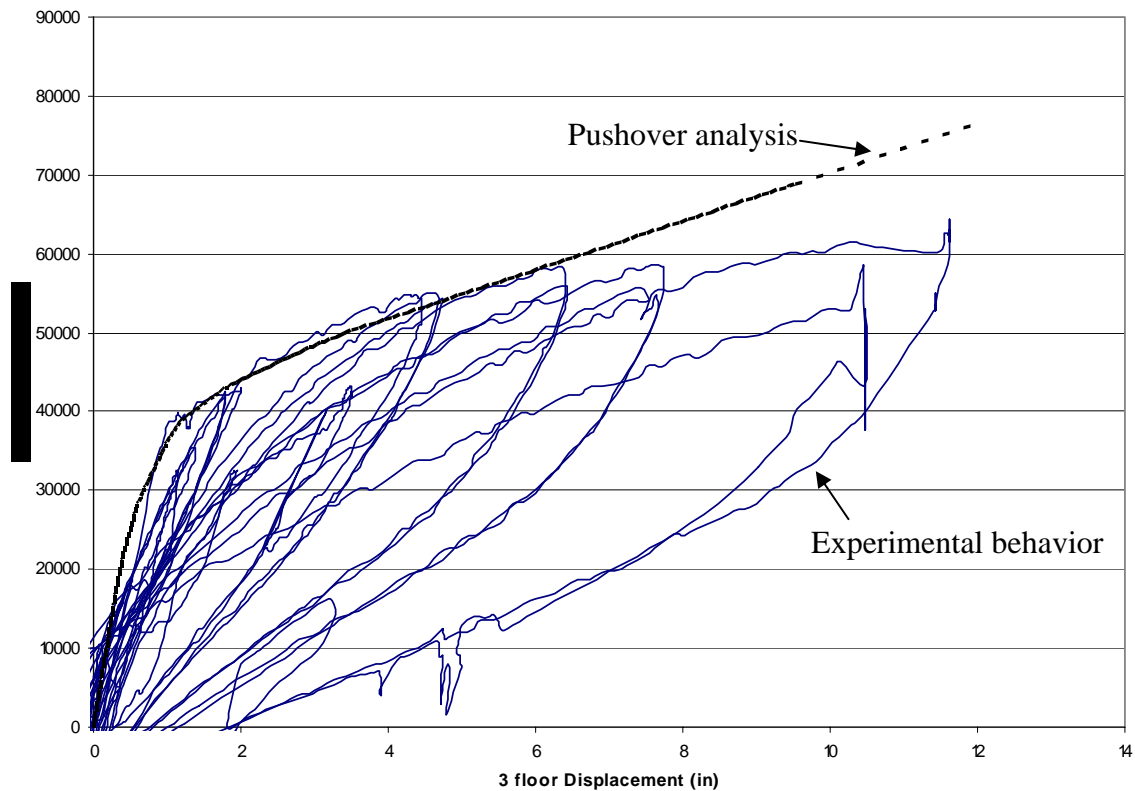


Figure 4.12 Comparison of experimental and calculated responses.

4.3.3 Dynamic Analyses

Dynamic analyses were conducted for the 2-D hybrid frame model using the input excitations that were used for the pseudodynamic testing of the PRESSS building. These records included short segments of input motions and were established to match four levels of earthquake acceleration response spectra. Labeled as EQ-I through EQ-IV, these input motions were derived using short segments of recorded earthquakes [60,61]. These four levels of earthquake motions were considered to correspond to performance levels of service, damage control, design, and survival limit states [62].

During the PRESSS test, it was realized that the original EQ-III and EQ-IV input motions demanded forces and displacements beyond the capacities of the hydraulic actuators used in the test. Therefore, testing in the frame direction of the PRESSS building was conducted using a modified version of EQ-III, which was established by reducing the high frequency content and will be referred to as EQ-III-M. No pseudodynamic testing was conducted at the EQ-IV level [55]. Figures 4.13 and 4.14 show the original and modified input motions, respectively. Since the PRESSS building represented the prototype building at 60 percent scale, the accelerations and time should be scaled by $1/0.6$ and 0.6 , respectively, which are included in the earthquake input motions shown in Figures 4.13 and 4.14. In order to use the PRESSS test data for validation of the hybrid frame model, the modified input motions were used in the first series of analysis. Note that the testing of the PRESSS building also included the $0.5EQ-I$ input motion. The response of the hybrid building to the original input motions is reported in Section 4.4.

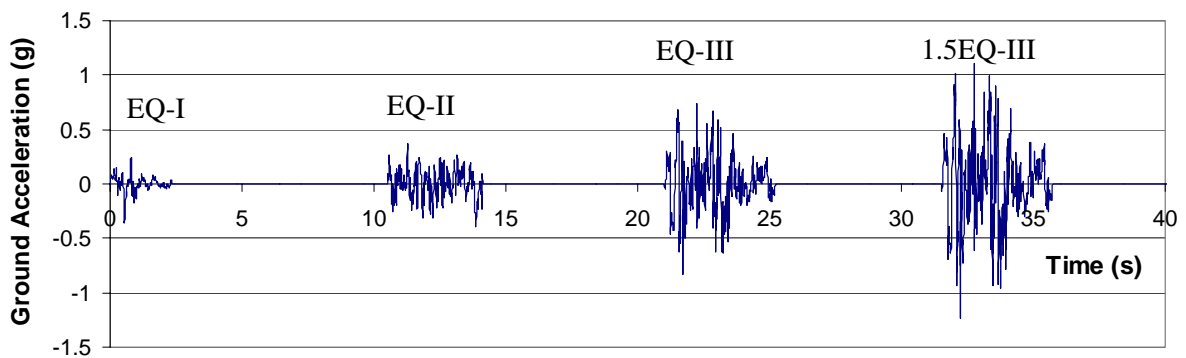


Figure 4.13 Acceleration time histories of the original input motions prepared for the PRESSS building that represented the prototype structure at 60% scale.

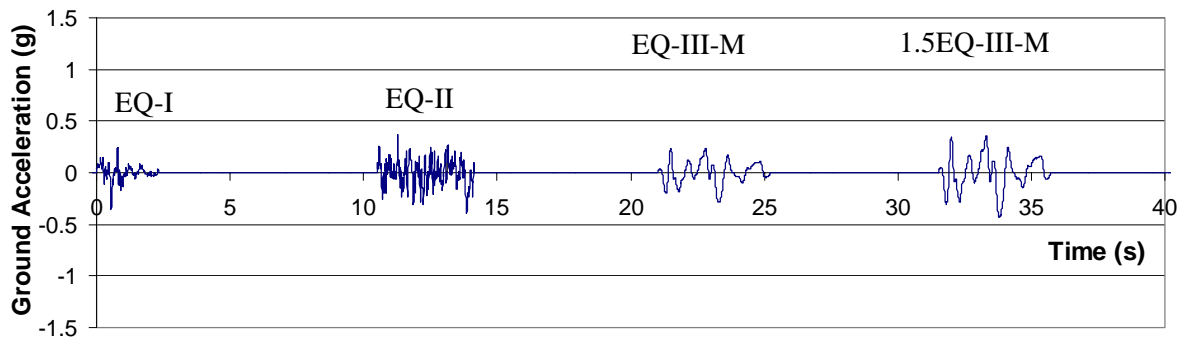


Figure 4.14 Modified input motions for the acceleration time histories shown in Figure 4.13.

At the end of each dynamic analysis for a given input segment, the hybrid building was allowed to experience free vibration for a sufficient duration of time. To adequately account for the strength and stiffness degradations experienced by the PRESSS test building, the hybrid frame building was analyzed using 0.5EQ-I, EQ-I, EQ-II and EQ-III-M in tandem as suggested by Pampanin et al. [18,63].

Lateral displacement and base moment time histories were used to characterize the building response under the earthquake input motions. Figure 4.15 shows the time histories of the third floor lateral displacement obtained from the dynamic analysis of the hybrid frame building and the PRESSS building test. A similar comparison for the base moment time histories is shown in Figure 4.16.

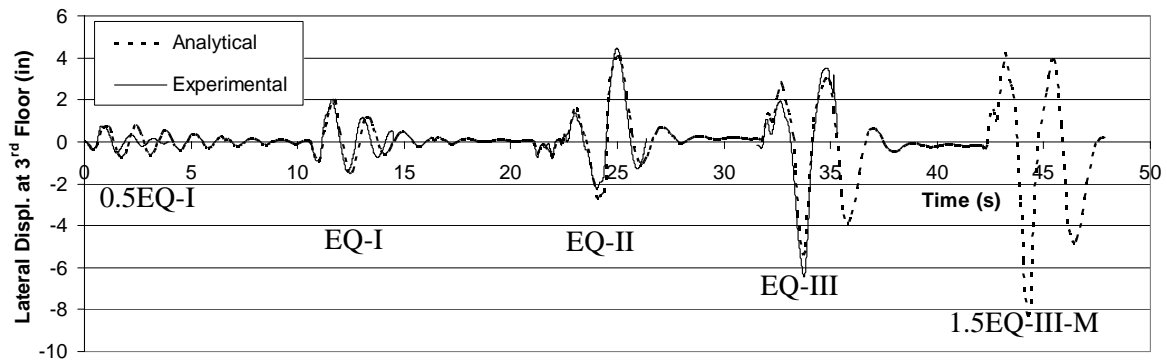


Figure 4.15 Third floor lateral displacement time histories obtained for the PRESSS and hybrid frame building.

It is observed from the comparison shown in Figure 4.15 that the peak displacements and the fundamental period reflected in the dynamic analysis results are slightly higher than the experimental values for 0.5EQ-I and EQ-I. However, a better agreement is seen between the analytical and experimental values for the EQ-II and EQ-III-M motions, indicating that the cracked section properties used for the beams and columns in the building model closely matched the conditions of the beams and columns of the test building during testing at EQ-II and EQ-III-M. At lower levels of excitation, the PRESSS building would have been stiffer than the model due to the formation of fewer flexural cracks in the beams and columns, contributing to the reduced period of the test building. Similar observations can also be made for the base moment histories shown in Figure 4.16.

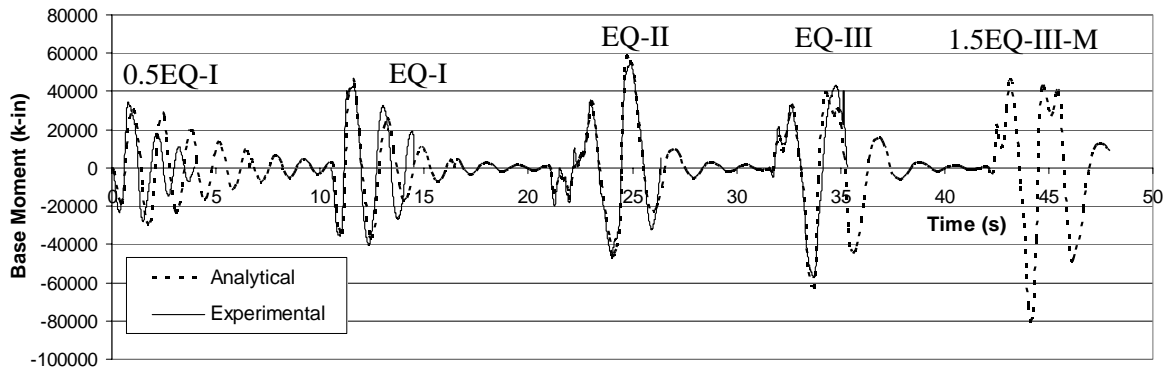


Figure 4.16 Base moment time histories obtained for the PRESSS and hybrid frame building.

The behavior of the PRESSS building was predicted in a previous study by Pampanin et al. [18, 63]. Their study differed from the current investigation in that they modeled the four jointed connection types used in the PRESSS building, and the moment-rotation behavior of various precast connections was based on the original expressions proposed for the strain estimates using the monolithic beam analogy. In the current study, the building is assumed to have only hybrid connections and the connection behavior was characterized using the modified expressions derived for the monolithic beam analogy, as described in Section 3.1. Therefore, it is of interest to compare the results obtained from the current study with that predicted by Pampanin et al. [18, 63]. Figure 4.17 compares the two analysis results obtained for the third floor lateral displacement with the test data. The response prediction obtained from the building model shown in Figure 4.10 more closely matches the observed response than that predicted by Pampanin et al. [18, 63].

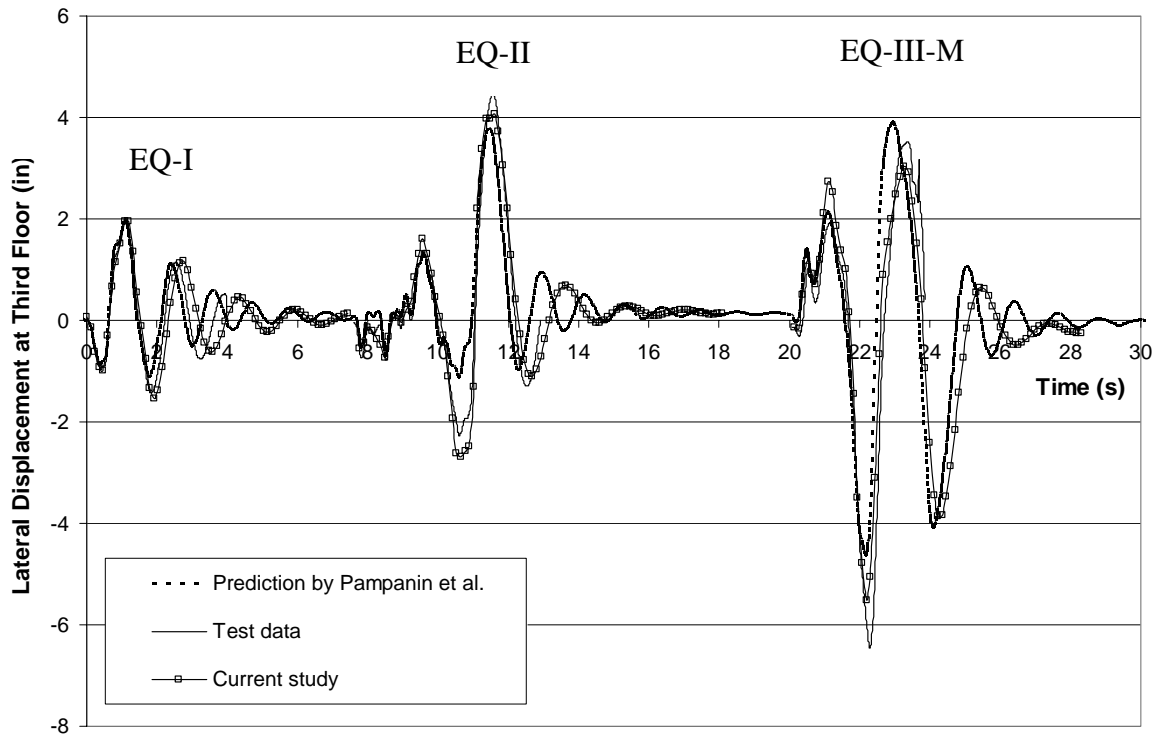


Figure 4.17 Third floor displacement time histories obtained from the PRESSS building and analytical models for the modified input motions.

Table 4.2 compares the peak displacement values for three input motions extracted from the plots shown in Figure 4.17. The table also shows the percentage differences between the predicted and experimental values. In addition to suggesting that the modeling approach used in the current study provides better prediction than that produced by Pampanin et al., the data in the table confirm that the analytical modeling of the five-story hybrid frame is satisfactory.

Table 4.2. Comparison of peak lateral displacements obtained at the third floor of the PRESSS and hybrid buildings.

Description		EQ-I		EQ-II		EQ-III-M	
		Positive	Negative	Positive	Negative	Positive	Negative
3rd Floor Displacement - Test Data (in.)		1.97	1.42	4.46	2.27	6.45	3.50
3 rd Floor Displacement Prediction (in.)	By Pampanin et al. [18,63]	1.87	1.11	3.75	1.12	4.64	3.92
	Current study	1.96	1.54	4.07	2.70	5.51	3.02
Percentage difference	By Pampanin et al. [18,63]	-5	-22	-16	-51	-28	12
	Current study	-1	8	-9	19	-15	-14

4.4 Performance Based Seismic Analysis

Performance based seismic engineering is generally regarded as the future direction for earthquake-resistant design, which has been addressed in the latest recommended design practice by the Structural Engineers Association of California (SEAOC) [62]. This concept requires multiple performance levels to be met in the design stage such that the seismic response of the structure will be satisfactory when subjected to earthquake ground motions with different intensities. This concept was followed when developing the four different levels of acceleration time histories for the PRESSS five-story building test [60]. Therefore, for the performance-based analysis of the five-story hybrid frame building, the original EQ-I, EQ-II, EQ-III, and 1.5EQ-III excitations were used as the input motion. Consistent with the SEAOC Blue book [62], 1.5EQ-III was assumed to represent an EQ-IV event.

For the dynamic analysis of the hybrid building, seismic weight at each floor level was assumed to be 702 kips, which corresponded to the floor weight of 3900 kips of the prototype building. The viscous damping for the building was defined using the Rayleigh damping model by assuming 5 percent and 17.5 percent for the first and fifth modes, respectively. As described in Section 4.2, the precast floors of the hybrid frame building were connected to the seismic frames using flexible floor links, which were represented as axial springs in the analytical model (see Figure 4.10).

The goal of the performance based seismic analysis was to examine various demand levels computed for the critical structural elements and compare the results against a specific set of acceptance criteria established for those demand levels. Since the lateral displacement drift of a building is considered a useful performance measure of damage under earthquake loading, the peak inter-story drifts were used to evaluate the performance of the hybrid building. The performance of the building was considered acceptable when the peak inter-story drifts were below the limits suggested for the performance based seismic response of special concrete moment frames [62].

Table 4.3 summarizes the peak inter-story drifts obtained at different floor levels from the dynamic analysis of the five-story hybrid frame building when subjected to the four levels of earthquake input motions. Also included in this table are the SEAOC recommended permissible drifts for the four intensities of ground motions. The performance of the hybrid building was remarkably good, producing drift demands about 63-73 percent of the recommended values for the damage control level (EQ-II), design level (EQ-III) and survival level (EQ-IV) earthquakes. At the service level, the drift demand in the building was exceeded by 20 percent at the first floor level while satisfying the recommended values at all

other floor levels. The reason for exceeding the inter-story drift limit of EQ-I at the first floor was believed to be due to the use of fully cracked section properties, which would be more suitable for higher intensity earthquake motions. With more realistic member properties, it is anticipated that the hybrid building would satisfy the performance limit state suggested in the SEAOC Blue book for the EQ-I input motion.

Table 4.3. Peak inter-story drifts obtained for different levels of earthquake input motions.

Earthquake intensity level	Peak inter-story drift (Percent)					
	Story level (Analytical values)					SEAOC recommended values
	1	2	3	4	5	
EQ-I	0.6	0.5	0.5	0.4	0.3	0.5
EQ-II	1.1	1.0	0.8	0.6	0.4	1.5
EQ-III	1.8	1.7	1.5	1.3	0.9	2.5
1.5EQ-III	2.4	2.3	2.3	2.1	1.8	3.8

4.5 Influence of Flexible Floor Links

For the dynamic analysis results reported in Section 4.4, the precast floors were assumed to be connected to the hybrid frames by flexible links. Using the same analytical model, the influence of the flexible floor links on seismic response of the five-story hybrid frame building was examined. By replacing the flexible floor links with rigid pin-ended links in the hybrid frame model shown in Figure 4.10, the analysis results were compared with those obtained in Section 4.4.

Table 4.4 summarizes the peak top floor lateral displacements and base moments obtained from the dynamic analyses of the hybrid frame model in Figure 4.10 with flexible and rigid floor links. Also included in the table are the percentage differences observed from the two analyses for the peak values of the top floor displacements and base moments at different earthquake intensities. Replacing the flexible floor links with rigid links increased the lateral displacements and reduced the base moments by only up to 2 percent for EQ-I, EQ-II, EQ-III, and 1.5EQ-III. The absolute values of the percentage differences obtained for the peak top floor displacement and base moment are similar for the EQ-I motion, to which the hybrid building responded in an elastic manner. For the input motions with higher intensities, inelastic responses were observed for the building. Overall, the two analyses showed no significant difference between the responses, which is attributed to the limited inelastic actions experienced by the floor links when modeled as flexible elements.

Table 4.4. Comparison of peak top floor displacements and total base moments obtained for the hybrid frame building with flexible and rigid floor links.

Description	EQ-I		EQ-II		EQ-III		1.5EQ-III	
	Peak displacement (in.)	Max. base moment (kip-in.)	Peak displacement (in.)	Max. base moment (kip-in.)	Peak displacement (in.)	Max. base moment (kip-in.)	Peak displacement (in.)	Max. base moment (kips-in.)
Flexible Link	2.59	42255	4.32	45701	8.51	57198	11.5	66599
Rigid Link	2.61	41937	4.33	45170	8.59	56410	11.6	65291
% Difference	0.77	-0.75	0.23	-1.16	0.94	-1.38	0.87	-1.96

4.6 Response Modification Factor

The response modification (R-) factor (or force reduction factor) is used in a forced-based design method to determine the design base shear and design moments for structures so that they can be forced to behave nonlinearly under design-level earthquakes. The R-factor enables design forces of a structure to be determined using elastic acceleration response spectra. The SEAOC Seismology Committee that was established in 1993 recommends that the R-factor consists of three parts: R_d that accounts for the global ductility capacity of the lateral force resisting systems, R_o that represents the overstrength inherent in the systems, and R_p that relates to the redundancy of the lateral load resisting systems. Ignoring the effect of R_p , the R-factor representing $R_d \times R_o$ was introduced in UBC 1997 [7]. A detailed description for the components of R-factor can be found in the SEAOC Blue Book [62].

As described in Section 1.2.2, hybrid frames are considered as a non-emulative structural system, for which a suitable R-factor is not recommended in the design codes [7, 13, 62]. Therefore, it is of interest to examine the R-factor for the hybrid frame building investigated in this study. Figure 4.18 shows the variation of base shear plotted against top floor lateral displacement for the hybrid building, which was obtained by performing a pushover analysis on the finite element model described in Section 4.3. Also included in this figure is the linear elastic response for the building that was established by replacing the inelastic springs modeling all hybrid connections including those located at the column bases with elastic springs in the finite element model and repeating the pushover analysis. Using the elastic and inelastic pushover analysis results, the following procedure is adopted to determine an R-factor for the five-story precast hybrid frame building.

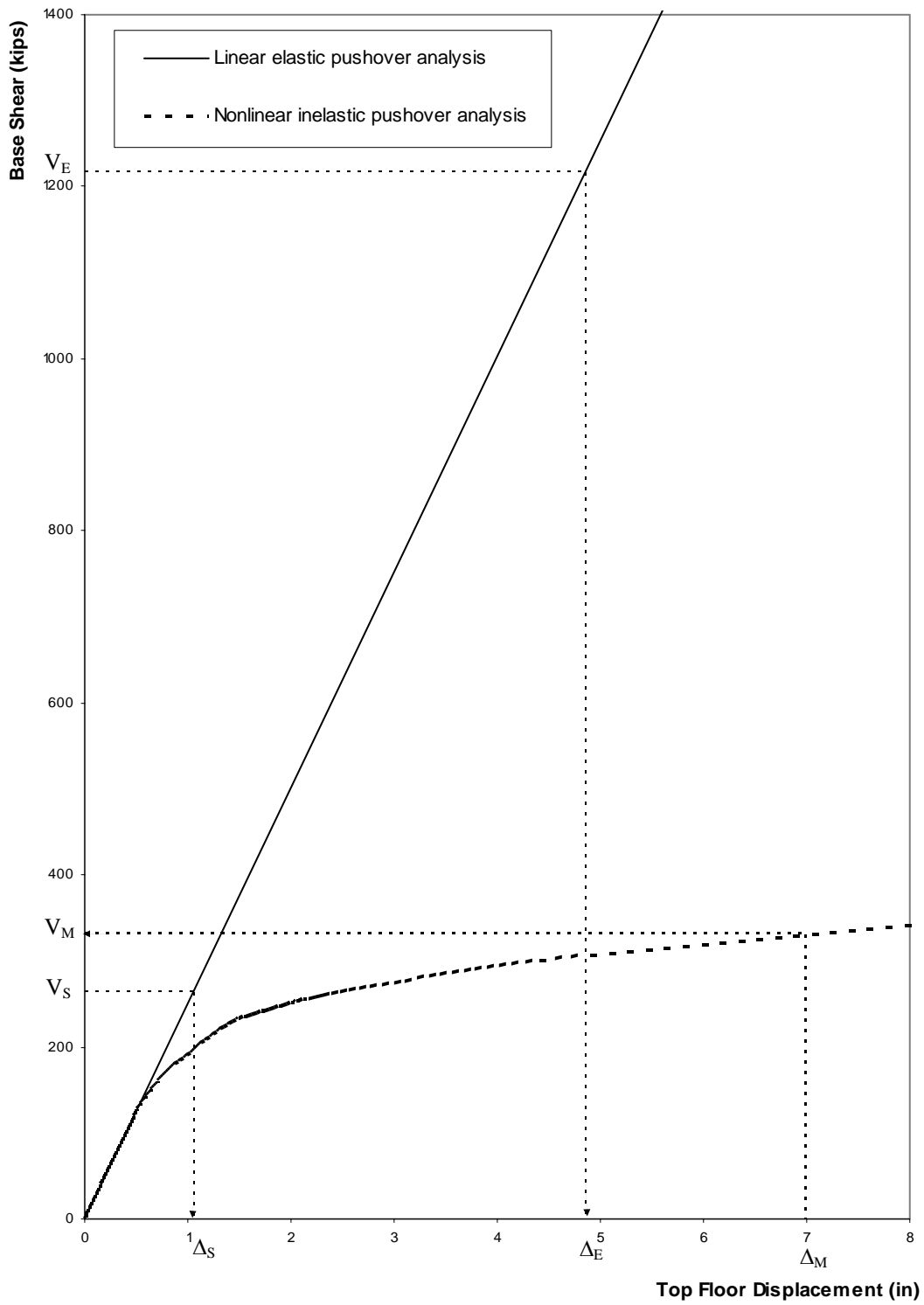


Figure 4.18 Linear and non-linear pushover analysis results for the hybrid frame model shown in Figure 4.10.

Consistent with recommendations in the SEAOC Blue Book [62] (see Figure 4.18),

$$R_d = \frac{V_E}{V_M} \quad (4.1)$$

$$\text{and } R_o = \frac{V_M}{V_S} \quad (4.2)$$

where V_E is the base shear corresponding to the elastic response of the structure, V_M is the probable maximum base shear capacity of the lateral load resisting system at inelastic response displacement, Δ_M , Δ_M is the maximum inelastic response displacement that occurs at a design-level earthquake, and V_S is the design base shear.

The five-story hybrid building used in this analysis was based on the PRESSSS test building, which was designed for seismic Zone 4 and soil profile type S_c using a direct-displacement based design (DBD) method. The fundamental period of the hybrid frame building was found to be 0.97 s by performing a modal analysis on the building model using the computer program RUAUMOKO. Using the corresponding period of 1.62 s at the prototype scale, V_E for the hybrid frame building was quantified as $0.346W$, where W is the seismic weight of the building and was equal to 3510 kips [61]. Therefore,

$$V_E = 0.346 \times 3510 \text{ kips.} = 1215 \text{ kips.}$$

Sritharan et al. [61] reported that the design team estimated a design base shear of 264 kips for the five-story PRESSSS building using the DBD approach. Hence, V_S for the hybrid frame building can be taken as 264 kips. Using the values for V_E and V_S , the corresponding elastic response displacements Δ_E and Δ_S can be found as shown in Figure 4.18.

The lateral top floor displacement Δ_M corresponds to the maximum inelastic response when the structure is subjected to a design-level ground motion. Since EQ-III represents a

design-level ground motion, Δ_M was obtained from the dynamic analyses of the building model reported in Section 4.4. Accordingly, Δ_M was equal to 6.99 in. and the corresponding V_M was determined using the nonlinear base shear vs. top floor lateral displacement envelope included in Figure 4.18. The estimated value for V_M was 331.0 kips. From Equations 4.1 and 4.2, the components of R-factor can be calculated as

$$R_d = (1215)/(331) = 3.67$$

$$R_o = (331)/(264) = 1.25$$

Therefore, a response modification factor for the hybrid frame building may be calculated as

$$R = R_d \times R_o = (3.67) \times (1.25) = 4.6$$

The R-factor of 4.6 calculated above appears to be noticeably smaller than a value of 8.5 recommended for concrete special moment resisting frames in design codes [7, 62]. The value of 8.5 is based on assuming $R_d = 3.4$ and $R_o = 2.5$. For the hybrid frame building, the calculated R_d closely related to the assumed value, but the R_o value is one-half of that suggested for design. Consistent with the direct-displacement based design, the design base shear was calculated at 2 percent inter-story drift, whereas V_S in the design codes correlates to the base shear when yielding occurs in the most stressed element in the structure [62]. According to this definition, a more suitable value for V_S for the hybrid frame building is 138 kips from Figure 4.18. This would imply an R_o value of 2.4 and an R-factor of 8.2. Hence, it is concluded that the behavior of the hybrid frame building is consistent with that expected for special moment resisting frames.

The calculation of V_E reported above was based on the elastic period estimated for the hybrid frame building using cracked section properties. Typically, the building codes use conservative estimates of periods when calculating the design base shear. If the two methods

suggested in the SEAOC Bluebook [62] for estimating the periods are followed, they would provide V_E values of 2257 kips and 2934 kips. When $V_S = 138$ kips is assumed, the corresponding R values for the hybrid frame building are 16.36 and 21.26, respectively. The reason for obtaining significantly high R-values for the hybrid frame building chosen for the current investigation may be attributed to: a) conservatively high estimates for V_E by the design codes by underestimating the period of the structure, and b) the use of lower V_S for the design of the hybrid frame building due to the application of the direct-displacement based design method. This is a benefit of using the DBD method for designing structures, which was also realized in the design of the PRESS building [54, 55].

Given the good performance of the hybrid frame building when subjected to different levels of earthquake input motions, the possibility of using higher R-factors in the design of such structures needs to be further investigated. The analysis results of the hybrid frame building also suggest that, by introducing methods for estimating realistic periods, the base-shear corresponding to the force based design method can be reduced. This aspect should also be further investigated by studying response of low- to high-rise hybrid frame buildings.

PAGE INTENTIONALLY BLANK

CHAPTER 5

CONCLUSIONS AND RECOMMENDATIONS

5.1 Overview

This research report focuses on an analytical investigation of precast concrete hybrid frames. First, a comprehensive literature review was completed addressing the performance of precast buildings in past earthquakes, experimental investigations of various precast framing concepts, analytical investigation of hybrid systems, and available design methods for hybrid frames. Next, an improved set of equations was established in accordance with the monolithic beam analogy concept to perform section level analysis for hybrid frame connections. A computer program, HYBRID, was then developed incorporating the improved set of equations, which enabled the investigation of hybrid systems at the member and system levels. The section level analysis results were compared with available experimental results to validate adequacy of the improved analysis results.

Utilizing the computer programs HYBRID and RUAUMOKO [59], dynamic response of a five-story hybrid frame building was investigated under different levels of earthquake input motions. After developing an analytical model to represent the hybrid frame building, the model was verified based on the test data from the PRESSS building. Using the analytical model, seismic behavior of the precast building was examined under multiple performance limit states. Using the analytical model, researchers also studied the influence of using flexible floor links in precast hybrid buildings and suitable R-factors for the force based design of hybrid frame buildings. Conclusions drawn from this study and recommendations for future research are presented below.

5.2 Literature Review

Conclusions drawn from the literature review are listed below under four different topics.

5.2.1 Performance of Precast Concrete Buildings in Past Earthquakes

1. Limited information on the performance of lateral load resisting moment frames incorporating only precast concrete members was generally found in earthquake reconnaissance reports. This limitation is believed to be due to restricted application of precast concrete technology in seismic regions.
2. Contrary to a popular belief, many precast buildings with and without other types of structural members performed satisfactorily during past earthquakes.
3. Although some of the buildings that incorporated precast structural members and other types of structural members in the gravity and/or lateral load resisting systems experienced severe earthquake damage, the cause of damage was not generally attributed to the use of precast structural members.
4. Common reasons for failure of structural systems in buildings that incorporated precast structural elements were the following:
 - Underestimation of design parameters
 - Poorly detailed connections between different precast structural members
 - Use of improper transfer mechanisms for the gravity and seismic forces within and between gravity and lateral load resisting systems
 - Brittle behavior of structural members, mainly due to the use of improper transfer mechanisms in design
 - Failure of floor panels due to unseating

- Use of inferior quality of materials in construction, and lack of supervision and implementation of quality control measures during construction

5.2.2 Experimental Investigation

Various framing concepts have been studied with an objective of introducing precast concrete buildings in seismic regions. These studies have primarily included the emulative systems and jointed systems that take advantage of the properties of precast concrete.

1. Several different precast framing concepts have been proposed by researchers with emulative connections. Generally, the emulative framing systems provided performance comparable to equivalent monolithic frame systems in terms of strength, ductility, and energy dissipation systems. However, some of the systems investigated did not provide adequate performance and require further research.
2. With added benefits, the jointed precast frame systems including the hybrid system have been shown to be a viable alternative to the emulation concept. Among several different jointed systems, extensive research has been conducted on the hybrid frame system which has shown to provide superior performance over the equivalent monolithic counterpart by providing ductile response with potential for energy dissipation and reduced residual displacements.

5.2.3 Analytical Investigation of Hybrid Systems

1. The strain incompatibility that exists between concrete and steel at the hybrid connections compelled researchers to develop analytical models based on several simplified assumptions. These assumptions, which are based on limited experimental

results, lead to analytical models that are less sophisticated than those available for monolithic concrete frames.

2. The monolithic beam analogy concept introduced by Pampanin et al. [18] provided an alternative analysis to characterize the connection behavior using a continuous moment-rotation envelope. However, the accuracy of the predicted results was not adequately investigated.

5.2.4 Design Methods for Hybrid Frame Systems

Due to the strain incompatibility issue discussed above, existing design methods were developed based on several simplified assumptions. These assumptions include the following:

1. Equivalent rectangular compression stress block is used to quantify the concrete compression force, ignoring the confinement effects.
2. Compression steel contribution is neglected.
3. The growth in the debonded length of the mild steel reinforcement is assumed to $5.5d_b$ based on limited test data, where d_b is the bar diameter.

5.3 Section Analysis of Hybrid Connections

Using the equivalent monolithic beam analogy concept suggested by Pampanin et al. [18], an improved set of equations were developed to estimate the strains at precast hybrid connections as a function of the interface rotation. Based on comparison of analysis results of three different connections with experimental data, the following conclusions were drawn:

1. The section analysis revealed that the moment-rotation envelope of a hybrid connection was not sensitive to the estimate of the extreme fiber concrete strain, which was consistent with a finding by Pampanin et al. [18]. However, the neutral axis depth, the strain in the post-tensioned steel, and strains in the mild steel reinforcing bars at the hybrid connection were found to be sensitive to the concrete strain.
2. The moment-rotation envelopes obtained for hybrid connections using the improved set of equations satisfactorily captured the stiffness and strength of the measured hysteresis responses.
3. The calculated neutral axis depths and tendon elongations were also found to correlate well with the experimental data.

5.4 Analysis of a Five-story Hybrid Frame Building

With dimensions identical to those of the PRESSSS building, a five-story hybrid frame building was analytically investigated using a 2-D nonlinear finite element model. The connection details assumed for the lower three floors of the hybrid building were identical to those used in the three-story hybrid frame included in the PRESSSS building. The behavior of the hybrid connections in the analytical model was based on the response envelopes obtained from the improved set of equations, which were developed for the monolithic beam analogy concept. Pushover and dynamic analyses were conducted on the building model, and the analysis results were compared with data from the PRESSSS building where appropriate. The conclusions drawn from this investigation are summarized below:

1. The base moment-lateral displacement response obtained from the pushover analysis of the hybrid building model satisfactorily matched the measured response of the PRESSSS building, indicating satisfactory representation of the connection behavior in the analysis model. At large inter-story drifts, discrepancies between the analytical and experimental results were observed, which was attributed to the strength degradation experienced by the PRESSSS building.
2. Analysis of the hybrid frame building under the input motions used for the PRESSSS test building led to good correlations between the analytical and experimental time histories of the base moments and lateral floor displacements, confirming that the analysis model satisfactorily represented the hysteresis behavior of the hybrid frame building.
3. A similar analytical investigation was conducted by Pampanin et al. [18] for the PRESSSS building using the original equations developed for the monolithic beam analogy concept. By comparing the peak displacements, it was found that the analysis results obtained from the improved set of equations more closely matched the experimental results. In some cases, the percentage difference obtained between the predicted maximum values and the experimental data using the original equations was reduced by more than 50 percent when the analysis was based on the improved set of equations.
4. A performance based seismic analysis was conducted for the hybrid frame building using four levels of earthquake input motions. For this analysis, the floors were assumed to be connected with flexible links. The peak inter-story drifts determined from this analysis were compared with the permissible limits recommended in the

- SEAOC Blue book [62] for concrete special moment frames. The hybrid building satisfied all drift limits, except at the first floor for the low intensity input motion. By using member properties more realistic for the low intensity motions, the corresponding drift limit was also expected to be satisfied.
5. The use of rigid links to connect the precast floors with the hybrid frames, instead of the flexible links, caused insignificant changes to the top floor displacements and base moments obtained for the hybrid building when subjected to the four levels of input motions. It was found that flexible elements were not subjected to significant inelastic actions during the seismic analysis.
 6. Depending on the drift assumed for defining the design base shear and how the period of the building is estimated, R-values ranging from 4.6 to 21.3 were shown to be possible for the design of the hybrid frame building. The possibility of using a large R-factor was supported by the direct-displacement design. A further investigation is necessary to finalize the suitable R-value for the force based design of hybrid buildings.

5.5 Recommendations

1. Previous experimental studies on hybrid frame systems did not provide adequate experimental data for adequately validating section analysis results of hybrid connections. More complete characterization of the connection behavior in the future experiments of hybrid frames would provide further verifications of the section analysis results including strains and neutral axis depths. Furthermore, the assumed

- plastic hinge length and growth in the debonded length of the mild steel reinforcement should also be verified using adequate experimental data.
2. Although dynamic analysis showed good correlations with experimental results, it is noted that no energy dissipation was assumed for the moment contribution by the unbonded post-tensioning tendons. Experimental data have shown that precast frames with unbonded post-tensioning tendons contribute to some energy dissipation. In recognition of this observation, more appropriate hysteresis rules should be established for the moment contributions by both the post-tensioning tendons and the mild steel reinforcement.
 3. The performance based seismic assessment, influence of flexible floor links and R-factor calculations were performed as demonstrations using one hybrid frame building. Using different buildings and several different input motions, these issues should be thoroughly investigated prior to generalizing the research outcomes for the design of precast hybrid frame buildings.

REFERENCES

- [1] Fintel, M. (1995). Performance of Buildings with Shear Walls in Earthquakes of the Last Thirty Years. *PCI Journal*, 40(3): 62–80.
- [2] Earthquake Engineering Research Institute (1995 and 1996). Northridge Earthquake Reconnaissance Reports. *Earthquake Spectra*, Supplement C to Vol. 11.
- [3] Earthquake Engineering Research Institute (2000). 1999 Kocaeli, Turkey, Earthquake Reconnaissance Report. *Earthquake Spectra*, Supplement A to Vol. 16.
- [4] Earthquake Engineering Research Institute (1989). Armenia Earthquake Reconnaissance Report. *Earthquake Spectra*, Special supplement.
- [5] Ghosh, S. K. (1995). Observations from the Bhuj Earthquake of January 26, 2001. *PCI Journal*, 46(2): 34–42.
- [6] Cheok, G. S., and Lew, H. S. (1991). Performance of Precast Concrete Beam-to-Column Connections Subject to Cyclic Loading. *PCI Journal*, 36(3): 56–67.
- [7] International Conference of Building Officials (1997). Uniform Building Code, Whittier, CA.
- [8] Park, R. (1995). A Perspective on the Seismic Design of Precast Concrete Structures in New Zealand. *PCI Journal*, 40(3): 40–60.
- [9] Paulay, T., and Priestley, M. J. N. (1992). *Seismic Design of Reinforced Concrete and Masonry Buildings*. John Wiley & Sons, Inc., New York.
- [10] Priestley, M. J. N. (1998). Displacement Based Approaches to Rational Limit States Design of New Structures. Keynote Lecture, *Proceedings of the Eleventh European Conference on Earthquake Engineering*, Paris.
- [11] Ghosh, S. K. (2001). Seismic Design Provisions for Precast Concrete Structures in ACI 318. *PCI Journal*, 46(1): 28–32.
- [12] Priestley, M. J. N. (1991). Overview of PRESSS Research Program. *PCI Journal*, 2(2): 50–57.
- [13] Cheok, G. S., Stone, W. C., and Nakaki, S. D. (1996). Simplified Design Procedure for Hybrid Precast Concrete Connections. *Report No. NISTIR 5765, National Institute of Standards and Technology*, Gaithersburg, MD.

- [14] Stanton, J. F., and Nakaki, S. D. (2002). Design Guidelines for Precast Seismic Structural Systems. *Report No. SM 01-02, Department of Civil Engineering, University of Washington, Seattle, WA.*
- [15] ACI Innovative Task Group 1 and Collaborators (2003). Special Hybrid Moment Frames Composed of Discretely Jointed Precast and Post-Tensioned Members (ACI T1.2-03) and Commentary (T1.2R-03). American Concrete Institute, Detroit, Michigan.
- [16] Ghosh, S. K. (2002). Seismic Design Provisions in U.S. Codes and Standards: A Look Back and Ahead. *PCI Journal*, 47(1): 94–99.
- [17] Celik, O. and Sritharan, S. (2004). An Evaluation of Seismic Design Guidelines Proposed for Precast Concrete Hybrid Frame Systems. *ISU-ERI-Ames Report ERI-04425, Department of Civil, Construction and Environmental Engineering, Iowa State University, Ames, Iowa, 172 pp.*
- [18] Pampanin, S., Priestley, M. J. N., and Sritharan, S. (2001). Analytical Modeling of Seismic Behavior of Precast Concrete ductile Frame Connection, *Journal of Earthquake Engineering*, 5(3): 329–367.
- [19] Mattock, A. H. (1979). Flexural Strength of Prestressed Concrete Sections by Programmable Calculator. *PCI Journal*, 24(1): 32–54.
- [20] John A. Martin & Associates, Inc. (1996 edition). Earthquake Images, <http://www.johnmartin.com/earthquakes/eqshow/index.htm>.
- [21] Kunze, W. E., Sbarounis, J. A., and Amrhein, J. E. (1965). Behavior of Prestressed Concrete Structures During the Alaskan Earthquake. *PCI Journal*, 10(2): 80–91.
- [22] Fintel, M. (1977). Performance of Precast Concrete Structures During Rumanian Earthquake of March 4, 1977. *PCI Journal*, 22(2): 10–15.
- [23] Fintel, M. (1986). Performance of Precast and Prestressed Concrete in Mexico Earthquake. *PCI Journal*, 31(1): 18–42.
- [24] Iverson, J. K. (1989). First Impression of Earthquake Damage in San Francisco Area. *PCI Journal*, 34(6): 108–124.
- [25] Iverson, J. K., and Hawkins, N. M. (1994). Performance of Precast/Prestressed Concrete Building Structures during the Northridge Earthquake. *PCI Journal*, 39(6): 38–55.
- [26] Ghosh, S. K. (1995). Observations on the Performance of Structures in the Kobe Earthquake of January 17, 1995. *PCI Journal*, 40(2): 14–22.

- [27] Earthquake Engineering Research Institute (2001). 1999 Chi-Chi, Taiwan, Earthquake Reconnaissance Report. *Earthquake Spectra*, Supplement A to Vol. 17.
- [28] International Conference of Building Officials (1977). Uniform Building Code, Whittier, CA.
- [29] García-Ranz, F., and Gómez, R. (1988). Seismic Design Regulations of the 1976 Mexico Building Code. *Earthquake Spectra*, 4(3): 427–440.
- [30] American Concrete Institute (1983). Building Code Requirements for Structural Concrete (ACI 318-83) and Commentary (ACI 318R-83). American Concrete Institute, Michigan.
- [31] United States Geological Survey (1995). The Mississippi Valley-"Whole Lotta Shakin' Goin' On". Reducing Earthquake Losses Throughout the United States, USGS fact sheet-168–95, <http://quake.wr.usgs.gov/prepare/factsheets/NewMadrid/index.html>.
- [32] Blakeley, R. W. G., and Park, R. (1971). Seismic Resistance of Prestressed Concrete Beam-to-Column Assemblies. *The Journal of the American Concrete Institute*, 68(9): 677–692.
- [33] Pillai, S. U., and Kirk, D. W. (1981). Ductile Beam-to-Column Connection in Precast Concrete. *The Journal of the American Concrete Institute*, 78(6): 480–487.
- [34] French, C. W., Hafner, M., and Jeyashankar, V. (1989). Connections between Precast Elements – Failure within Connection Region. *ACSE ACSE Journal of Structural Engineering*, 115(12): 3171–3192.
- [35] Seckin, M., and Fu, H. C. (1990). Beam-to-Column Connections in Precast Reinforced Concrete Construction. *ACI Structural Journal*, 87(3): 252–261.
- [36] Restrepo, J. I., Park, R., and Buchanan, A. H. (1995). Tests on Connections of Earthquake Resisting Precast Reinforced Concrete Perimeter Frames of Buildings. *PCI Journal*, 40(4): 44–61.
- [37] Alcocer S. M., Carranza, R., Perez-Navarrete, D., and Martinez, R. (2002). Seismic Tests on Beam-to-Column Connections in a Precast Concrete Frame. *PCI Journal*, 47(3): 70–89.
- [38] French, C. W., Amu, O., and Tazikhan, C. (1989). Connections between Precast Elements – Failure outside Connection Region. *ACSE Journal of Structural Engineering*, 115(2): 316–340.
- [39] Ersoy, U., and Tankut, T. (1993). Precast Concrete Members with Welded Plate Connections under Reversed Cyclic Loading. *PCI Journal*, 38(4): 94–100.

- [40] Ochs, J. E., and Ehasani, M. (1993). Moment Resisting Connections in Precast Connection Frames for Seismic Regions. *PCI Journal*, 39(5): 46–59.
- [41] Nakaki, S. D., Englekirk, R. E., and Plaehn, J. L. (1994). Ductile Connectors for Precast Concrete Frame. *PCI Journal*, 39(5): 46–59.
- [42] Cheok, G. S., and Lew, H. S. (1991). Performance of Precast Concrete Beam-to-Column Connections Subject to Cyclic Loading. *PCI Journal*, 36(3): 56–67.
- [43] International Conference of Building Officials (1985). Uniform Building Code, Whittier, CA.
- [44] Cheok, G. S., and Lew, H. S. (1993). Model Precast Concrete Beam-to-Column Connections Subject to Cyclic Loading. *PCI Journal*, 38(3): 80–92.
- [45] Priestley, M. J. N., and Tao, J. T. (1993). Seismic Response of Precast Prestressed Concrete Frames with Partially Debonded Tendons. *PCI Journal*, 38(1): 58–69.
- [46] Stone, W. C., Cheok, G. S., and Stanton, J. F. (1995). Performance of Hybrid Moment-Resisting Precast Beam-Column Concrete Connections Subjected to Cyclic Loading. *ACI Structural Journal*, 92(2): 229–249.
- [47] Stanton, J., Stone, W. C., and Cheok, G. S. (1997). A Hybrid Reinforced Precast Frame for Seismic Regions. *PCI Journal*, 42(2): 20–32.
- [48] Priestley, M. J. N., and MacRae, G. A. (1996). Seismic Tests of Precast Beam-to-Column Joint Subassemblages with Unbonded Tendons. *PCI Journal*, 41(1): 64–81.
- [49] Englekirk, R. E. (1989). An Analytical Approach to Establishing the Seismic Resistance Available in Precast Concrete Frame Structures. *PCI Journal*, 34(1): 92–101.
- [50] Sritharan S. (1998). Analysis of Concrete Bridge Joints Subjected to Seismic Actions, Ph.D. Dissertation, *Department of Applied Mechanics and Engineering Sciences*, University of California, San Diego, CA.
- [51] International Conference of Building Officials (1994). Uniform Building Code, Whittier, CA.
- [52] Mander, J. B., Priestley, M. J. N., and Park, R. (1988). Theoretical Stress-Strain Model for Confined Concrete. *ASCE Journal of the Structural Engineering*, 114(8), 1804–1826.

- [53] Dodd L. L., and Restrepo-Posada, J. I. (1995). Model for Predicting Cyclic Behavior of Reinforcing Steel. *ASCE Journal of Structural Engineering*, 121(3): 433–445.
- [54] Nakaki, S. D., Stanton, J. F., and Sritharan, S. (1999). An Overview of the PRESSS Five-Story Precast Concrete Test Building. *PCI Journal*, 44(2): pp 26–37.
- [55] Priestley, M. J. N, Sritharan, S., Conley, J. R., and Pampanin, S. (1999). Preliminary Results and Conclusions from the PRESSS Five-Story Precast Concrete Test Building. *PCI Journal*, 44(6): 42–67.
- [56] Sritharan, S. (2002). Performance of Four Jointed Precast Frame Systems under Simulated Seismic Loading. *Proceedings of the Seventh U. S. National Conference on Earthquake Engineering*, Paper No. 480, Boston, Massachusetts.
- [57] Sritharan, S., and Vernu, S. (2003). Analysis and Design of Precast Hybrid Frames. *Proceedings of the Pacific Conference on Earthquake Engineering*, Christchurch, New Zealand.
- [58] Thomas D., and Sritharan S. (2004). An Evaluation of Seismic Design Guidelines Proposed for Precast Concrete Jointed Wall Systems. *ISU-ERI-Ames Report, Department of Civil, Construction and Environmental Engineering*. Iowa State University, Ames, Iowa.
- [59] Carr, A. J. (2000). RUAUMOKO – Inelastic Dynamic Analysis Program, University of Canterbury, Christchurch.
- [60] Sritharan, S., Igarashi, A., Priestley, M. J. N., and Seible, F. (1999). Test Design of the PRESSS Five-Story Precast Concrete Building. *Proceedings of the 68th SEAOC Annual Convention*, Structural Engineers Association of California, Santa Barbara, pp. 255–261.
- [61] Sritharan, S., S. Pampanin, and Conley J. (2002). Design Verification, Instrumentation & Test Procedures. PRESSS-3: The Five-Story Precast Test Building, Vol. 3-3. *ISU-ERI-Ames Report ERI-04425, Department of Civil and Construction Engineering*, Iowa State University, Ames.
- [62] Seismology Committee. (1999). Recommended Lateral Force Requirements and Commentary (SEAOC Blue Book). Structural Engineers Association of California (SEAOC), California.
- [63] Pampanin, S., Priestley, M. J. N., and Sritharan, S. (2000). Frame direction Response. PRESSS-3: The Five-Story Precast Test Building, Vol. 3-4. *Report No. SSRP – 2000/08, Department of Structural Engineering*, University of California at San Diego, CA.